Doctoral Dissertation
Doctoral Program in Civil and Environmental Engineering (35thcycle)

A formulation to exactly integrate multiple discontinuities in 2D/3D finite elements by means of equivalent polynomials in XFEM analysis

By

Sebastiano Fichera
******

Supervisor(s):
Prof. G. Ventura, Supervisor

Doctoral Examination Committee:
Prof. E. Benvenuti , Referee, Università degli Studi di Ferrara
Prof. M. Fagone, Referee, Università degli Studi di Firenze

Politecnico di Torino
2023

Declaration

I hereby declare that, the contents and organization of this dissertation constitute my own original work and does not compromise in any way the rights of third parties, including those relating to the security of personal data.

<div align="right">

Sebastiano Fichera

2023

</div>

Acknowledgements

Abstract

Numerical integration of discontinuous functions is a longstanding problem explored by numerous authors over time. This topic acquired even greater attention in fracture mechanics, particularly in the eXtended finite element method (XFEM) context, in which the exact integration of discontinuous functions is essential in order to obtain precise and accurate results. In this scope, equivalent polynomials stand as an efficient method to address the problem harnessing traditional Gauss quadrature rule to exactly integrate polynomials times step function. Specific situations, however, require polynomials times multiple step functions to be integrated (i.e., problems involving crack branching, kinking, and junctions within a single finite element).

This Thesis focuses on the development of a method to exactly integrate polynomials times multiple step functions over various 2D and 3D domain shapes using standard Gauss quadrature, without splitting the integration domain. Traditional integration methods adopted in the XFEM framework may struggle to handle step functions, resulting in inaccurate numerical solutions or requiring multiple domain subdivisions. To address this issue, the research explores the mathematical foundations of equivalent polynomials for the integration of polynomials times step function in the context of XFEM analysis. The concept is then extended to the case of multiple step functions within the integration domain in order to deliver a formulation to smooth the overall integration process.

As a first step towards the integration of an arbitrary number of discontinuities, a closed form solution for the exact numerical integration of polynomials times double step function over quadrilateral domains is proposed. A software implementation of the proposed formulation, the Fortran library *double discontinuity equivalent polynomials* (*DD_EQP*), is also presented, delivering a practical application of the method and demonstrating its ease of implementation, precision and effectiveness. The *DD_EQP* is used to validate the proposed solution by means of numerical testing,

providing exact results. The presented formulation is then extended to triangular, tetrahedral and hexahedral domains, demonstrating its effectiveness and the accuracy for each analysed element shape. Additionally, by means of isoparametric mapping, the solution can be employed on 2D and 3D elements however defined in a global coordinate system, bringing them back to a regular parent element geometry. The effect on the results accuracy in the case of distorted elements is also discussed and mitigation strategies are explored. The extension of the proposed method to an arbitrary number of discontinuities is then addressed and a closed form solution for standard bi-dimensional quadrilateral domains is presented. The results demonstrate that the presented formulation offers an accurate and robust method for the exact integration of polynomials times multiple step functions, which is crucial for the stiffness matrix evaluation of enriched elements in XFEM simulations. The proposed technique provides a mathematical framework which can be also used as a reliable numerical tool to integrate polynomials over complex geometries and non-trivial domain shapes by way of standard Gauss quadrature.

In conclusion, the proposed method provides new pathways for exactly numerically integrate polynomials times multiple step functions, which is essential in simulations of complex physical phenomena in engineering and scientific applications. Moreover, the proposed formulation, as well as the *DD_EQP* library, have a wide application range, not limited to XFEM and fracture mechanics, but also including computational mechanics, mathematical computing of complex geometric regions, and computer graphics.

Contents

List of Figures

List of Tables

Chapter 1

Introduction

1.1 Background and motivation

The problem of exactly integrating discontinuous functions by way of standard quadrature rule is a challenging topic which has been explored by numerous authors over the years [1–8]. This problem gained particular attention in the context of fracture mechanics, in which modelling discontinuities by means of discontinuous and singular functions caused the traditional finite element method (FEM) to be ill-suited to handle such problems, being a piecewise differentiable polynomial approximation [9]. The finite element mesh, in fact, must be precisely defined in accordance with the discontinuity interface in order to produce accurate results, the use of FEM in such problems is dependent on an accurate and time-consuming discretisation process [10, 9]. Additionally, to track the path of the discontinuity as it develops (i.e., crack growth problems), the mesh must be regenerated at each step of the analysis [10], which results in high computational costs [11]. Such problems required the development and definition of specific numerical techniques for this scope, which has been tackled by various authors. In this scope, partition of unity methods (PUM) and element-free Galerkin-based formulations have been proposed by numerous authors [12, 13]. PUM enables the definition of solution spaces with user-defined local properties [14, 5]. Babuška and Melenk [14] developed the method specifically to address issues where standard FEM fails or the solutions are prohibitively expensive [11]. The PUM serves as the foundation for methods like GFEM and XFEM that are specifically created to address issues involving discontinuities, singularities,

localised deformations, and complex geometries [15]. GFEM, is a variant of the conventional FEM used in numerical analysis and has been introduced by Strouboulis, Babuška and Copps [16]. To better capture localised phenomena like singularities, discontinuities, or highly variable solutions, it enables the incorporation of additional enrichment functions or enrichment techniques. By enhancing the basis functions used in the approximation, GFEM improves the capabilities of FEM and increases the accuracy of the solution in the regions of interest [17]. The elements embedding enrichment functions posses additional degrees of freedom associated with the enrichment, in order to allow a more precise representation of the solution. Enrichment functions are usually defined based on the solution local behaviour [11]. The use of meshes that are partially or completely independent of the domain geometry and the enrichment of the approximation by way of special functions of interest are the main characteristics of this approach. On the other hand, XFEM is a particular kind of GFEM, presented by Belytschko et al. [18, 7], for engineering problems involving discontinuous and singular functions. In XFEM, additional degrees of freedom and enrichment functions, such as the Heaviside step function, that can model the displacement field around discontinuities avoiding meshing the crack surfaces [15], are introduced [11]. This makes XFEM especially helpful for fracture mechanics problems involving crack propagation or complex geometries. By simply including more basis functions in the approximation, XFEM allows for the introduction of a discontinuous displacement field along the crack surface. Additionally, the geometry and displacement field of a crack can be defined in terms of the original mesh nodal values when XFEM and level sets are used together. These advantages are especially important when the geometry changes, such as in the case of a growing crack [15]. The application of XFEM and GFEM to analyse the mechanical behaviour of structures and solids embedding cracks in their continuum has made the problem of exactly integrating discontinuous functions especially important in recent times [19–21]. In fact, although such methods over standard FEM enable a regular discretisation and not require remeshing [7], they introduce highly localised functions and discontinuous functions (such as the Heaviside step function) in the solution field [15]. These functions produce discontinuous terms in the finite element stiffness matrix, resulting in a non-negligible computational error when integrating using a traditional quadrature rule, due to the non-polynomial nature of the integrand [22]. In this context, it is common to achieve quadrature of terms embedding discontinuous and singular functions by dividing the elements crossed by discontinuities into

quadrature subdomains [7, 18, 15], though additional quadrature techniques, such as adaptive quadrature [23], nonconvex polygons [24], and a regularised form of the Heaviside step function, have also been proposed [25, 26]. Nonetheless, the elegance of XFEM and its main benefit of not requiring remeshing fall apart as quadrature subcells are introduced when the integration domain is divided into subdomains. In this context, an effective solution has been presented by Ventura in [22, 27], in which the concept of equivalent polynomials has been introduced, which has demonstrated its effectiveness in exact numerical integration of polynomials times step functions over a variety of domain shapes [22, 27, 28, 11].

1.2   Main objectives

The current research explores the problem of integrating multiple discontinuities without splitting the integration domain, with reference to the discussed above contexts of XFEM and fracture mechanics, by means of equivalent polynomials. To summarise, the equivalent polynomials concept has been explored in order to define an integration technique to exactly integrate two (or more) discontinuous functions over various domain shapes, without the need for defining subdomains.

Firstly, the formulation presented in [22, 27] has been thoroughly analysed and a Fortran library, *EQP*, has been developed as a practical application for the integration of polynomials times step function by means of equivalent polynomials. The precise results delivered by the library for various finite element shapes, however defined in a global coordinate system, have been the stepping stone for extending the use of equivalent polynomials also to multiple discontinuities.

The case of a standard 2×2 bilinear quadrilateral element crossed by two discontinuities in the XFEM context has been explored. In such scenario, the problem of integrating a double step function over the element domain arises when the element stiffness matrix has to be computed. This situation is not uncommon and can be encountered when scenarios such as crack branching, kinking or junction occur [29, 21, 30–36, 11]. A closed form solution by means of equivalent polynomials has been defined and an exact numerical integration technique for this specific element shape has been proposed. The presented method has been developed to address the integration problems that occur when more than one discontinuity is present within a single enriched finite element of an XFEM discretisation, delivering

an exact numerical solution without splitting the domain. The significance of this work, however, goes much deeper; it aims to provide a technique that could be incredibly helpful not only in XFEM/GFEM fracture mechanic problems, but also in computational geometry and as a mathematical tool to easily solve integrals over complex shape domains. Moreover, the proposed formulation has been embedded in a Fortran library *double discontinuity equivalent polynomials* (*DD_EQP*), which is a a double discontinuity version of the *EQP* library. The library has been used to carry out numerical tests on the proposed method and prove its efficiency on exactly integrating polynomials times double step function on quadrilateral domains, however defined in a global coordinate system. The proposed formulation has also been extended to the standard linear triangular element and to three-dimensional elements such as linear tetrahedron and trilinear hexahedron. Numerical tests have been performed for each element and the validity of the presented method has been proven. The results provided by the proposed formulation have been demonstrated to be exact as long as the determinant of the Jacobian matrix is constant. Approximations in the results or non-negligible computational errors are introduced in the case of distorted quadrilateral and hexahedral elements.

Finally, an extension for the presented formulation to the case of an arbitrary number of discontinuities within a bilinear quadrilateral element has been investigated and a general solution has been proposed. As for the case of two discontinuities, the extension of the proposed solution for an arbitrary number of discontinuities to triangular elements, as well as tetrahedral and hexahedral elements is straightforward.

1.3   Organisation of the thesis

This dissertation consists of six chapters, organised as follows:

Chapter 2: The problem of discontinuities and singularities in the finite element method (FEM) is introduced. A literature review of the the existing methods to address the problem is presented, as well as an overview of various applications of the extended finite element method (XFEM).

Chapter 3: The XFEM is presented and its formulation is discussed in detail. Moreover, the use of the Heaviside step function as enrichment function in the case

of strong discontinuities and the numerical integration strategies and possible issues in the XFEM are also analysed.

Chapter 4: The integration of XFEM elements containing a single discontinuity by means of equivalent polynomials over various domain shapes is analysed. The Fortran *equivalent polynomials* library, *EQP*, is presented as a practical implementation of the aforesaid formulation and some numerical tests are carried out in order to prove the exactness of the results. An extension of the equivalent polynomials formulation to non-polygonal elements is also briefly discussed.

Chapter 5: A formulation to exactly integrate polynomials times double step function over various 2D and 3D domain shapes is presented. The integration technique is discussed in detail and some numerical tests to validate it are carried out. Moreover, a software implementation of the proposed method, the Fortran *double discontinuity equivalent polynomials* library (*DD_EQP*), is introduced as a handy tool for the integration of polynomials times double step function over quadrilateral domains. Finally, an analysis about the loss of precision in the results in the case of distorted elements and the extension of the formulation to an arbitrary number of discontinuities are also discussed.

Chapter 6: The conclusions of the presented work are outlined and possible further applications and research are explored.

Chapter 2

Discontinuities in the Finite Element Method: a literature review

2.1 Introduction

The purpose of this Chapter is to introduce the Finite Element Method (FEM), its applications in the context of fracture mechanics and the formulations proposed to handle the problem of discontinuities and singularities within finite elements in various contexts. FEM is one of the most popular numerical methods for obtaining the approximate solutions of partial differential equations [9]. It has been effectively used to analyse, simulate, and forecast the behaviour of structures in many fields of engineering sciences. Instead of using differential equations to operate, the FEM rewrites starting value and continuous boundary problems into analogous variational forms [9]. The domain must be partitioned into non-overlaying areas known as *elements* in order to use the FEM. In the FEM, individual elements are linked to one another creating a *mesh*, and the fields within each element are represented using a local polynomial [37]. The quality of the mesh has a role in the outcome, and it is a vital necessity that the mesh adhere to the geometry. FEM primary benefit is that it handles complicated boundaries with relative ease, but there are several problems with FEM. The FEM places limitations on how well the technique may be applied in a variety of situations. Because the FEM depends on the approximation characteristics of polynomials, smooth solutions are frequently necessary to achieve the highest level of accuracy [9]. Nevertheless, the FEM becomes computationally

expensive to optimally converge if the solution involves non-smooth behaviour, such as high gradients or singularities in the stress and strain fields, or severe discontinuities in the displacement field, as in the case of cracked structures [38]. The modelling of fracture and damage phenomena is one of the issues in solid

Fig. 2.1 Buildings destroyed by a 7.8 magnitude earthquake on April 16, 2016 in Ecuador. (Source: J. Lance (European Union/ECHO) [CC BY-NC-ND 2.0 (http://creativecommons.org/licenses/by-nc-nd/2.0/)], via Flickr; http://www.flickr.com/photos/eu_echo/26571713861)

mechanics that has attracted the greatest attention (Fig. 2.1). When engineering constructions are subjected to heavy loads, the body may experience stresses that are greater than the material tensile strength, leading to progressive failure. During the last several decades, there has been an increase in interest in the correct modelling and evolution of smeared and discrete discontinuities, and there have been some important advancements in computational methods in recent years [9]. In early numerical methods for modelling discontinuities in finite elements [39, 40], using a multi-field variational concept, the shear band localisation has been characterised as a *weak* (strain) discontinuity that might pass through the finite element mesh [9]. The notion of virtual work statement has been thereafter modified [41] to consider *strong* discontinuities. A unified approach for modelling strong discontinuities by accounting for the interface traction-displacement connection and the softening constitutive rule has been subsequently proposed [42]. The displacement in the

strong discontinuity method is made up of regular and enhanced components, where the enhanced component results in a leap over the surface of the discontinuity [38]. The enriched degrees of freedom (DOF) are statically condensed on an element level using an assumed improved strain variational formulation to produce the element tangent stiffness matrix [9]. The non-smooth displacement close to the fracture tip is essentially captured in the FEM by locally tightening the mesh. Particularly in three-dimensional applications, the DOF count may dramatically rise. Moreover, repeated remesh operations are required for the incremental calculation of fracture development [38]. Re-evaluating the solution onto the revised mesh is an expensive process that also runs the risk of lowering the quality of the final outcome. The traditional FEM has reached the limits of its capacity to address fracture mechanics issues. A novel solution to the problem involves taking into consideration the a priori knowledge of the precise answer in order to avoid these computational issues [9]. With the definition of a partition of unity (PU) based enrichment approach for discontinuous fields [43], also known as the eXtended Finite Element Method (XFEM), a substantial advancement in crack modelling was demonstrated [9, 8]. The finite element approximation in the XFEM is enhanced with specific functions utilising the PU framework. Two-dimensional linear-elastic asymptotic crack tip displacement fields and discontinuous functions like the Heaviside step function are utilised to represent cracks. This makes it possible to use finite elements to describe the domain without directly meshing the fracture surfaces [38, 9]. One especially interesting aspect is that the discrete equations are obtained using the single-field (displacement) variational approach while maintaining the finite element framework and associated features, such as sparsity and symmetry [9]. This method offers a precise and reliable numerical approach to simulate strong discontinuities [18, 7]. By adding the discontinuous enrichment functions to the finite element approximation in order to account for the crack existence, a minimum remeshing FEM for crack growth is provided. The fundamental concept was to enhance the approximation space, which already contained a discontinuous displacement field [38, 8]. As a result, the approach enables the fracture to be positioned anywhere inside the mesh. The technique takes advantage of the observation that the sum of the shape functions for finite components must be one [5], known as the PU property. This characteristic is well-known because it relates to the shape functions capacity to replicate a constant that stands in for translation and is essential for convergence [9]. A strong tool for adding details from asymptotic solutions and other physics-related

information to solution spaces is the XFEM. This has shown to be especially helpful for fractures and dislocations where the PU technique may integrate near-field solutions to significantly improve the accuracy of reasonably coarse meshes [8]. The method has potential applications in the treatment of phenomena including void evolution, and models of interface behaviour, among others. As a result, the XFEM significantly increased the FEM power for many problems of interest in materials mechanics [9]. This chapter objective is to present an XFEM overview with a focus on modelling issues and applications of the method.

2.2   Methods and Formulations

2.2.1   Enriched FEM

Unquestionably, FEM has emerged as the most well-liked and effective analytical tool for analysing the behaviour of a variety of engineering and physical problems: from simple mechanical problems through fracture mechanics, fluid dynamics, civil engineering, material science, and so on. Also, several software programmes based on FEM methodologies have been created [9]. The study of fracture mechanics has shown to be a very good fit for the FEM. Yet, due to the altered mesh topology, it is challenging to represent fracture propagation using a finite element mesh. It is essential to fit the discretisation to the discontinuity in order to correctly simulate discontinuities with FEM. When addressing the problems with growing discontinuities, where the mesh must be generated at each step, this poses a significant challenge. Re-evaluating the solution onto the revised mesh is an expensive process that also has the potential of lowering the quality of the final outcome [9, 8]. Because the mesh must fit the discontinuity surfaces, modelling moving discontinuities with the traditional FEM is rather laborious and mesh generation of complicated geometries can be extremely time-consuming. The mesh must adhere to physical surfaces, which presents the biggest challenge. Voids, fractures, and material interface discontinuities may not intersect mesh elements. Moreover, it might be challenging to follow the geometrical and topological variation in fracture propagation problems and to modify the mesh close to discontinuities [9, 38]. Furthermore, reliable ways to transfer the solution to the new mesh are required when geometries change and history-dependent models are used [9]. This problem is crucial since the fields that are defined on

such discontinuities are frequently the most relevant ones. The generalised finite element method (GFEM) [44–46] and the XFEM have been developed to simplify the modelling of arbitrary moving discontinuities by the partition of unity method (PUM) [47], whose main idea is to extend a classical approximate solution basis by a set of enrichment functions that carry information about the nature of the solution (such as singularities or discontinuities) in order to overcome mesh-dependent difficulties [9]. The PUM offers flexibility in modelling moving discontinuities without altering the base mesh, while the enrichment functions evolve with the interface geometry. This is because it allows arbitrary functions to be locally embedded in the FEM or the meshfree approximation [38]. By permitting the incorporation of arbitrary functions in its basis, enrichment not only makes it easier to describe moving discontinuities but also improves the local approximation quality of the solution space. For problems involving boundary layers or singularities, this is very helpful [9]. The GFEM and the XFEM are effectively flexible instruments for the study of problems that are characterised by discontinuities, singularities, and complicated geometries. Several material modelling problems, such as the spread of fractures, and the development of dislocations may be resolved much more easily using these techniques [9, 8]. These approaches have the benefit that the structure of these entities can be fully independent of the finite element mesh. The traditional Finite Element approximation with the PUM is combined with the analytically known or numerically evaluated handbook functions within some scope of their applicability in the GFEM and the XFEM to improve the local and global accuracy of the computed solution [9]. Most of the theoretical and numerical advancements in Finite Elements may be easily expanded and used since the FEM is employed as the basic component in the XFEM and the GFEM. Moreover, the XFEM and GFEM enable the precise resolution of engineering problems in complicated domains that may be very hard to resolve using the traditional FE (Finite Element) approach [8]. The XFEM was designed for discontinuities, such as cracks, and employed local enrichments; the GFEM, on the other hand, was initially concerned with global enrichments of the approximation space. Nonetheless, the two techniques are essentially equivalent [9]. One can utilise both unstructured and structured meshes with the XFEM and GFEM. Many materials science investigations find structured meshes to be more appealing to evaluate the characteristics of a material unit cell. However, because it is frequently desirable to conform the mesh to the external boundaries of the component, unstructured meshes are frequently used for the analysis of engineering structures

and components, even though some methods currently being developed can handle even complex geometries with structured meshes [15]. By adding the analytically or numerically produced solution to a particular boundary value problem to the FE space, the GFEM offers precise numerical solutions with coarse meshes. On the other hand, the XFEM focuses primarily on the necessary node enrichment to simulate the internal boundary (inclusion or fracture) of interest. As a result, the XFEM offers more flexibility and is less reliant on established closed form solutions [9].

2.2.2   eXtended FEM

The benefits of the XFEM in reproducing the discontinuity of the displacement field throughout the crack surface and singularity at the crack tip without the requirement for remeshing have attracted a lot of interest in the last 20 years. With the help of the XFEM, fields containing jumps, kinks, singularities, and other non-smooth characteristics inside the elements may be approximated accurately [48]. This is accomplished by including extra terms (enrichments) into the traditional FE approximations. These terms provide the approximation the ability to capture non-smooth characteristics regardless of the mesh. Fracture mechanics has utilised the XFEM to the fullest extent possible [8]: such applications include discontinuities over the surface of the fracture and singularities at the fracture tip [9]. An appropriate mesh that takes these properties into account must be created and maintained in the traditional FEM; this is particularly challenging for crack growth, especially in three dimensions. Nevertheless, the XFEM can handle these problems on fixed meshes and takes crack propagation into account by dynamic enrichment of the approximation [9]. Belytschko and Black [18] initially described crack propagation using an enhanced FEM approach, which covers three key areas: the discretised formulation, the crack description, and the crack update criteria. By employing the PUM to take into consideration the crack presence, the meshing process is simplified in this technique by enriching the elements close to the crack tip and along its edges with the leading singular crack tip asymptotic displacement fields [38]. A mapping technique is utilised to match the discontinuities with the crack geometry when it is necessary to enrich numerous crack segments utilising the near-tip fields [9]. By adapting the generalised Heaviside function, Moës, Dolbow, and Belytschko [7] presented a much more elegant method to introduce a discontinuous field across the fracture faces away from the crack-tip and created straightforward rules for the

introduction of discontinuous and crack tip enrichments. As the XFEM does not use a mesh that adapts to fractures, voids, or inhomogeneities like the standard FEM does, it is a practical alternative. In XFEM, the conventional FE mesh for the problem is first built without taking the geometric object into consideration. By adding more functions to the basic displacement approximation, the existence of fractures, voids, or inhomogeneities is then described independently of the mesh [9]. For crack modelling, the displacement-based FE approximation is supplemented through the PUM with both discontinuous displacement fields along the fracture faces and the leading singular crack tip asymptotic displacement fields [38]. Furthermore, the XFEM offers a smooth way to incorporate specific finite elements or higher order elements without substantially altering the formulation. The XFEM enhances accuracy in cases where appropriate enrichment functions may be applied and some elements of the functional behaviour of the solution field are known a priori [9, 8]. Several approaches employed in the XFEM have direct connections to earlier methods created for mesh-free technologies [9].

2.3   XFEM Applications Overview

2.3.1   The Level-Set Method

The Level-set Method (LSM) is frequently used in the context of the XFEM to define implicitly where non-smooth features are located [49, 9]. The LSM is a perfect companion to the XFEM since it indicates where and how to enhance. The extension of the LSM to the description of crack paths in two dimensions has been proposed by Storlaska [50, 51]; other Authors [52–54] described crack surfaces in three dimensions. While both kinds of information, including crack surface as well as the crack front, may be directly derived from the level set functions, for crack problems, one enrichment is often required at the crack surface and further enrichments are needed at the fracture front. The level set function that saves the signed distance to the surface immediately affects the discontinuous enrichment function that catches the jump in the displacement field throughout the fracture surface [9]. The level-set functions, which imply a coordinate system whereby the enrichment functions are assessed, are indirectly responsible for the enrichment functions ability to capture the strong gradients at the crack front. As a result, it is

clear that the LSM offers significant benefits when used with XFEM. The XFEM, on the other hand, is just one stage in the modelling of crack propagation that results in an accurate estimate of the displacement, stress, and strain fields. The state at the crack tip is described in the next phase, whereby the crack increment is inferred [9]. In fact, the direction and length of the increment at the tip of the crack in two dimensions, or at specific points on the crack front in three dimensions, can be modelled using fracture parameter information such as stress intensity factors (SIFs), configurational forces, the J-integral, threshold stress and strain measures, etc. The third and last stage is updating the crack description in order to ensure that increments are taken into consideration properly [55]. Under the extended FE framework, Stolarska demonstrated the first use of LSM for simulating crack propagation, in which the LSM effectively handled interface evolution [50]. According to Sukumar [56], the level set function was utilised to describe the local enrichment for material interfaces while modelling holes and inclusions using the LSM [9]. For the three-dimensional study of crack issues, Moës, Gravouil, and Belytschko [53, 52] used the XFEM with the LSM to create arbitrary discontinuities. In the element-free Galerkin approach, Ventura, Xu, and Belytschko [57] developed the vector LSM for modeling of propagating cracks. For two-phase flow with surface tension effects, Chessa and Belytschko [58, 59] developed a combined XFEM and LSM, where the velocity was enhanced by the signed distance function. Moreover, the same Authors [60] used the LSM and the XFEM to simulate arbitrary space-time discontinuities along a moving hypersurface. Legay, Chessa, and Belytschko [61] suggested an Eulerian-Lagrangian technique for fluid-structure interaction based on the LSM, where the formulation of the fluid-structure interaction issue is derived from the level set description of the interface. Sethian [62] presented an expansion of the LSM based on the rapid marching technique. This strategy eliminates the requirement to describe the interface topology during its evolution; it is computationally appealing for fronts that advance monotonically [9]. In Sukumar, Chopp, and Moran [54] implementation of the mixed XFEM and fast marching approach, the fast marching method was employed to manage the development of the planar three-dimensional fatigue crack under fatigue growth circumstances. Chopp and Sukumar [63] used a method based on combining the XFEM with the fast marching approach to describe the fatigue crack propagation of numerous coplanar cracks. Sukumar [64] suggested a numerical method based on a linked XFEM and the fast marching method for non-planar three-dimensional linear elastic crack development simulation.

2.3.2   Linear Elastic Fracture Mechanics

FEM modelling of fracture propagation is laborious because the mesh must be up-dated to match the geometry of the crack surface [9]. Various FE approaches have been developed to describe cracks and fracture propagation. One of the most potent methods created using an enrichment approach for finite elements on the basis of a PU is the XFEM. In order to account for the existence of the crack, discontinuous enrichment functions were initially included to the FE approximation by Belytschko and Black [18], who also presented a minimum remeshing FEM for crack growth [9]. The traditional displacement-based approximation was enriched close to a crack by using both discontinuous fields and near-tip asymptotic fields through a PUM [7]. This was done to describe crack growth over the crack sides away from the fracture tip. The XFEM was improved by other Authors to represent crack problems with several branches, holes, and cracks originating from holes [34], and also to describe three-dimensional fracture mechanics problems through the PU concept, adding a discontinuous function and the two-dimensional asymptotic crack tip displacement fields to the FE approximation [6, 9]. The LSM was utilised to represent the crack position, including the location of crack-tips, in Stolarska method [50], which links the LSM with the XFEM to simulate crack growth. By describing the crack geometry in terms of two signed distance functions, Moës, Gravouil, and Belytschko [53] extended the XFEM to handle arbitrary non-planar cracks in three dimensions. This allowed them to create a near tip asymptotic field with a discontinuity that con-forms to the crack, even when it is curved or kinked near a tip [9]. For deriving the SIFs for common three-dimensional fracture situations, Ayhan and Nied [65] developed an enhanced FE technique. Using enhanced quadratic interpolations, Stazi [66] provided a technique for Linear Elastic Fracture Mechanics (LEFM) in which the geometry of the crack was described by a level set function interpolated on the same quadratic FE discretization. A combination of the XFEM and the mesh superposition method was proposed by Lee [67], whereby the near-tip field was modelled by superimposed quarter point elements on an overlaid mesh and the remaining portion of the discontinuity was implicitly described by a step function on the PU, in which the two displacement fields were paired through a transition region. This method was used for modelling stationary and growing cracks [9]. In order to account for the junction of fractures in both homogeneous and inhomogeneous brittle materials, Budyn [68] proposed the XFEM for multiple crack growth, which

does not need remeshing as the cracks expand. Zi [69] suggested a similar strategy for simulating the development and coalescence of fractures in a quasi-brittle cell with numerous cracks. Researchers have undertaken more current investigations on complex LEFM challenges. In order to apply the Dirichlet boundary conditions within the XFEM, Moës, Béchet, and Tourbier [70] proposed building a corrected Lagrange multiplier space on the border that retains the best rate of convergence. Employing discontinuous/non-differentiable enrichment functions in the XFEM, Ventura [22] proposed a technique for preventing the introduction of quadrature sub-cells by substituting the discontinuous/non-differentiable functions with equivalent polynomials. An XFEM for simulating cracks in orthotropic media was proposed by Asadpoure, Mohammadi, and Vafai [71]. It is based on a discontinuous function and two-dimensional asymptotic fracture tip displacement fields. In order to replicate orthotropic cracked materials, Asadpoure and Mohammadi [72] updated their prior model by introducing additional enrichment functions [9]. The necessary near tip enrichment functions were produced by extracting fundamental terms from complex solutions close to the crack tip. The impact of crack shielding and amplification of several configurations of microcracks, including many randomly aligned microc-racks, on the SIFs of a macro-crack was examined by Loehnert and Belytschko [73] using the XFEM [9]. By integrating the XFEM with the fast marching approach, Sukumar [64] presented a computational method for non-planar three-dimensional elastic crack development simulations. For two-dimensional crack development modelling, Tabarraei and Sukumar [74] used the XFEM on polygonal and quadtree finite element meshes. For convex polygonal meshes, basis functions were built using the Laplace interpolant, while mean value coordinates were used for non-convex elements [9]. The blending elements, which are established between enriched and standard elements and are frequently essential for a successful local partition of unity enrichments, are one of the key problems with the XFEM approach. To boost the effectiveness of local PU enrichments, Chessa and Belytschko [75] used the enhanced strain method in blending elements. By enriching an entire defined region surrounding the crack tip, Laborde [76] changed the conventional XFEM to get past issues with blending elements for the occurrence of crack problems. For address-ing arbitrary discontinuities in a finite element context, Fries and Belytschko [77] proposed an intrinsic XFEM technique without blending elements, where no new unknowns were added at the nodes whose supports are crossed by discontinuities. Based on a linearly decreasing weight function for enrichment in the blending ele-

ments, Fries [78] developed a corrected XFEM technique without blending elements problems [9]. Gracie [79] proposed a discontinuous Galerkin formulation that divides the domain into enriched and unenriched sub-domains, with the continuity being enforced via an internal penalty technique, avoiding blending elements. For the transition from continuous to discontinuous displacements, Benvenuti, Tralli, and Ventura [25] proposed a regularised XFEM model, where the developing strain and stress fields were handled separately using certain constitutive assumptions. In order to address the issue of blending elements, Shibanuma and Utsunomiya [80] proposed an alternate formulation for the XFEM based on the idea of the PU FEM, which ensures numerical correctness over the whole domain. The original corrected XFEM approach introduced by Fries was generalised to finite deformation theory and used to the three-dimensional scenario by Loehnert, Mueller-Hoeppe, and Wriggers [81]. The use of the XFEM in dynamic fracture has mainly been concentrated on estimating the dynamic SIFs for arbitrary two- and three-dimensional cracks and modelling of dynamic crack propagation. In order to describe dynamic fracture and time-dependent problems that provide evidence of stability of the numerical scheme in linear fracture mechanics, Réthoré, Gravouil, and Combescure [82] suggested an energy-conserving scheme inside the framework of the XFEM [9]. Menouillard [83, 84] presented an explicit time-stepping method for enriched elements based on a mass matrix lumping technique, and showed that the critical time step for an enriched element is of the same order as the critical time step for the corresponding element without extended DOF. Elguedj, Gravouil, and Maigre [85] developed a traditional element-by-element approach that links the conventional central difference scheme with the unconditionally stable-explicit scheme to offer a generic explicit time integration technique for XFEM dynamic simulations with a standard critical time step. In the context of the XFEM for moving interfaces, Fries and Zilian [86] investigated the convergence characteristics of several time integration approaches, including one-step time-stepping schemes, the implicit Euler method, the trapezoidal rule, and the implicit midpoint rule. The meshless approximation was utilised by Menouillard and Belytschko [87] to enhance the XFEM for dynamic fracture problems by smoothing the stress state around the crack tip during propagation and reducing oscillations in the stress caused by the propagation of the discontinuity. The same Authors later presented a technique based on ensuring the continuity of forces corresponding to the richer DOF to gradually release the tip element as the crack tip passes through it [88]. In the scope of the XFEM, Menouillard [89] introduced a new

enrichment approach with a time-dependent enrichment function and investigated the impact of several directional criteria on the crack path [9]. By assessing the dynamic SIFs utilising the domain separation integral approach, Motamedi and Mohammadi [90, 91] developed a dynamic crack analysis for composites based on the orthotropic enrichment functions in the XFEM context. Several academics have examined at the significance of error estimation in the XFEM numerical analysis. By utilising a cut-off function to localise the singular enrichment region in a convergence investigation for a variation of the XFEM on cracked domains, Chahine, Laborde, and Renard [92] showed that the suggested variant convergence error is of order h for a linear FEM [9]. Based on the superconvergent patch recovery (SPR) method for the XFEM framework, Ródenas [93] proposed a stress recovery strategy that offers precise estimates of the discretisation error for LEFM problems. By assessing the discretisation error for quantities of interest computed in the XFEM using the idea of constitutive relation error, Panetier, Ladeveze, and Chamoin [94] developed a technique to find the local error boundaries in the context of fracture mechanics. For LEFM issues, Ródenas [95] proposed a recovery-type error estimator that uses the XFEM to produce local equilibrium and upper limits on the error in energy norm. For problems involving fracture mechanics, Shen and Lew [96, 97] developed an optimally convergent discontinuous Galerkin-based XFEM, in which an optimal order of convergence was observed in comparison to existing XFEM variations. In the XFEM study of crack problems, Prange, Loehnert, and Wriggers [98] provided a straightforward recovery-based error estimator for the discretisation error [9]. The XFEM analysis of linear elastic fracture mechanics has been investigated by researchers in more innovative concepts. For two-dimensional and three-dimensional problems, as well as those involving arbitrarily shaped triangles and tetrahedra, Park [99] devised a mapping technique for integrating weak singularities that arise from enrichment functions in the GFEM/XFEM. In order to establish the Gauss quadrature rule over components of any shape in two dimensions without the necessity for partitioning, Mousavi [100] provided an alternative Gaussian integration scheme. This method proved effective and precise in evaluating weak form integrals. By applying strain smoothing to higher order elements, Bordas [101] examined at the accuracy and convergence of enriched finite element approximations. He concluded that polynomial enrichment functions are the best type of enrichment function for strain smoothing in enriched approximations. In addition to introducing a straightforward and adaptable quadrature rule based on the same geometric methodology, Richardson [102] offered

a technique for modelling quasi-static crack growth that combines the XFEM with a broad strategy for cutting triangulated domains [9]. By combining the benefits of explicit and implicit crack descriptions, Fries and Baydoun [103, 104] presented a method for two-dimensional and three-dimensional crack propagation. They also described a propagation criterion for three-dimensional fracture mechanics using the proposed hybrid explicit-implicit approach [9]. Using the interaction integral approach created by the XFEM in LEFM, Minnebo [105] proposed a three-dimensional integral strategy for numerical integration of singular functions in the computation of stiffness matrix and SIFs. In the three-dimensional XFEM analysis of regularised interfaces, Benvenuti [26] proposed the Gauss quadrature of integrals of discontinuous and singular functions [9].

2.3.3   Cohesive Fracture Mechanics

LEFM is effective only when the fracture process zone (FPZ) at the crack tip is small compared to the size of the crack and the size of the specimen LEFM useful [106]. In order to account for the FPZ, other models must be chosen [9]. A traction-displacement relation across the fracture faces near the tip can be used to depict the cohesive crack model, one of the simplest ones. By incorporating the idea of fracture energy into the cohesive crack model and defining a variety of traction-displacement equations for concrete, Hillerborg, Modéer, and Petersson [107] further refined the model that Dugdale and Barenblatt [108] introduced in the early 1960s for metals. By incorporating the displacement jump into the conventional FEM and using the jump function as an enrichment function for the entire cohesive crack, Wells and Sluys [109] proposed the first application of an enriched FEM into cohesive fracture mechanics [9]. In this case, the path of the discontinuity was completely independent of the mesh structure. For simulating the formation of arbitrary cohesive cracks, Moës and Belytschko [110] designed the cohesive crack model within the XFEM framework. This model required the SIFs at the cohesive zone's tip to disappear in order for the cohesive zone to grow. In order to avoid the need for local PU blending, Zi and Belytschko [111] introduced an XFEM for the cohesive crack model with a new formulation for elements containing crack tips. In this formulation, the entire crack was modelled with just one type of enrichment function, namely the signed distance function, including the elements containing the crack tip. The crack was modelled as a group of cohesive segments with a finite length, and the segments

were added to finite elements by using the partition of unity property of the finite element shape functions [9]. Remmers, de Borst, and Needleman [112] presented this method for modelling crack nucleation and discontinuous crack growth regardless of the structure of the finite element mesh. Using a cubic displacement discontinuity, Mariani and Perego [113] described a method for simulating the propagation of quasi-static cohesive cracks in quasi-brittle materials. The process zone at the tip of a cohesive fracture was modelled to have a cusp-like appearance [9]. Belytschko [114] proposed the XFEM for modelling dynamic crack propagation based on switching from a continuum to a discrete discontinuity, where the loss of hyperbolicity was modelled by a hyperbolicity indicator that allows determining both the crack speed and crack direction for a given material model [9]. A theoretical and computational framework for linear and nonlinear fracture behaviours was published by Larsson and Fagerström [115]. It was based on the inverse deformation issue and employed discontinuous deformation that was separated from continuous deformation using the XFEM approach. There is a connection between fracture mechanics and strain softening. The fact that strain softening results from damage and frequently precedes fracture is one reason for this interest. In actuality, it is a symptom of energy release that occurs gradually during microscopic decohesion before a macroscopic break becomes visible [9]. Areias and Belytschko [116] presented a numerical method for the quasi-static analysis of three-dimensional crack propagation in brittle and quasi-brittle solids. This method coupled an XFEM formulation with a regularised "crack-band" version of the XFEM with a viscosity-regularized continuum damage constitutive model [9]. An incremental-secant modulus iteration method employing the XFEM/GFEM was presented by Xiao, Karihaloo and Liu [117] to model the cracking process in quasi-brittle materials defined by cohesive crack models whose softening law was composed of linear segments. Based on additional enrichment of the cracked elements with the capabilities to model variations in the discontinuous displacement field on both sides of the discontinuity to obtain a better stress distribution on crack faces, Asferg, Poulsen, and Nielsen [118] developed a partially cracked XFEM element for cohesive crack growth. For the transition from continuous to discontinuous displacements, Benvenuti [119] and Benvenuti, Tralli, and Ventura [25] introduced a regularised XFEM model, in which the emerging strain and stress fields were modelled separately using particular constitutive assumptions that can address cohesive interfaces with vanishing and finite thickness in a unified manner. In a thorough investigation, Zamani, Gracie, and Eslami [120] employed the SIF criterion and

the stress criterion with both linear and nonlinear cohesive laws to use higher-order terms of the crack tip asymptotic fields as enrichment functions of the XFEM for cohesive and traction-free cracks. By including the constitutive conditions in front of the crack tip as direct unknowns in the FEM equations along with the crack growth parameters in an incremental form of the virtual work, Mougaard, Poulsen, and Nielsen [121] presented a complete tangent stiffness for modelling crack growth in the XFEM [9]. XFEM has been widely utilised in cases where failure is followed by the development of discrete cracks and localised damage zones, such as in concrete structures and rock mechanics problems, to simulate crack growth. For a discrete crack simulation of concrete utilising an adaptive crack growth method, Unger, Eckardt, and Könke [122] used the XFEM [9]. Several criteria were used to forecast the direction of the expansion of a cohesive fracture. Deb and Das [123] presented the XFEM for simulating cohesive discontinuities in rock masses. The displacement discontinuities were simulated by modelling using three- and six-nodded triangular elements. To examine the impacts of fracture criteria in cohesive zone models for mixed-mode fractures, Xu and Yuan [124] presented a cohesive zone model with a threshold in conjunction with the XFEM. Benvenuti and Tralli [125] proposed a regularised XFEM approach that can simulate the formation of a process zone with finite width and its subsequent collapse into a macro-crack in concrete-like materials [9]. This approach can deal with the entire process from strain localization to crack inception and propagation in a unified and smooth manner. A numerical method based on the XFEM was published by Zhang, Wang, and Yu [126] with particular reference to the dynamic study of the Koyna Dam during the 1967 Koyna earthquake. The method was designed for a seismic analysis of crack development in concrete gravity dams [9].

2.4   Conclusions

The present chapter has provided a comprehensive overview of XFEM, outlining its theoretical foundations and practical implementation, as well as highlighting some of its key advantages and limitations. By examining a number of representative examples from the literature, we have demonstrated how XFEM can be used to solve challenging problems that would be difficult or even impossible to tackle with traditional FEM. Overall, it is clear that the XFEM method represents a significant

advance in the field of numerical simulation, and has the potential to revolutionise the way in which a variety of engineering problems are approached. There are still some challenges to be addressed, particularly in terms of computational efficiency and robustness, that will be further discussed in this Thesis. In conclusion, XFEM represents a powerful numerical tool that allows for the efficient and accurate simulation of complex engineering problems involving discontinuities and singularities. Through its ability to seamlessly incorporate the effects of such features into the underlying mesh, XFEM provides a flexible and versatile framework that is well-suited for a wide range of applications, including fracture mechanics, fluid-structure interaction, and contact problems, among others.

Chapter 3

eXtended Finite Element Method: Formulation and Challenges

3.1 Introduction

As a piecewise differentiable polynomial approximation, the FEM approximation is unsuitable to describe problems including discontinuities (either in the unknown field or its gradient), singularities, and boundary layers [9]. It is required to adapt the discretisation to the line or surface of the discontinuity in order to properly model discontinuities using the FEM. When addressing problems with growing discontinuities, where the mesh needs to be re-generated at each step, this poses a significant challenge. The standard FEM requires extensive mesh refinement in the areas where the field gradients are high in order to resolve singularities or boundary layers. In fact, updating the mesh topology to adhere to the discontinuity geometry makes modelling discontinuities using the FEM troublesome (Figure 3.1) [9]. The existence of fractures, shear bands, and inclusions in structural problems are prominent examples of the discontinuity in a system field variables. Discontinuous fields can also exist between two distinct fluids in fluid mechanics problems. Discontinuities are usually grouped into two categories: *strong discontinuities* and *weak discontinuities*. The former refers to discontinuities in the field variables of a model, while the latter represents discontinuities in the field variables gradients. Cracks and interfaces between different materials represent strong and weak discontinuities in structural problems. An adequate management of the interface in the approximation of the

(a) Crack propagation in a plate containing a hole and subjected to a tensile stress.

(b) Example of standard *FEM* mesh following the interfaces geometry.

(c) Example of *XFEM* mesh. Yellow elements are enriched.
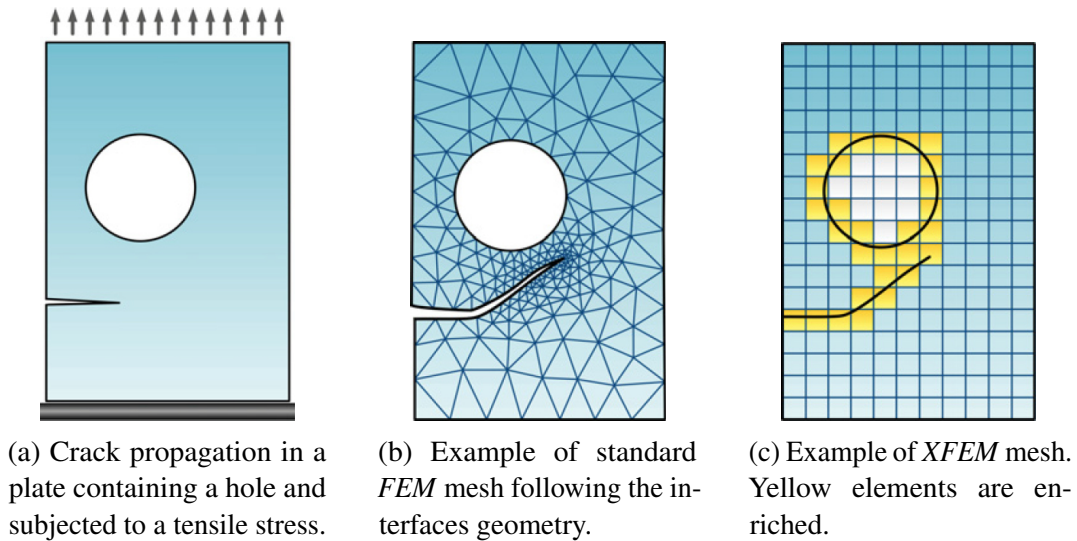
Fig. 3.1 Comparison between standard *FEM* and *XFEM* modelling of a plate containing a crack and a hole and subjected to a tensile stress. (Source: *Extended Finite Element Method: theory and applications* (p. 32) by A. R. Khoei, 2015, John Wiley & Sons. [Copyright (2015) by title of publisher]. Used with permission.)

discontinuous field is required for good convergence of the solution. As shown in the crack tip area, the solution may, for instance, have a particular behaviour at the interface, such as strong discontinuities or singular derivatives [9]. In such cases, the numerical method involved in the approximation may be enhanced to represent these characteristics of the solution. The essential feature is the incorporation of enrichment functions that contain a discontinuous field. The standard FEM relies on the local approximation properties of polynomials [5]. However, for jumps, kinks, or singularities in the solution within elements, polynomials have poor approximation properties [127]. Consequently, the accuracy of a standard finite element analysis is, in general, quite poor for problems involving arbitrary discontinuities [128]. Various formulations have been developed with the capability to introduce particular solution characteristics into the approximation space, such as the partition of unity finite element method (PU-FEM) [14], the GFEM [45, 46], and the XFEM [18, 7]. These techniques include the PUM, which adds unique enrichment functions to the conventional approximation space. In this Chapter the mathematical formulation for the XFEM will be introduced with reference to solid mechanics problems and its robustness as well as its potential flaws will be discussed. It includes the definition of PUM, enrichment elements and enrichment functions, as well as XFEM formulation numerical integration. In particular, in Section 3.7, the quadrature problems that

arise due to the introduction of discontinuous enrichment functions will be anal-
ysed and the existing methods to circumvent the issue, with their advantages and
disadvantages, will be examined.

3.2   The Partition of Unity Method and Enriched Fi-nite Elements

A partition of unity in a domain Ω is a set of functions such that

$$\sum_i^{\mathcal{N}} \phi_i(\boldsymbol{x}) = 1, \forall \boldsymbol{x} \in \Omega \tag{3.1}$$

The basis for the definition of the PU is the notion of *clouds*, which are overlapping
open sets Ω_i of arbitrary shape centred in $\boldsymbol{x}_i$ and covering the solution domain Ω of
a boundary value problem with $\Omega \subset \cup_{i=1}^{\mathcal{N}} \Omega_i$ [129]. A PU is an ensemble of global
functions $\phi_i(\boldsymbol{x})$ whose support is contained in a cloud and whose values add up to
one at each point $\boldsymbol{x}$ in the solution domain (Eq. (3.1)). By means of an arbitrary
function $\psi(\boldsymbol{x})$ defined on Ω, Eq. (3.1) becomes

$$\sum_i^{\mathcal{N}} \phi_i(\boldsymbol{x}) \psi(\boldsymbol{x}_i) = \psi(\boldsymbol{x}) \tag{3.2}$$

Since in the FE approach the shape function collection is generally a PU, by taking
$\phi_i(\boldsymbol{x}) \equiv N_i(\boldsymbol{x})$, the solution field $\boldsymbol{u}(\boldsymbol{x})$ can be written as

$$\boldsymbol{u}(\boldsymbol{x}) = \sum_i^{\mathcal{N}} N_i(\boldsymbol{x}) \bar{\boldsymbol{u}}_i \tag{3.3}$$

where $\mathcal{N}$ represents the number of each finite element nodal points and N_i are the
standard shape functions. Nonetheless, the interpolation field can be enhanced by
expressions that adhere to the analytical solution [9]. A mathematical framework
for generating an *enriched* solution can be developed using the notion of PU. The
enrichment is the process of enhancing the discretisation approximation depending
on the characteristics of the problem. In this approach, the behaviour of the analysed
phenomena is added to the approximation space used to solve the problem. The main
method for obtaining the enriched solution is to increase the order of completeness,

which leads to a greater approximation accuracy by including the information acquired from the analytical solution [9]. Enrichment can be characterised by knowing the particular behaviour of the solution (e.g. in case of singularities, discontinuities, etc.), embedding this information into the FE space, in opposition to standard FEM, where singular solution behaviour are generally resolved refining the mesh. Several interpolation functions set can be employed to better estimate the problem solution than polynomial spaces. The PU concept introduction for the enrichment of solution spaces of numerical solutions to partial differential equation is generally credited to Melenk and Babuška [5], who introduced the PUM: the precursor of XFEM and GFEM [15], and defined some interpolation functions used for the solution of the Laplace equation, Helmholtz equation, and the elasticity equation. The key feature is based on the multiplication of enrichment functions by nodal shape functions. Limiting the enrichment to the nodes of a region of interest, the enrichment can acquire a local form [9]. Therefore, the FE approximation of the enriched domain can be written as

$$\boldsymbol{u}(\boldsymbol{x}) = \underbrace{\sum_{i}^{\mathscr{N}} N_i(\boldsymbol{x})\bar{\boldsymbol{u}}_i}_{\text{standard interpolation}} + \underbrace{\sum_{i}^{\mathscr{N}} N_i(\boldsymbol{x})(\sum_{j}^{\mathscr{M}} p_j(\boldsymbol{x})\bar{\boldsymbol{a}}_{ij})}_{\text{enriched interpolation}} \qquad (3.4)$$

where $\bar{\boldsymbol{u}}_i$ are the standard nodal DOF associated to the basis $N_i(\boldsymbol{x})$ and $\bar{\boldsymbol{a}}_{ij}$ are the DOF associated to the basis $p_j(\boldsymbol{x})$. $\mathscr{M}$ represents the enrichment functions number for the i-th node. In Eq. (3.4) the standard FE interpolation field indicates the base field upon the enriched interpolation field is overlapped to improve the displacement field interpolation $\boldsymbol{u}(\boldsymbol{x})$ by means of the enriched terms. In the mathematical literature the enriched part of the interpolation is usually called the *ansatz*. As the enrichment is adjusted to best reproduce the current solution ($p_j(\boldsymbol{x})$ is frequently based on asymptotic solutions, which are not perfect solutions), the nodal values $\bar{\boldsymbol{a}}_{ij}$ are unknown parameters. Therefore, the ansatz need not be a precise local solution for the issue at hand [15]. Another benefit of this approximation structure is that the discrete equations for the system will be sparse if the functions $\phi_i(\boldsymbol{x})$ have compact support (e.g. are only nonzero across a tiny subdomain of the problem). In contrast, if an enrichment function were simply added to the approximation, non-sparse discrete equations would result, which are far more computationally burdensome. Notice that the approximation in Eq. (3.4) reproduces the function $p_j(\boldsymbol{x})$ identically when $\bar{\boldsymbol{a}}_{ij} = 1$ and $\bar{\boldsymbol{u}}_i$, according to the partition of unity condition.

It should be highlighted that, despite what was stated above, the shape functions for the conventional approximation and enrichment do not necessarily need to be the same functions. Instead, usually speaking, $\phi_i(\boldsymbol{x}) = N_i(\boldsymbol{x})$ is employed [15]. Since the partition of unity criteria enables a FE approximation to accurately represent rigid body translation, all Lagrangian FE shape functions possess this property, which is required for convergence and passing the patch test. Many meshfree approximations also meet this requirement [15].

3.3   Enriched Elements

The core concept of the standard FEM is the approximation properties of polynomials [37, 19]. Standard FEM may perform quite poorly if the solution exhibits noticeable non-polynomial behaviour, such as weak or strong discontinuities. In fact, the discontinuity or singularity, for instance at the crack tip location, cannot be accurately represented by the standard FEM in an adequate way. Numerous strategies have been proposed in order to get over these problems, but one of the most effective ones to utilise to capture weak or strong discontinuities is the enrichment of approximation space [9]. The degree of consistency of the approximation or the versatility of the approximation to recreate a certain complex field of interest may be attributed to the enrichment. Enhancing the order of completeness is essentially the same as the enrichment principle. However, the enrichment aims to improve the approximation accuracy by including information from the analytical solution. In the case of PUM (Section 3.2) and XFEM/GFEM, the approximation space is enhanced through "*extrinsic enrichment*" of the approximation by adding enrichment functions to standard approximation (Eq. (3.4)) [9]. While enrichment functions are defined over the entire domain in standard PUM, a *local* extrinsic enrichment of the approximation is used by the XFEM. Since discontinuities usually have local effects, enrichment can be restricted to certain zones rather than enriching the whole solution domain, dramatically reducing the computational time and the memory usage. XFEM enrichment gives elements the capability to replicate the internal interfaces of both strong and weak discontinuities [9]. The former refers to discontinuities that primarily affect the main variables, such as displacement in crack surfaces, while the latter refers to discontinuities in gradients, such as displacement gradient, or strain, in the boundaries of material changes (*bimaterial problems*). The solution field in

XFEM can be described as

$$\boldsymbol{u}(\boldsymbol{x}) = \sum_{i=1}^{\mathcal{N}} N_i(\boldsymbol{x})\bar{\boldsymbol{u}}_i + \sum_{k=1}^{\mathcal{P}} \sum_{j=1}^{\mathcal{M}_k} \bar{N}_j(\boldsymbol{x})\,\psi_k(\boldsymbol{x})\bar{\boldsymbol{a}}_{kj} \tag{3.5}$$

where $\mathcal{M}_k \subseteq \mathcal{N}$ are the set of nodal points enriched by $\psi_k(\boldsymbol{x})$. Given the fact that $\sum_{j=1}^{\mathcal{M}_k} \bar{N}_j(\boldsymbol{x})$ is only a PU in the elements where all nodes are enriched, this technique must be acknowledged as not being entirely compatible with the standard PU notion. In fact, the enriched approximation is capable of exactly define the $\psi_k(\boldsymbol{x})$ functions only in these elements. However, issues can occasionally arise for enrichment functions in elements for which only some of the nodes are enriched, also known as *blending elements* [75, 76]. The local extrinsic enrichment of the XFEM in fact produce a systematic error in partly enriched elements.

3.4 XFEM Approximation

One of the most employed enriched PUM approaches for numerical modelling of discontinuous problems is the XFEM [9]. It is a potent and precise method used to model both weak and strong discontinuities without taking into account their geometries. This approach incorporates specific functions that rely on the nature of discontinuity into the finite element approximation without considering them during the mesh generation procedure. The technique goal is to model weak and strong discontinuities minimising the enrichment. Fractures, voids, contact surfaces, and so on, have no impact on mesh configurations in XFEM [9]. Problems involving moving discontinuities, such as changing of phase, fracture propagation, and shear banding, are well suited for this approach. To introduce the notion of *discontinuous enrichment*, let us consider a body Ω containing a discontinuity Γ_d (as shown in Figure 3.2). The objective is to build a discontinuous FE approximation of the field $\boldsymbol{u} \in \Omega$ along the discontinuity Γ_d. The standard FEM approach is to create a mesh in which the elements conform and align to the discontinuity (Figure 3.1b). This technique is clearly burdensome and computationally expansive, especially in the case of a growing discontinuity or if multiple discontinuities have to be modelled. In XFEM the discontinuity Γ_d is modelled by means of enrichment functions, so that the uniform mesh in Figure 3.1c can reproduce the discontinuity in $\boldsymbol{u} \in \Omega$ within the
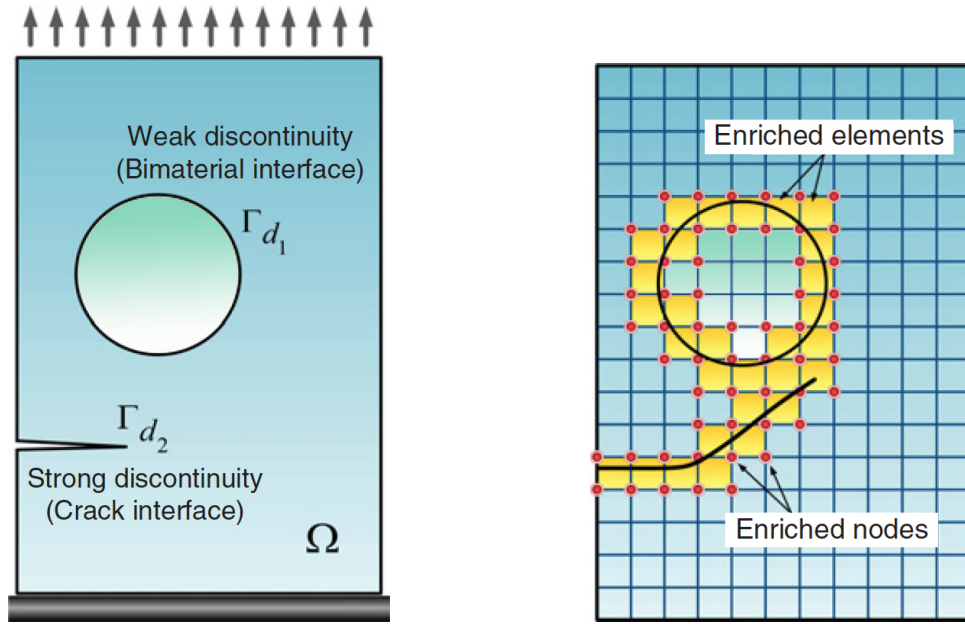
(a) Internal interfaces definition for the discontinuities.

(b) Uniform mesh with enriched nodes (with additional DOF) and enriched elements highlighted.

Fig. 3.2 Enriched-FEM technique to model weak and strong discontinuities. (Source: *Extended Finite Element Method: theory and applications* (p. 38) by A. R. Khoei, 2015, John Wiley & Sons. [Copyright (2015) by title of publisher]. Used with permission.)

enriched elements [9]. The approximation for a single interface Γ_d can be written as

$$\boldsymbol{u}(\boldsymbol{x}) = \sum_{i=1}^{\mathscr{N}} N_i(\boldsymbol{x})\bar{\boldsymbol{u}}_i + \sum_{j=1}^{\mathscr{M}} \bar{N}_j(\boldsymbol{x})\psi(\boldsymbol{x})\bar{\boldsymbol{a}}_j \tag{3.6}$$

where the enriched component $\bar{N}_j(\boldsymbol{x})$ shape functions are selected similar to the FE shape functions $N_i(\boldsymbol{x})$. In this equation, $psi(\boldsymbol{x})$ is the enrichment function, $N(\boldsymbol{x})$ is the standard shape function, $\bar{\boldsymbol{u}}_i$ is the standard nodal displacement, and $\bar{\boldsymbol{a}}_j$ is the nodal DOF corresponding to the enrichment function. $\mathscr{N}$ is the set of all nodal points of the domain in Eq. (3.6), and $\mathscr{M}$ is the set of all the elements nodes on the discontinuity Γ_d. The PUM and the *enrichment of displacement field* are two methods that are simultaneously used in the XFEM to treat elements containing discontinuities. PUM is employed to improve the approximation, including the enrichment functions to the standard approximation. By adding discontinuous fields using a PUM, the displacement field enrichment is used to correct the conventional

displacement-based approximation. As an application of the PU principle, it must be highlighted that the enrichment differs from node to node and that many do not need enrichment [9]. The variety of problem types in XFEM require the identification of suitable enrichment functions. The enrichment function can be defined using a variety of methods; these methods depend on the type of discontinuity and how it affects the solution form. These approaches are based on several mathematical functions, including the signed distance function, level set function, branch function, Heaviside jump function, and others [9]. The problem conditions affect the choice of enrichment functions in displacement approximation. The level set function can be suggested as an enrichment function if the discontinuity results from various kinds of material properties (Figure 3.3a); however, the Heaviside function is appropriate if the discontinuity is caused by different displacement fields on each side of the discontinuity (Figure 3.3b). The *Heaviside step function* is well suited for crack

(a) Weak discontinuity mod-
elling.

(b) Strong discontinuity mod-
elling.
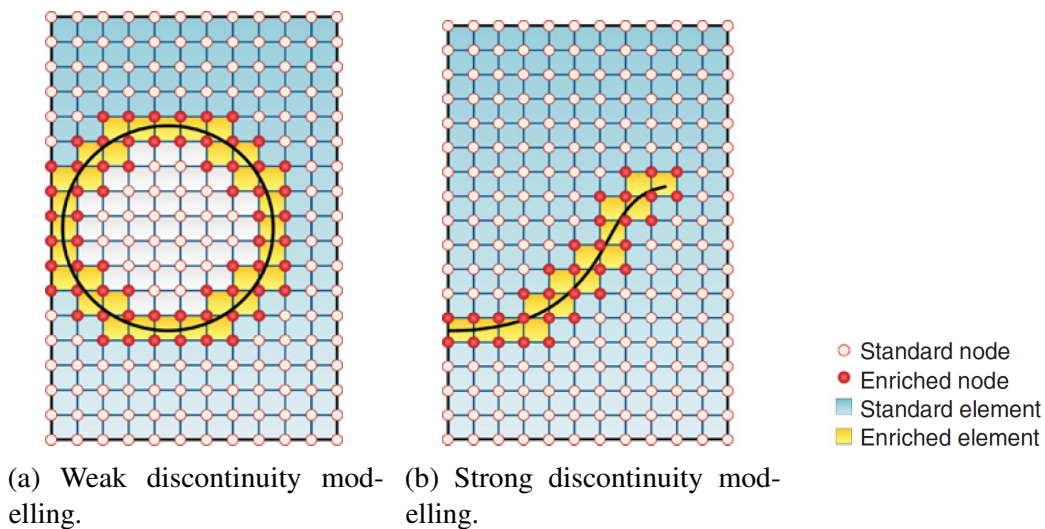
Fig. 3.3 XFEM discontinuity modelling. (Source: *Extended Finite Element Method: theory and applications* (p. 39) by A. R. Khoei, 2015, John Wiley & Sons. [Copyright (2015) by title of publisher]. Used with permission.)

problems discontinuous across the crack line [33]. The crack tip singularity can be modelled in linear fracture mechanics by means of *branch functions* that extend the near tip asymptotic solution for a crack tip [33]. The interface motion can be tracked by means of the *level set method*, where the interface is described as a zero level set of a function of one higher dimension [130]. This technique for predicting boundary geometry stands out as a viable choice for inhomogeneous fields, and

it finds significant effectiveness in enriching the domains where the strain field is discontinuous [9].

3.5   Heaviside Step Function

The term *strong discontinuity* refers to a jump in the displacement field that is frequently seen in fracture problems. When the displacement fields on the two sides of a fracture are completely different from one another, there is a discontinuity in the displacement. In such instances, the Heaviside function can be used to characterise the kinematics of the strong discontinuity [9]. Commonly, there are two ways to define the Heaviside function, one as

$$H(\boldsymbol{x}) = \varphi(\boldsymbol{x}) = \begin{cases} 1 & if \; \varphi(\boldsymbol{x}) > 0 \\ 0 & if \; \varphi(\boldsymbol{x}) < 0 \end{cases} \tag{3.7}$$

and the other as

$$H(\boldsymbol{x}) = \varphi(\boldsymbol{x}) = \begin{cases} 1 & if \; \varphi(\boldsymbol{x}) > 0 \\ -1 & if \; \varphi(\boldsymbol{x}) < 0 \end{cases} \tag{3.8}$$

where $\varphi(\boldsymbol{x})$ is the signed distance function, defined as

$$\varphi(\boldsymbol{x}) = \|\boldsymbol{x} - \boldsymbol{x}^*\| sign(\boldsymbol{n}_{\Gamma_d}(\boldsymbol{x} - \boldsymbol{x}^*)) \tag{3.9}$$

in which (as shown in Figure 3.4) $\boldsymbol{x}^*$ is the projection of $\boldsymbol{x}$ onto the discontinuity Γ_d, $\boldsymbol{n}_{\Gamma_d}$ is the normal to the interface at point $\boldsymbol{x}^*$, and $\| \quad \|$ denotes the Euclidean norm. The definition in Eq. (3.7) is known as the original Heaviside *step function*, while the one in Eq. (3.8) is known as the Heaviside *sign function*. Heaviside enrichment function is discontinuous at the interface. It ought to be noted that smoothed functions could be required to prevent numerical problems such instabilities in the numerical solution. This aspect will be discussed more in detail in Section 3.7. Moreover, the proposed numerical implementation of the equivalent polynomials method presented by Ventura [22, 27] in the case of domains containing a single discontinuity, and the proposed formulation to overcome numerical problems in quadrangular domains containing double discontinuities will be presented in Chapters 4 and 5. Using the
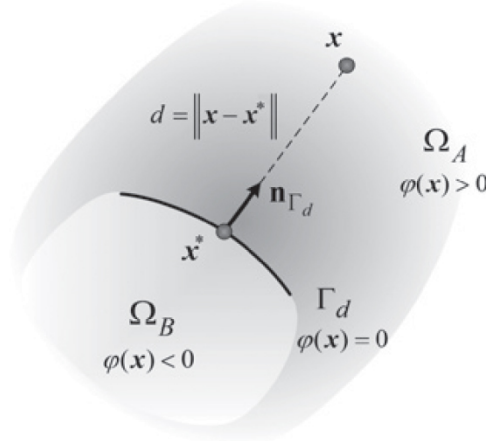
Fig. 3.4 Signed distance function definition. (Source: *Extended Finite Element Method: theory and applications* (p. 40) by A. R. Khoei, 2015, John Wiley & Sons. [Copyright (2015) by title of publisher]. Used with permission.)

Heaviside function $H(\boldsymbol{x})$ as enrichment function, Eq. (3.6) becomes

$$\boldsymbol{u}(\boldsymbol{x}) = \sum_{i=1}^{\mathcal{N}} N_i(\boldsymbol{x})\bar{\boldsymbol{u}}_i + \sum_{j=1}^{\mathcal{M}} \bar{N}_j(\boldsymbol{x})H(\boldsymbol{x})\bar{\boldsymbol{a}}_j \tag{3.10}$$

The consequences of Heaviside enrichment function in the approximation field (Eq. (3.10)) are illustrated in Figure 3.5 in the context of a monodimensional body embedding a strong discontinuity at point x_c. In Figure 3.5 a monodimensional body (i.e. a bar) containing a strong discontinuity at an arbitrary location x_c between nodes 2 and 3 is considered. The shape function for each finite element are defined referring to a monodimensional two-nodes *parent element* in a *parent coordinate system* (ξ) as

$$\begin{cases} N_i(\xi) &= (1-\xi) \\ N_f(\xi) &= \xi \end{cases} \tag{3.11}$$

where i is the starting node of the parent element and f is its end node. The correspondence between the parent coordinate system (ξ) and the global coordinate system (x) is definied by means of *isoparametric mapping* [9]. In the middle (enriched) element it is $\varphi(x_c) = 0$. The Heaviside definition in Eq. (3.8) is considered in order to enrich nodes 2 and 3, thus it will be

$$\begin{cases} H(\varphi(x_2)) &= -1 \\ H(\varphi(x_3)) &= 1 \end{cases} \tag{3.12}$$
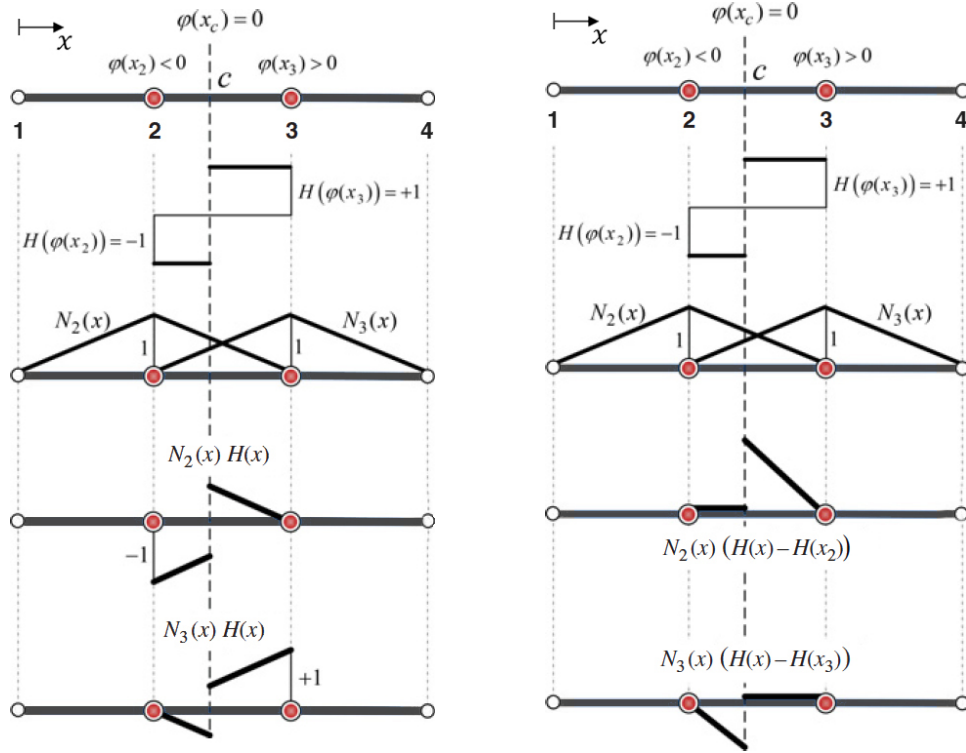
(a) Enrichment without *shifting $N_j(x)H(x)$*. (b) Enrichment with *shifting $N_j(x)(H(x) - H(x_j))$*.

Fig. 3.5 XFEM enrichment applied on a monodimensional body containing a strong discontinuity at point x_c. Enriched nodes are in red.

The enriched Heaviside shape functions $N_j(x)H(x)$ are shown in Figure 3.5a for nodes 2 and 3. The displacement value at an enriched node k can be deducted from Eq. (3.10) as

$$u(x_k) = \bar{u}_k + H(\varphi(x_k))\bar{a}_k \tag{3.13}$$

As $H(\varphi(x_k))$ is not zero by definition, Eq. (3.13) is not equal to the real nodal value $\bar{u}_k$ [9]. The enriched displacement field in Eq. (3.10) can be revised as

$$\boldsymbol{u}(\boldsymbol{x}) = \sum_{i=1}^{\mathcal{N}} N_i(\boldsymbol{x})\bar{\boldsymbol{u}}_i + \sum_{j=1}^{\mathcal{M}} \bar{N}_j(\boldsymbol{x})(H(\boldsymbol{x}) - H(\boldsymbol{x}_j))\bar{\boldsymbol{a}}_j \tag{3.14}$$

in which the term $H(\boldsymbol{x}) - H(\boldsymbol{x}_j)$ in Eq. (3.14) guarantees the expected $u(x_k) = \bar{u}_k$. The approximation in Eq. (3.14) is known as *shifting* [33] and the enriched field of the shifted Heaviside function $N_j(x)(H(x) - H(x_j))$ are shown in Fig. 3.5b for

nodes 2 and 3 [9]. Clearly, a jump in the displacement field arises when using the Heaviside enrichment function.

3.6   XFEM Governing Equation Discretisation

In order to obtain the XFEM formulation for a continuum body embedding a discontinuity, let us consider a body $\Omega = \Omega_A + \Omega_B$ containing an internal discontinuous boundary Γ_d (Figure 3.6). The static equilibrium equation for the body in Figure 3.6
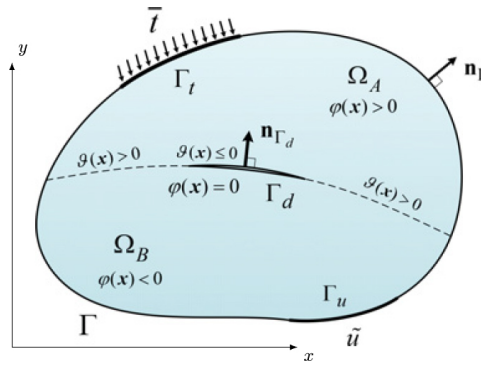
Fig. 3.6 A body $\Omega = \Omega_A + \Omega_B$ containing an internal discontinuous boundary Γ_d. (Source: *Extended Finite Element Method: theory and applications* (p. 40) by A. R. Khoei, 2015, John Wiley & Sons. [Copyright (2015) by title of publisher]. Used with permission.)

is

$$\nabla \cdot \boldsymbol{\sigma} + \boldsymbol{b} = \boldsymbol{0} \quad in \quad \Omega \tag{3.15}$$

where ∇ indicates the gradient operator, $\boldsymbol{\sigma}$ is the Cauchy stress tensor and $\boldsymbol{b}$ is the body force vector [9]. Assuming that the material behaviour is linear-elastic, its constitutive relation can be written as

$$\boldsymbol{\sigma} = \boldsymbol{D}\boldsymbol{\varepsilon} \tag{3.16}$$

with $\boldsymbol{D}$ being the tangential constitutive matrix and $\boldsymbol{\varepsilon}$ being the strain tensor. The problem boundary conditions are

$$\begin{aligned}
\boldsymbol{\sigma} \cdot \boldsymbol{n}_\Gamma &= \bar{\boldsymbol{t}} & on & \quad \Gamma_t \\
\boldsymbol{u} &= \bar{\boldsymbol{u}} & on & \quad \Gamma_u \\
\boldsymbol{\sigma} \cdot \boldsymbol{n}_{\Gamma_d} &= \bar{\boldsymbol{t}}_d & on & \quad \Gamma_d
\end{aligned} \tag{3.17}$$

where $\bar{\boldsymbol{u}} = (\bar{\boldsymbol{u}}_x, \bar{\boldsymbol{u}}_y)^T$ is the prescribed displacement on the boundary Γ_u, $\bar{\boldsymbol{t}} = (\bar{\boldsymbol{t}}_x, \bar{\boldsymbol{t}}_y)^T$ is the prescribed traction vector on the boundary Γ_t, and $\boldsymbol{n}_\Gamma$ is the outward normal vector to the external boundary Γ. In the case of weak discontinuities $\bar{\boldsymbol{t}}_d$ indicates the transferred traction across the discontinuity Γ_d. In the case of strong discontinuities, the traction-free condition is $\boldsymbol{\sigma} \cdot \boldsymbol{n}_{\Gamma_d} = \boldsymbol{0}$. The *Galerkin discretisation method* is utilised to derive the weak form of equilibrium equation in Eq. (3.15), integrating the product of the equilibrium equation multipied by *admissible test function* over the domain [9]. The *trial function* $\boldsymbol{u}(\boldsymbol{x}, t)$ must satisfy the boundary conditions in Eq. (3.17) and be smooth enough to define the equations derivatives. Moreover, $\delta\boldsymbol{u}(\boldsymbol{x}, t)$ have the same properties of trial function, since it is defined in the same approximation space [9]. Let us define a continuous function $\boldsymbol{G}$. By means of the *Divergence theorem* the integral of $\boldsymbol{G}$ over the domain Ω can be set equal to the integration over the boundary Γ as

$$\int_\Omega \text{div}\boldsymbol{G}\,d\Omega = \int_\Gamma \boldsymbol{G} \cdot \boldsymbol{n}_\Gamma\,d\Gamma \tag{3.18}$$

In order to adapt Eq. (3.18) to discontinuous problems, let us consider the domain Ω as in Figure 3.6, which it is divided into two distinct parts Ω_A and Ω_B by the discontinuity Γ_d, so that

$$\int_\Omega \text{div}\boldsymbol{G}\,d\Omega = \int_{\Omega_A} \text{div}\boldsymbol{G}\,d\Omega + \int_{\Omega_B} \text{div}\boldsymbol{G}\,d\Omega \tag{3.19}$$

By applying the Divergence theorem on the two subdomains in Eq. (3.19) it is

$$\int_\Omega \text{div}\boldsymbol{G}\,d\Omega = \int_\Gamma \boldsymbol{G} \cdot \boldsymbol{n}_\Gamma\,d\Gamma - \int_{\Gamma_{d_A}} \boldsymbol{G} \cdot \boldsymbol{n}_{\Gamma_d}\,d\Gamma + \int_{\Gamma_{d_B}} \boldsymbol{G} \cdot \boldsymbol{n}_{\Gamma_d}\,d\Gamma \tag{3.20}$$

where the value of $\boldsymbol{G}$ over Γ_{d_A} and Γ_{d_B} can be denoted by $\boldsymbol{G}_A$ and $\boldsymbol{G}_B$. Moreover, defining as $[\boldsymbol{G}] = \boldsymbol{G}_A - \boldsymbol{G}_B$ Eq. (3.20) becomes

$$\int_\Omega \text{div}\boldsymbol{G}\,d\Omega = \int_\Gamma \boldsymbol{G} \cdot \boldsymbol{n}_\Gamma\,d\Gamma - \int_{\Gamma_d} [\boldsymbol{G}] \cdot \boldsymbol{n}_{\Gamma_d}\,d\Gamma \tag{3.21}$$

which is the Divergence theorem expression for discontinuous problems[9]. Multiplying Eq. (3.15) by $\boldsymbol{u}(\boldsymbol{x}, t)$ and integrating over the entire domain Ω it is

$$\int_\Omega \delta\boldsymbol{u}(\boldsymbol{x}, t)(\nabla \cdot \boldsymbol{\sigma} + \boldsymbol{b})\,d\Omega = 0 \tag{3.22}$$

By applying the expression of the Divergence theorem for discontinuous problems in Eq. (3.21), Eq. (3.22) becomes

$$\int_\Omega \nabla \delta \boldsymbol{u} : \boldsymbol{\sigma} \, \mathrm{d}\Omega + \int_{\Gamma_d} [\delta \boldsymbol{u} \cdot \boldsymbol{\sigma}] \boldsymbol{n}_{\Gamma_d} \, \mathrm{d}\Gamma - \int_{\Gamma_t} \delta \boldsymbol{u} \cdot \bar{\boldsymbol{t}} \, \mathrm{d}\Gamma - \int_\Omega \delta \boldsymbol{u} \cdot \boldsymbol{b} \, \mathrm{d}\Omega = 0 \qquad (3.23)$$

which can be generally simplified in the case of weak and strong discontinuities [9] as

$$\int_\Omega \nabla \delta \boldsymbol{u} : \boldsymbol{\sigma} \, \mathrm{d}\Omega - \int_{\Gamma_t} \delta \boldsymbol{u} \cdot \bar{\boldsymbol{t}} \, \mathrm{d}\Gamma - \int_\Omega \delta \boldsymbol{u} \cdot \boldsymbol{b} \, \mathrm{d}\Omega = 0 \qquad (3.24)$$

To discretise Eq. (3.24), the XFEM discretisation is applied using the approximation field described in Eq. (3.6). The displacement field of an enrichment element can be written as

$$\begin{aligned}
\boldsymbol{u}(\boldsymbol{x},t) &= \sum_{i=1}^{\mathscr{N}} N_i(\boldsymbol{x}) \bar{\boldsymbol{u}}_i + \sum_{j=1}^{\mathscr{M}} N_j(\boldsymbol{x}) (\psi(\boldsymbol{x}) - \psi(\boldsymbol{x}_j)) \bar{\boldsymbol{a}}_j \\
&\equiv \boldsymbol{N}^{std}(\boldsymbol{x}) \bar{\boldsymbol{u}} + \boldsymbol{N}^{enr}(\boldsymbol{x}) \bar{\boldsymbol{a}}
\end{aligned} \qquad (3.25)$$

where the shifted enrichment function $\psi((\boldsymbol{x}))$ and the notation $N_i^{std}(\boldsymbol{x}) \equiv N_i(\boldsymbol{x})$ and $N_j^{enr}(\boldsymbol{x}) \equiv N_j(\boldsymbol{x})(\psi(\boldsymbol{x}) - \psi(\boldsymbol{x}_j))$ have been used. It is possible to define the test function $\delta \boldsymbol{u}(\boldsymbol{x},t)$ as

$$\begin{aligned}
\delta \boldsymbol{u}(\boldsymbol{x},t) &= \sum_{i=1}^{\mathscr{N}} N_i(\boldsymbol{x}) \delta \bar{\boldsymbol{u}}_i + \sum_{j=1}^{\mathscr{M}} N_j(\boldsymbol{x}) (\psi(\boldsymbol{x}) - \psi(\boldsymbol{x}_j)) \delta \bar{\boldsymbol{a}}_j \\
&\equiv \boldsymbol{N}^{std}(\boldsymbol{x}) \delta \bar{\boldsymbol{u}} + \boldsymbol{N}^{enr}(\boldsymbol{x}) \delta \bar{\boldsymbol{a}}
\end{aligned} \qquad (3.26)$$

From Eq. (3.25) it is possible to define the strain vector $\boldsymbol{\varepsilon}(\boldsymbol{x},t)$ as

$$\begin{aligned}
\boldsymbol{\varepsilon}(\boldsymbol{x},t) &= \sum_{i=1}^{\mathscr{N}} \frac{\delta N_i(\boldsymbol{x})}{\delta \boldsymbol{x}} \bar{\boldsymbol{u}}_i \\
&\quad + \sum_{j=1}^{\mathscr{M}} \left[\frac{\delta N_j(\boldsymbol{x})}{\delta \boldsymbol{x}} (\psi(\boldsymbol{x}) - \psi(\boldsymbol{x}_j)) + N_j(\boldsymbol{x}) \frac{\delta}{\delta \boldsymbol{x}} (\psi(\boldsymbol{x}) - \psi(\boldsymbol{x}_j)) \right] \bar{\boldsymbol{a}}_j \\
&\equiv \boldsymbol{B}^{std}(\boldsymbol{x}) \bar{\boldsymbol{u}} + \boldsymbol{B}^{enr}(\boldsymbol{x}) \bar{\boldsymbol{a}}
\end{aligned} \qquad (3.27)$$

The strain field variation $\delta\boldsymbol{\varepsilon}(\boldsymbol{x},t)$ can be obtained as

$$
\begin{aligned}
\delta\boldsymbol{\varepsilon}(\boldsymbol{x},t) = {} & \sum_{i=1}^{\mathcal{N}} \frac{\delta N_i(\boldsymbol{x})}{\delta \boldsymbol{x}} \delta\bar{\boldsymbol{u}}_i \\
& + \sum_{j=1}^{\mathcal{M}} \left[\frac{\delta N_j(\boldsymbol{x})}{\delta \boldsymbol{x}} (\psi(\boldsymbol{x}) - \psi(\boldsymbol{x}_j)) + N_j(\boldsymbol{x}) \frac{\delta}{\delta \boldsymbol{x}} (\psi(\boldsymbol{x}) - \psi(\boldsymbol{x}_j)) \right] \delta\bar{\boldsymbol{a}}_j \\
\equiv {} & \boldsymbol{B}^{std}(\boldsymbol{x})\delta\bar{\boldsymbol{u}} + \boldsymbol{B}^{enr}(\boldsymbol{x})\delta\bar{\boldsymbol{a}}
\end{aligned} \tag{3.28}
$$

Substituting the test functions $\delta\boldsymbol{u}(\boldsymbol{x},t)$ and $\delta\boldsymbol{\varepsilon}(\boldsymbol{x},t)$ from eqs. (3.26) and (3.28) into Eq. (3.24) it is

$$
\begin{aligned}
& \int_{\Omega} (\boldsymbol{B}^{std}(\boldsymbol{x})\delta\bar{\boldsymbol{u}} + \boldsymbol{B}^{enr}(\boldsymbol{x})\delta\bar{\boldsymbol{a}})^T \boldsymbol{\sigma}\, d\Omega \\
& - \int_{\Gamma_t} (\boldsymbol{N}^{std}(\boldsymbol{x})\delta\bar{\boldsymbol{u}} + \boldsymbol{N}^{enr}(\boldsymbol{x})\delta\bar{\boldsymbol{a}})^T \bar{\boldsymbol{t}}\, d\Gamma \\
& - \int_{\Omega} (\boldsymbol{N}^{std}(\boldsymbol{x})\delta\bar{\boldsymbol{u}} + \boldsymbol{N}^{enr}(\boldsymbol{x})\delta\bar{\boldsymbol{a}})^T \boldsymbol{b}\, d\Omega = 0
\end{aligned} \tag{3.29}
$$

which can be rearranged as

$$
\begin{aligned}
& \delta\bar{\boldsymbol{u}}^T \left\{ \int_{\Omega} (\boldsymbol{B}^{std})^T \boldsymbol{\sigma}\, d\Omega - \int_{\Gamma_t} (\boldsymbol{N}^{std})^T \bar{\boldsymbol{t}}\, d\Gamma - \int_{\Omega} (\boldsymbol{N}^{std})^T \boldsymbol{b}\, d\Omega \right\} \\
& + \delta\bar{\boldsymbol{a}}^T \left\{ \int_{\Omega} (\boldsymbol{B}^{enr})^T \boldsymbol{\sigma}\, d\Omega - \int_{\Gamma_t} (\boldsymbol{N}^{enr})^T \bar{\boldsymbol{t}}\, d\Gamma - \int_{\Omega} (\boldsymbol{N}^{enr})^T \boldsymbol{b}\, d\Omega \right\} = 0
\end{aligned} \tag{3.30}
$$

Defining $\bar{\boldsymbol{U}}^T = [\bar{\boldsymbol{u}}^T, \bar{\boldsymbol{a}}^T]$ as the unknowns vector at the nodal points, from Eq. (3.30) it is possible to obtain the discrete system of XFEM equations as

$$
\boldsymbol{K}\bar{\boldsymbol{U}} - \boldsymbol{F} = \boldsymbol{0} \tag{3.31}
$$

where $\boldsymbol{K}$ is the total stiffness matrix and $\boldsymbol{F}$ is the external force vector [9]. The system of equations in Eq. (3.31) can be written as

$$
\begin{bmatrix} \boldsymbol{K}_{uu} & \boldsymbol{K}_{ua} \\ \boldsymbol{K}_{au} & \boldsymbol{K}_{aa} \end{bmatrix} \begin{Bmatrix} \bar{\boldsymbol{u}} \\ \bar{\boldsymbol{a}} \end{Bmatrix} = \begin{Bmatrix} \boldsymbol{F}_u \\ \boldsymbol{F}_a \end{Bmatrix} \tag{3.32}
$$

where

$$K = \begin{bmatrix} \int_{\Omega} (\boldsymbol{B}^{std})^T \boldsymbol{D} \boldsymbol{B}^{std} \, d\Omega & \int_{\Omega} (\boldsymbol{B}^{std})^T \boldsymbol{D} \boldsymbol{B}^{enr} \, d\Omega \\ \int_{\Omega} (\boldsymbol{B}^{enr})^T \boldsymbol{D} \boldsymbol{B}^{std} \, d\Omega & \int_{\Omega} (\boldsymbol{B}^{enr})^T \boldsymbol{D} \boldsymbol{B}^{enr} \, d\Omega \end{bmatrix} \tag{3.33}$$

and

$$\boldsymbol{F} = \left\{ \begin{array}{l} \int_{\Gamma_t} (\boldsymbol{N}^{std})^T \bar{\boldsymbol{t}} \, d\Gamma + \int_{\Omega} (\boldsymbol{N}^{std})^T \boldsymbol{b} \, d\Omega \\ \int_{\Gamma_t} (\boldsymbol{N}^{enr})^T \bar{\boldsymbol{t}} \, d\Gamma + \int_{\Omega} (\boldsymbol{N}^{enr})^T \boldsymbol{b} \, d\Omega \end{array} \right\} \tag{3.34}$$

3.7   Numerical Integration in XFEM

The Gauss quadrature rule can be effectively utilised to calculate the stiffness matrix integral in the conventional FEM since the standard shape functions are expressed in terms of polynomial order. The enriched shape functions in the XFEM, however, may be expressed in terms of non-polynomial order. Additionally, because an enriched element may have a weak or strong discontinuity, the enrichment functions over the element may not be smooth. Therefore, if the element is split by a discontinuity, the conventional Gauss quadrature rule cannot be applied, and essential changes are required for numerical integration over an enriched element [9]. The main strategy, based on the increased number of Gauss integration points, as shown in Figure 3.7a, may be proposed; nevertheless, this technique may cause a significant loss in accuracy. Two methods: the triangular/quadrilateral partitioning approach and the rectangular sub-grids method, are developed for the numerical integration of an enriched element in order to get around these problems. The element bisected by the interface is separated into triangle and quadrilateral sub-elements using the triangular/quadrilateral partitioning technique, as illustrated in Figure 2.14b, and the Gauss integration rule is applied to each sub-polygon. This decomposition does not introduce any new unknowns or require the sub-polygons to be compliant. The zero level set is defined by $\varphi(\boldsymbol{x}) = \sum_{i=1}^{\mathcal{N}} N_i(\boldsymbol{x}) \varphi_i = 0$ because the interface is often specified by a discretised level set function that is interpolated by the common FE shape functions. The interface, which is $\varphi(\boldsymbol{x})$ zero-level, is often curved and is defined by finding the roots in the reference element and projecting those points onto the geometry of the real element [9]. In actuality, only linear interpolants with 3-noded triangular elements have an interface that is planar within the elements. For

(a) Standard Gauss integration points.

(b) Triangular/quadrilateral partitioning method.

(c) Rectangular sub-grids method.
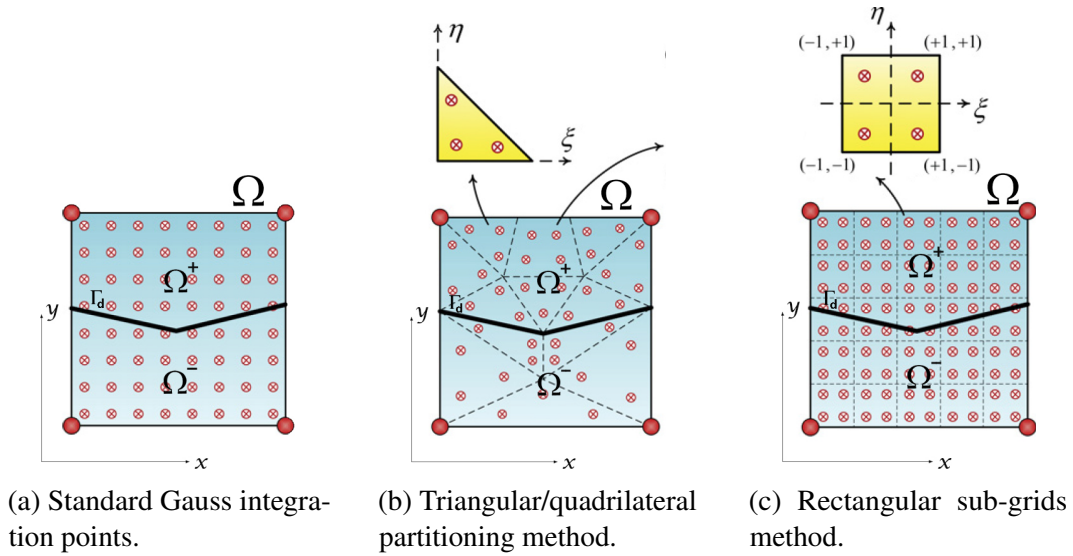
Fig. 3.7 Numerical integration of enriched XFEM element. (Source: *Extended Finite Element Method: theory and applications* (p. 58) by A. R. Khoei, 2015, John Wiley & Sons. [Copyright (2015) by title of publisher]. Used with permission.)

quadrilateral elements, it is acceptable to substitute a straight line for the curved interface based on where the interface intersects the edges of the element. Because they represent a constraint in this situation, it is challenging to design the precise interpolation functions of $\varphi(\boldsymbol{x})$ [9]. Since the interface is therefore always piecewise straight and triangular sub-elements for integration purposes are easily obtained, it is frequently preferred to breakdown the cut quadrilateral reference elements into sub-triangles and utilise linear interpolation in each sub-triangle. But when a level set function is used to discretise a curved interface that cuts through an element with linear shape functions, the level set function is unable to accurately capture the curvature of the interface. To expand the number of sub-polygons and preserve the accuracy of the integration in such a situation, additional points can be added along the interface [9]. Let us consider a body $\mathscr{B}$ defined in a *global coordinate system* ($\boldsymbol{x}$). Let us assume that $\mathscr{B}$ is discretised by means of *isoparametric elements* and let us consider an element Ω of its mesh. To compute the Ω stiffness matrix in Eq. (3.33) it is convenient to refer to a *parent coordinate system* ($\boldsymbol{\xi}$) in which *parent element* $\mathscr{P}$ is defined and a correspondence between the global coordinate system and the parent coordinate system is ensured by means of *isoparametric mapping* such as

$$\boldsymbol{x} = \sum_{i=1}^{\mathcal{N}} N_i(\boldsymbol{\xi})\boldsymbol{x}_i \tag{3.35}$$

where $\mathcal{N}$ is the number of nodes of the isoparametric element. Since the derivatives of both standard and enriched shape functions ($\boldsymbol{B}^{std}$ and $\boldsymbol{B}^{enr}$ respectively) are defined in the global coordinate system, a relation between the derivatives in the global and parent coordinate system have to be defined. This can be accomplished by means of Jacobian matrix $\boldsymbol{J}$ for the mapping function in Eq. (3.35) as

$$\frac{\delta N}{\delta \boldsymbol{\xi}} = \boldsymbol{J} \frac{\delta N}{\delta \boldsymbol{x}} = \frac{\delta \boldsymbol{x}}{\delta \boldsymbol{\xi}} \frac{\delta N}{\delta \boldsymbol{x}} \tag{3.36}$$

Finally, from eqs. (3.35) and (3.36), the total stiffness matrix in Eq. (3.33) is

$$\boldsymbol{K}_{ij(\boldsymbol{x})}^{\alpha\beta} = \int_{\Omega} \left(\boldsymbol{B}_{i(\boldsymbol{x})}^{\alpha} \right)^{T} \boldsymbol{D} \boldsymbol{B}_{j(\boldsymbol{x})}^{\beta} \, \mathrm{d}\Omega = \int_{\mathscr{P}} \left(\boldsymbol{B}_{i(\boldsymbol{\xi})}^{\alpha} \right)^{T} \boldsymbol{D} \boldsymbol{B}_{j(\boldsymbol{\xi})}^{\beta} \det \boldsymbol{J} \, \mathrm{d}\mathscr{P} \tag{3.37}$$

Let us suppose that Ω split in two parts, Ω^{+} and Ω^{-}, by a discontinuity Γ_d as shown in Figure 3.7. The numerical integration of the stiffness matrix in Eq. (3.37) can be performed decomposing the domains into quadrilateral and triangles (Figure 3.7b), in order to employ the Gauss quadrature rule over each sub-element as

$$\begin{aligned}
\boldsymbol{K}_{ij(\boldsymbol{x})}^{\alpha\beta} = & \sum_{l=1}^{\mathscr{N}_{sub}^{+}} \left(\sum_{k=1}^{\mathscr{N}_{GP}^{+}} \left(\boldsymbol{B}_{i(\boldsymbol{\xi})}^{\alpha} \right)^{T} \boldsymbol{D} \boldsymbol{B}_{j(\boldsymbol{\xi})}^{\beta} w_k \right)_{l} \\
& + \sum_{l=1}^{\mathscr{N}_{sub}^{-}} \left(\sum_{k=1}^{\mathscr{N}_{GP}^{-}} \left(\boldsymbol{B}_{i(\boldsymbol{\xi})}^{\alpha} \right)^{T} \boldsymbol{D} \boldsymbol{B}_{j(\boldsymbol{\xi})}^{\beta} w_k \right)_{l}
\end{aligned} \tag{3.38}$$

where $\mathscr{N}_{sub}^{+}$ and $\mathscr{N}_{sub}^{-}$ are the sub-polygons number in Ω_{+} and Ω_{-} respectively, $\mathscr{N}_{GP}^{+}$ and $\mathscr{N}_{GP}^{-}$ are the Gauss points for each sub-polygon in Ω_{+} and Ω_{-} respectively, and w_k is the quadrature point weight. Although the integration of polynomials (up to a certain order) is mathematically exact for the triangular sub-elements, this property cannot be always guaranteed for quadrilaterals sub-elements. In fact, distorted quadrilateral sub-elements may arise when the element partitioning is performed (Figure 3.7b), which may lead to a loss of precision in the integral computation, therefore the exact integration property can be lost [131, 132, 9]. An alternative method is dividing the element by the interface into rectangular sub-grids, illustrated in Figure 3.7c. In this method, it is not required to conform the sub-quadrilaterals to the interface geometry, but there must be enough subdivisions to lessen the numerical integration error. The natural coordinates of the Gauss quadrature points are independent at each sub-quadrilateral based on the rectangular sub-grids integration.

An exact solution may be obtained by increasing the number of sub-quadrilaterals. It should be noted that since the interface does not correspond with the rectangular edges, it may create some approximation in the numerical simulation [133, 134, 9]. Both methods have benefits and weaknesses, but they are both very accurate and often employed in the extended FE framework. Since the domain is divided into smooth sub-domains in the triangular-partitioning approach, the integration might be considerably more precise; nevertheless, developing partitioning for different interface configurations would be extremely laborious. Additionally, the likelihood of updating the interface as a result of its temporal development, particularly owing to crack propagation, may result in the position of the Gauss points changing throughout the solution, necessitating transferring information between the old and new Gauss points. Contrarily, the rectangular sub-grids technique does not need to transfer information since the sub-grids are independent of the interface configuration. Rectangular sub-grid integration is obviously more simpler to construct than the triangle partitioning approach, but accuracy cannot be guaranteed in those sub-grids that are divided by the interface. The finer sub-grids may often be used to limit such events in order to eliminate the inaccuracies associated with this strategy. Practical observations show that the rectangular sub-grids system produces a sufficient level of precision [134, 9]. Another numerical integration method to be mentioned is adaptive quadrature. It is a numerical technique that dynamically adjusts the integration mesh based on local error estimations. It aims to improve the accuracy of numerical integration by refining the mesh in regions where the integrand exhibits significant variations or irregularities. This adaptive refinement process allows for a more efficient allocation of computational resources. Adaptive quadrature in the context of XFEM has been discussed by various Authors [8, 7, 135], highlighting its importance for accurately integrating singular terms arising from cracks, improving the accuracy and efficiency of the numerical integration process. However, it is worth noting that adaptive quadrature, like any numerical method, does have certain limitations and challenges. Some potential disadvantages of adaptive quadrature in XFEM may include:

- Computational Cost: Adaptive quadrature requires additional computational effort compared to fixed or uniform quadrature schemes. The adaptive refinement process involves dynamically adjusting the integration mesh based on error estimations, which can increase the computational overhead.

- Implementation Complexity: Implementing adaptive quadrature algorithms can be more complex compared to simpler integration techniques. Developing efficient error estimation strategies and managing the refinement process may require advanced programming and algorithmic considerations.

- Mesh Sensitivity: Adaptive quadrature relies on accurately identifying regions that require refinement based on error estimations. In some cases, the algorithm may struggle to effectively capture localised irregularities or rapidly varying integrands, leading to potential inaccuracies.

Although a high precision in the numerical integration result can be met when using those techniques to integrate the expression in Eq. (3.37), an exact numerical integration is not always guaranteed, or it comes at a highly computational cost. To overcome these issues, a solution that allow to integrate exactly Eq. (3.37) without partitioning the integration domain has been proposed by Ventura [22, 27] by means of equivalent polynomials and will be discussed in detail in Chapter 4. A practical application of this formulation has been carried out in the course of this PhD: a software library, *EQP library* that allows to integrate exactly various 2D/3D FE domains containing an arbitrary discontinuity, that will be also presented in Chapter 4.

3.8   Conclusions

This Chapter has provided a comprehensive exploration of the XFEM approximation and the numerical integration techniques in the context of the XFEM. Several integration methods have been discussed and their advantages and disadvantages have been examined. Various integration methods, such as the Gaussian quadrature, composite quadrature, and adaptive quadrature, offer distinct benefits and limitations. The Gaussian quadrature method demonstrated excellent accuracy and efficiency for problems with smooth integrands and simple geometries. On the other hand, composite quadrature methods showed better performance for complex geometries by dividing the domain into smaller subdomains and applying numerical integration techniques separately within each subdomain. Additionally, adaptive quadrature methods exhibited the ability to adaptively refine the integration mesh based on local error estimations, resulting in improved accuracy while minimising computational

cost. However, the adaptive quadrature methods may be more computationally demanding and complex to implement compared to other techniques. Moreover, a numerical integration technique based on equivalent polynomials that overcomes some of the limits of these methods has been introduced and will be extensively discussed in Chapter 4, together with its software implementation, specifically tailored for XFEM applications to achieve improved accuracy and efficiency and to provide a foundation for future developments in this field. Overall, the choice of numerical integration method in XFEM should be carefully considered based on the specific characteristics of the problem, such as geometry complexity, smoothness of integrands, and desired precision.

Chapter 4

Integration of XFEM Elements Containing a Single Discontinuity[1]

4.1 Introduction

The representation of discontinuities in the displacement or strain fields in conventional finite-element studies necessitates mesh boundary alignment to the discontinuity line or surface. Fracture problems or material interfaces, where the element boundaries line up with the boundaries of the materials, are common examples where the mesh is regenerated as the crack develops [22]. As seen in Chapter 3, the numerical integration of the stiffness matrix in the elements crossed by a discontinuity leads to well-known issues. Gauss quadrature implicitly adds a polynomial approximation of the integrand function, making it impossible to apply it to elements with non-differentiable or discontinuous functions since significant errors occur. This is frequently resolved using the techniques discussed in Section 3.7, (i.e., by dividing the elements into quadrature subcells with continuous and differentiable integrands). In order to implement those methods, automated mesh generators or tailored domain subdivision techniques usually have to be implemented to correctly split the element domain into quadrature subcells. Although the quadrature subcells generation neither adds new nodal variables nor changes XFEM approximation qualities, it somehow creates a "mesh" requirement that compromises the formal

---

[1]Part of the work described in this Chapter has been previously published in: G. Mariggiò, S. Fichera, M. Corrado, G. Ventura. EQP - A 2D/3D library for integration of polynomials times step function. SoftwareX 12:100636 (2020).

beauty of the local PU method [22]. In this Chapter, the problem of discontinuous or non-differentiable function quadrature in enriched elements is investigated and the methodology proposed by Ventura [22, 27] to avoid the quadrature subcell generation is explored. The method is based on the investigation of the element stiffness integrand. Let the level set function be the signed distance from the discontinuity surface. It is shown that an *equivalent polynomial function*, whose integral reveals the precise values of the discontinuous/non-differentiable function integrated on subcells, exists based on the nodal values of the level set. Since the polynomial is specified over the whole element domain, Gauss quadrature can be used to easily integrate it without the need to create any quadrature subdomains. In this case, the polynomial is supplied in closed form and takes the role of the enrichment function in the element stiffness evaluation [22]. In this context, a software library (*EQP Library*) to integrate various 2D and 3D FE domains containing an arbitrary linear discontinuity has been developed as part of the research work in this PhD Thesis and it is presented in Section 4.4. Its functionalities, precision and easiness of implementation are reported and some practical example are carried out to demonstrate its effectiveness in solving numerical integration problems on domains embedding discontinuities. This Chapter is structured as follows. In Section 4.2 the problem of the integration of polynomials times Heaviside step function is presented. The formulation proposed in [22, 27] by means of equivalent polynomials is introduced in Section 4.3, with proper mathematical demonstrations for each analysed domain shape. Finally the software library implementation for this formulation is presented in Section 4.4, along with some numerical examples to prove its effectiveness.

4.2   Problem definition

Let us consider a body $\mathscr{B}$, let $\delta\mathscr{B}$ be its boundary, and let $\boldsymbol{u}$ be the displacement field. Let us define the boundary partition $\delta\mathscr{B}_u$ where the displacements are prescribed, so that $\boldsymbol{u} = \bar{\boldsymbol{u}}$, and the partition $\delta\mathscr{B}_q$ where the traction $\boldsymbol{q}$ is given, so that $\delta\mathscr{B}_u \cap \delta\mathscr{B}_q = \emptyset$ [22]. The local PU approximation for the displacement field defined in Eq. (3.6) thus becomes

$$\boldsymbol{u}(\boldsymbol{x}) = \sum_{i=1}^{\mathscr{N}} N_i(\boldsymbol{x})(\boldsymbol{u}_i + \boldsymbol{a}_i \psi(\boldsymbol{x})) \qquad (4.1)$$

in which $\mathscr{N}$ are the FE mesh nodes, N_i are the FE shape functions and $\boldsymbol{u}_i$ and $\boldsymbol{a}_i$ are to be determined by means of the application of a variational principle or weak form to the discrete displacement field in Eq. (4.1), as discussed in Section 3.6. Supposing that Γ is a discontinuity surface and $d(\boldsymbol{x})$ is the signed distance from Γ to a point $\boldsymbol{x}$, a discontinuity in the displacement field generated from a crack can be described assuming the Heaviside step function $H(\boldsymbol{x})$ as the enrichment function $\psi(\boldsymbol{x})$ (see eqs. (3.7) and (3.8)) [33].

Typically, the enrichment component is only applied to the nodes of the elements that are affected by the discontinuity, leading to the term *enriched elements* for them. Thus, at nodes of non-enriched elements, the coefficients $\boldsymbol{a}_i$ are not present. Using traditional Gauss quadrature to obtain the element stiffness matrix is inappropriate when the elements enriched through Eq. (4.1) contain the enrichment function $H(\boldsymbol{x})$ [22]. The common method is to divide the element domain into quadrature subdomains following the discontinuity surface path, as extensively described in Section 3.7. Let us analyse an enriched element Ω of the discretisation of body $\mathscr{B}$. Considering $H(\boldsymbol{x})$ its enrichment function, from Eq. (3.33) its stiffness matrix $\boldsymbol{K}$ can be written as

$$
\boldsymbol{K} = \int_{\Omega} \begin{bmatrix} \left(\boldsymbol{B}^{std}\right)^T \boldsymbol{E}\boldsymbol{B}^{std} & H\left(\boldsymbol{B}^{std}\right)^T \boldsymbol{E}\boldsymbol{B}^{std} \\ H\left(\boldsymbol{B}^{std}\right)^T \boldsymbol{E}\boldsymbol{B}^{std} & H^2\left(\boldsymbol{B}^{std}\right)^T \boldsymbol{E}\boldsymbol{B}^{std} \end{bmatrix} d\Omega \tag{4.2}
$$

where $\left(\boldsymbol{B}^{std}\right)^T \boldsymbol{E}\boldsymbol{B}^{std}$ and $H^2\left(\boldsymbol{B}^{std}\right)^T \boldsymbol{E}\boldsymbol{B}^{std}$ are continuous and differentiable functions (since $H^2 = 1$ in Ω), and $H\left(\boldsymbol{B}^{std}\right)^T \boldsymbol{E}\boldsymbol{B}^{std}$ are piecewise continuous and differentiable functions [22]. As a consequence, only the off-diagonal part of matrix $\boldsymbol{K}$ in Eq. (4.2), $H\left(\boldsymbol{B}^{std}\right)^T \boldsymbol{E}\boldsymbol{B}^{std}$, cannot be integrated using standard Gauss quadrature over the entire domain Ω, that has to be split along the discontinuity surface Γ into two subdomains, Ω^+ and Ω^- so that

$$
\int_{\Omega} H\left(\boldsymbol{B}^{std}\right)^T \boldsymbol{E}\boldsymbol{B}^{std} d\Omega = \int_{\Omega^-} H\left(\boldsymbol{B}^{std}\right)^T \boldsymbol{E}\boldsymbol{B}^{std} d\Omega
$$
$$
+ \int_{\Omega^+} H\left(\boldsymbol{B}^{std}\right)^T \boldsymbol{E}\boldsymbol{B}^{std} d\Omega \tag{4.3}
$$

The solution proposed by Ventura [22] consists on substituting the two integrals over Ω^- and Ω^+ at the right-hand side of Eq. (4.3) with one defined on Ω that yields the same numerical result. To achieve this, let $\tilde{H}$ be a polynomial defined by the formal

relation

$$\int_{\Omega} \tilde{H} \left(\boldsymbol{B}^{std} \right)^{T} \boldsymbol{E} \boldsymbol{B}^{std} \, \mathrm{d}\Omega = \int_{\Omega^{-}} H \left(\boldsymbol{B}^{std} \right)^{T} \boldsymbol{E} \boldsymbol{B}^{std} \, \mathrm{d}\Omega$$
$$+ \int_{\Omega^{+}} H \left(\boldsymbol{B}^{std} \right)^{T} \boldsymbol{E} \boldsymbol{B}^{std} \, \mathrm{d}\Omega \tag{4.4}$$

If the aforesaid polynomial $\tilde{H}$ exits, it is

$$\boldsymbol{K} = \int_{\Omega} \begin{bmatrix} \left(\boldsymbol{B}^{std} \right)^{T} \boldsymbol{E} \boldsymbol{B}^{std} & \tilde{H} \left(\boldsymbol{B}^{std} \right)^{T} \boldsymbol{E} \boldsymbol{B}^{std} \\ \tilde{H} \left(\boldsymbol{B}^{std} \right)^{T} \boldsymbol{E} \boldsymbol{B}^{std} & H^{2} \left(\boldsymbol{B}^{std} \right)^{T} \boldsymbol{E} \boldsymbol{B}^{std} \end{bmatrix} \, \mathrm{d}\Omega \tag{4.5}$$

such that the integration may be carried out using standard Gauss quadrature on the whole element domain Ω [22]. A closed form solution for the case of a straight line discontinuity (for 2D integration domains) and a plane surface discontinuity (for 3D integration domains) is discussed in Section 4.3.

4.3   Closed form solution for 2D/3D integration domains

In this Section, the closed form solution [22] for the problem defined in Section 4.2 are analysed for the case of 2D integration domains crossed by a straight discontinuity line and for 3D integration domains crossed by a plane discontinuity surface, as a fundamental part in the *EQP Library* implementation.

4.3.1   2D case

The two-dimensional case depends on the element type and the point at which the discontinuity surface intersects it. The closed form solution [22] is analysed for the three-node triangle and the four-node quadrilateral elements. Since isoparametric mapping may be used in the general situation, all calculations are done in the parent reference system (ξ, η). The discontinuity surface Γ is assumed as a line intersecting the element at points $\boldsymbol{P}_1 = (\xi_1, \eta_1)$ and $\boldsymbol{P}_2 = (\xi_2, \eta_2)$, that can be easily determined

by means of level set data, since the signed distance from each node of the element to the discontinuity is known.

Linear triangular element

Let us consider a three-node triangular parent element, as in Figure 4.1a and let us suppose it is intersected by a discontinuity surface Γ at points $\boldsymbol{P}_1 = (\xi_1, \eta_1)$ and $\boldsymbol{P}_2 = (\xi_2, \eta_2)$ (Figure 4.1b). Its shape functions are
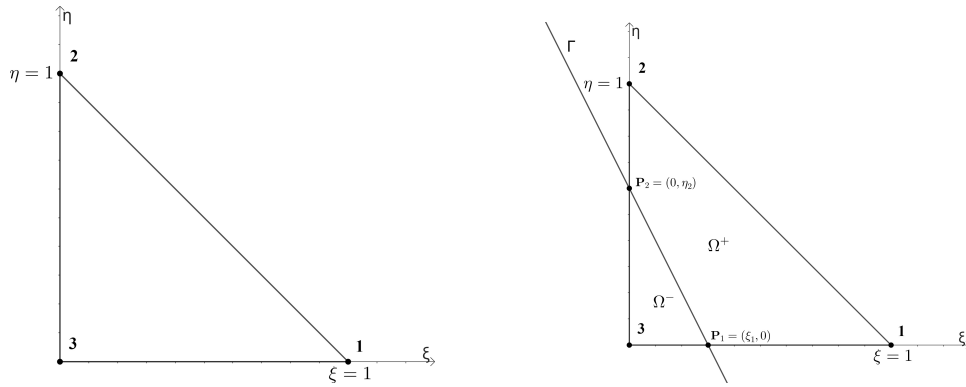
(a) Triangular FE in the parent domain.   (b) Triangular FE in the parent domain intersected by a discontinuity Γ.

Fig. 4.1 Triangular FE in the parent domain and its intersection with a discontinuity Γ.

$$N_1(\xi, \eta) = \xi \tag{4.6a}$$

$$N_2(\xi, \eta) = \eta \tag{4.6b}$$

$$N_3(\xi, \eta) = 1 - \xi - \eta \tag{4.6c}$$

so that, from the evaluation of $\left(\boldsymbol{B}^{std}\right)^T \boldsymbol{E} \boldsymbol{B}^{std}$, each component is a constant [22]. Thus, only one independent equation may be derived from Eq. (4.4) in scalar form (all the equations are linearly dependent). Since $\tilde{H}$ is considered to be a zero degree polynomial, its value can be found by applying the specific form of Eq. (4.4) to the current scenario

$$\int_{\Omega} \tilde{H} \, d\Omega = \int_{\Omega^-} H \, d\Omega + \int_{\Omega^+} H \, d\Omega \tag{4.7}$$

Considering $H > 0$ in Ω^+, Eq. (4.7) becomes

$$\int_\Omega \tilde{H}\,d\Omega = \int_{\Omega^-}(-1)\,d\Omega + \int_{\Omega^+}(+1)\,d\Omega \tag{4.8}$$

thus $\tilde{H}$ is

$$\tilde{H} = 2\xi_1\eta_2 - 1 \tag{4.9}$$

and the element stiffness matrix $\boldsymbol{K}$ can be evaluated from Eq. (4.2).

Bilinear quadrilateral element

Let us analyse a quadrilateral element defined in the parent reference system (ξ, η), as shown in Figure 4.2 and let us suppose it is intersected by a discontinuity surface Γ at points $\boldsymbol{P}_1 = (\xi_1, \eta_1)$ and $\boldsymbol{P}_2 = (\xi_2, \eta_2)$. The two possible scenarios are shown in Figure 4.2a and Figure 4.2b. The shape functions for the bilinear quadrilateral
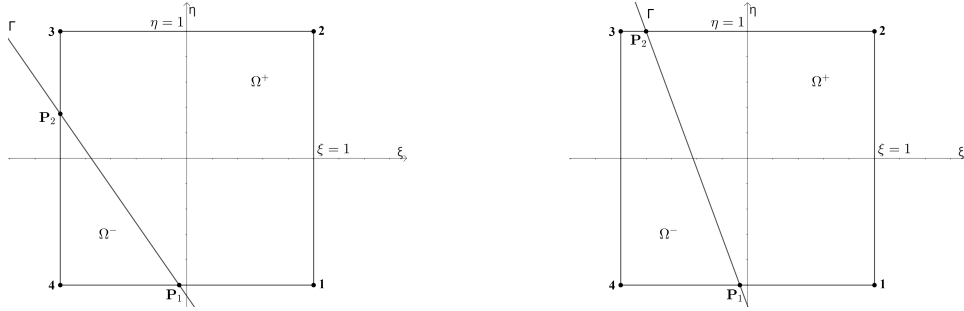
(a) Quadrilateral FE in the parent domain intersected by a discontinuity Γ on two adjacent sides.

(b) Quadrilateral FE in the parent domain intersected by a discontinuity Γ on two opposite sides.

Fig. 4.2 Quadrilateral FE in the parent domain and its intersection scenarios with a discontinuity Γ.

element are

$$N_1(\xi, \eta) = \frac{1}{4}(1+\xi)(1-\eta) \tag{4.10a}$$

$$N_2(\xi, \eta) = \frac{1}{4}(1+\xi)(1+\eta) \tag{4.10b}$$

$$N_3(\xi, \eta) = \frac{1}{4}(1-\xi)(1+\eta) \tag{4.10c}$$

$$N_4(\xi, \eta) = \frac{1}{4}(1-\xi)(1-\eta) \tag{4.10d}$$

so that, from the evaluation of $\left(\boldsymbol{B}^{std}\right)^T \boldsymbol{E}\boldsymbol{B}^{std}$, each component can be represented by a quadratic polynomial of the kind $\mathscr{P} = c_0 + c_1\xi + c_2\eta + c_3\xi\eta + c_4\xi^2 + c_5\eta^2$ [22]. Thus, from Eq. (4.4), the equivalent polynomial function $\tilde{H}(\xi,\eta)$ can be defined through

$$\int_\Omega \tilde{H}\,\mathrm{d}\Omega = \int_{\Omega^-} H\,\mathrm{d}\Omega + \int_{\Omega^+} H\,\mathrm{d}\Omega \tag{4.11a}$$

$$\int_\Omega \tilde{H}\xi\,\mathrm{d}\Omega = \int_{\Omega^-} H\xi\,\mathrm{d}\Omega + \int_{\Omega^+} H\xi\,\mathrm{d}\Omega \tag{4.11b}$$

$$\int_\Omega \tilde{H}\eta\,\mathrm{d}\Omega = \int_{\Omega^-} H\eta\,\mathrm{d}\Omega + \int_{\Omega^+} H\eta\,\mathrm{d}\Omega \tag{4.11c}$$

$$\int_\Omega \tilde{H}\xi\eta\,\mathrm{d}\Omega = \int_{\Omega^-} H\xi\eta\,\mathrm{d}\Omega + \int_{\Omega^+} H\xi\eta\,\mathrm{d}\Omega \tag{4.11d}$$

$$\int_\Omega \tilde{H}\xi^2\,\mathrm{d}\Omega = \int_{\Omega^-} H\xi^2\,\mathrm{d}\Omega + \int_{\Omega^+} H\xi^2\,\mathrm{d}\Omega \tag{4.11e}$$

$$\int_\Omega \tilde{H}\eta^2\,\mathrm{d}\Omega = \int_{\Omega^-} H\eta^2\,\mathrm{d}\Omega + \int_{\Omega^+} H\eta^2\,\mathrm{d}\Omega \tag{4.11f}$$

$$\tag{4.11g}$$

It is crucial to emphasise the conceptual significance of Eq. (4.11): The discontinuous function H can multiply any polynomial of type $\mathscr{P}$ when computing the element stiffness matrix [22]. All of the independent single equations in Eq. (4.11) must hold for the corresponding continuous and differentiable function $\tilde{H}$ to allow for linear combination

$$\int_\Omega \tilde{H}\mathscr{P}\,\mathrm{d}\Omega = \int_{\Omega^-} H\mathscr{P}\,\mathrm{d}\Omega + \int_{\Omega^+} H\mathscr{P}\,\mathrm{d}\Omega \tag{4.12}$$

Assuming $\tilde{H}(\xi,\eta) = a + b\xi + c\eta + d\xi\eta + e\xi^2 + f\eta^2$, equations (4.11) can be considered a linear system in the six unknowns a,b,c,d,e,f, and they can be evaluated by means of the Gauss theorem, as described in detail in [22], finding a closed form solution for both the case of discontinuity line intersecting two adjacent element sides and for the case of discontinuity line intersecting two opposite element sides [22]. It has to be noted that the coefficients a,b,c,d,e,f defining $\tilde{H}(\xi,\eta) = a + b\xi + c\eta + d\xi\eta + e\xi^2 + f\eta^2$, consent to evaluate eqs. (4.2), (4.4) and (4.5), so that the integration is defined on the entire domain of the element and its splitting into Ω^- and Ω^+ is no longer required. However, since the integrand function in Eq. (4.2) has a higher polynomial degree than the one in Eq. (4.5) ($\tilde{H}$ is a quadratic polynomial), a higher-order Gauss quadrature is needed [22].

4.3.2   3D case

As seen in Subsection 4.3.1, the three-dimensional case depends on the element type and the point at which the discontinuity surface intersects it. The closed form solution is presented for the four-node tetrahedron [22] and the eight-node hexahedron elements. Since isoparametric mapping may be used in the general situation, all calculations are done in the parent reference system (ξ, η, ζ). The discontinuity surface Γ is assumed as a plane intersecting the element at points $P_i = (\xi_i, \eta_i, \zeta_i)$, where $i = 1, ..., 3$ for the tetrahedron element and $i = 1, ..., 4$ for the hexahedron element. All intersection points P_i can be easily determined by means of level set data, since the signed distance from each node of the element to the discontinuity is known.

Linear tetrahedral element

Let us consider a four-node tetrahedron parent element, as in Figure 4.3a and let us suppose it is intersected by a discontinuity surface Γ at points $P_1 = (\xi_1, \eta_1, \zeta_1)$, $P_2 = (\xi_2, \eta_2, \zeta_2)$ and $P_3 = (\xi_3, \eta_3, \zeta_3)$ (Figure 4.3b). Its shape functions are

(a) Tetrahedral FE in the parent domain.

(b) Tetrahedral FE in the parent domain intersected by a discontinuity Γ.
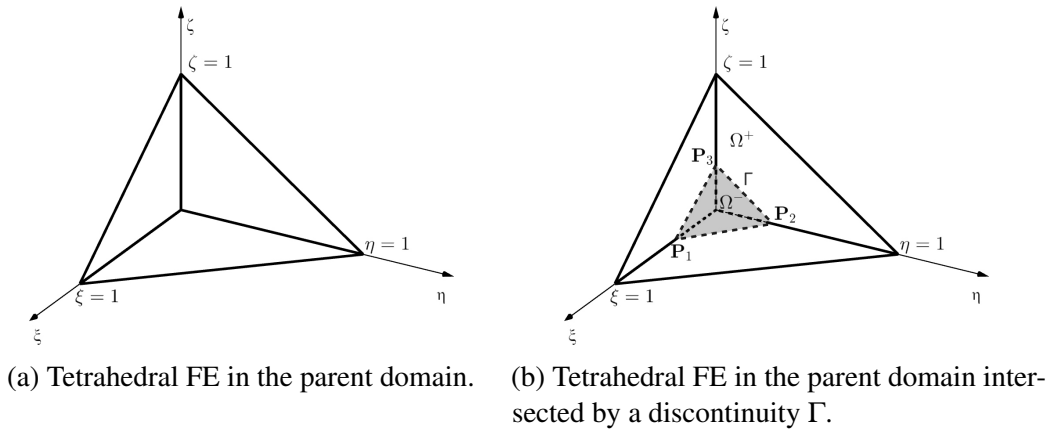
Fig. 4.3 Tetrahedral FE in the parent domain and its intersection with a discontinuity Γ.

$$N_1(\xi, \eta, \zeta) = \xi \tag{4.13a}$$

$$N_2(\xi, \eta, \zeta) = \eta \tag{4.13b}$$

$$N_3(\xi, \eta, \zeta) = \zeta \tag{4.13c}$$

$$N_4(\xi, \eta, \zeta) = 1 - \xi - \eta \tag{4.13d}$$

The same procedure seen in 4.3.1 is followed. From the evaluation of $\left(\boldsymbol{B}^{std}\right)^T \boldsymbol{E} \boldsymbol{B}^{std}$, each component is a constant [22]. Thus, only one independent equation may be derived from Eq. (4.4) in scalar form (all the equations are linearly dependent). Since $\tilde{H}$ is considered to be a zero degree polynomial, its value can be found by applying the specific form of Eq. (4.4) to the current scenario (Eq. (4.7)). Considering $H > 0$ in Ω^+, Eq. (4.7) can be rewritten as in Eq. (4.8) thus $\tilde{H}$ is

$$\tilde{H} = 2\xi_1\eta_2\zeta_3 - 1 \tag{4.14}$$

and the element stiffness matrix $\boldsymbol{K}$ can be evaluated from Eq. (4.2).

Trilinear hexahedral element

A hexahedral element defined in the parent reference system (ξ, η, ζ), as shown in Figure 4.4 has been analysed. To evaluate the equivalent polynomial for the
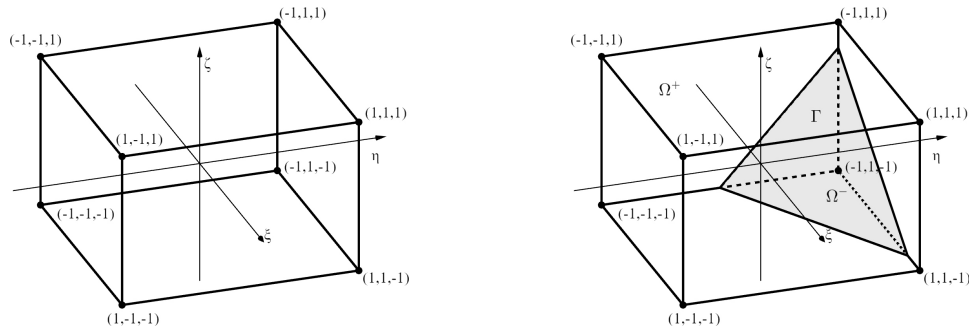
(a) Hexahedral FE in the parent domain.　　(b) Hexahedral FE in the parent domain intersected by a discontinuity Γ.

Fig. 4.4 Hexahedral FE in the parent domain and its intersection with a discontinuity Γ.

hexahedral element, a regularised expression of the Heaviside function (4.15) has

been taken into account [27].

$$H_\rho = \frac{2}{e^{-\rho x} + 1} - 1 \qquad (4.15)$$

where e is the Euler number and ρ is a regularisation parameter, such that as $\rho \to +\infty$ the Heaviside function H is reproduced by $H_{\rho \to \infty}$ (Figure 4.5). Therefore, it is
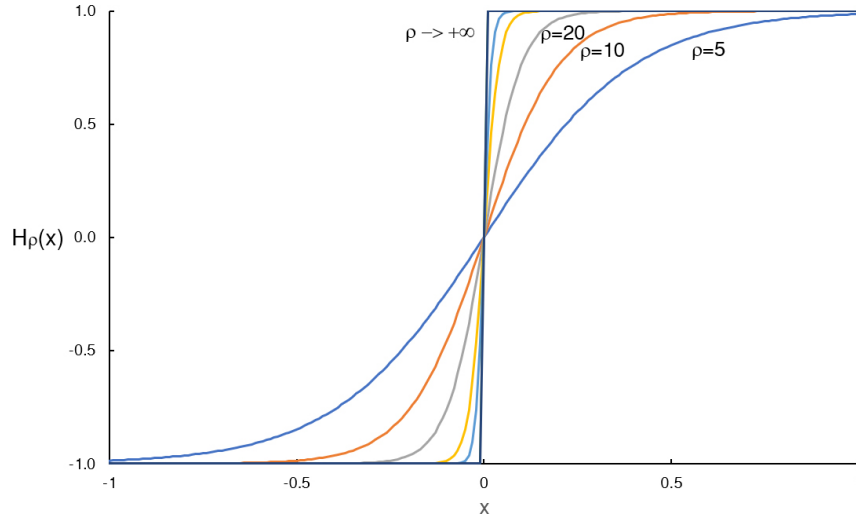
Fig. 4.5 Graphs of H_ρ for various values of the parameter ρ. As $\rho \to +\infty$, the function H_ρ reproduces H

possible to evaluate the equivalent polynomials $\tilde{H}_\rho$ and H_ρ from the relation

$$\int_\Omega \tilde{H}_\rho m^{(i)} \mathrm{d}\Omega = \int_\Omega H_\rho m^{(i)} \mathrm{d}\Omega \quad i = 1, ..., n \qquad (4.16)$$

being $m^{(i)}$ a i-degree monomial. Thus, Eq. (4.16) is a system of n linear equations in n unknowns, that are the coefficient of the equivalent polynomial $\tilde{H}$ [27]. In fact, applying the limit for $\rho \to +\infty$ to Eq. (4.16), it is

$$\lim_{\rho \to +\infty} \int_\Omega \tilde{H}_\rho m^{(i)} \mathrm{d}\Omega = \lim_{\rho \to +\infty} \int_\Omega H_\rho m^{(i)} \mathrm{d}\Omega \quad i = 1, ..., n \qquad (4.17)$$

and by applying the bounded convergence theorem it is

$$\int_\Omega \lim_{\rho \to +\infty} \tilde{H}_\rho m^{(i)} \mathrm{d}\Omega = \int_\Omega \lim_{\rho \to +\infty} H_\rho m^{(i)} \mathrm{d}\Omega \quad i = 1, ..., n \qquad (4.18)$$

where

$$\lim_{\rho \to +\infty} H_\rho m^{(i)} = H m^{(i)} \quad i = 1, ..., n \tag{4.19}$$

and from eqs. (4.17) and (4.18)

$$\tilde{H} m^{(i)} = \lim_{\rho \to +\infty} H_\rho m^{(i)} \quad i = 1, ..., n \tag{4.20}$$

so that

$$\tilde{H} = \lim_{\rho \to +\infty} H_\rho \tag{4.21}$$

Thus, equivalent polynomial $\tilde{H}$ can be obtained from $\lim_{\rho \to +\infty} \tilde{H}_\rho$ [27]. Unlike the 2D elements and the linear tetrahedron presented in [22] and previously discussed, where an explicit intersection with the element faces and edges is required, Eq. (4.15) continuity and differentiability qualities allow for seamless integration throughout the parent element domain [27]. In these hypotheses, the discontinuity Γ can be defined as a plane of equation

$$\Gamma(\xi, \eta, \zeta) = a\xi + b\eta + c\zeta + d \tag{4.22}$$

where $\sqrt{a^2 + b^2 + c^2} = 1$. Thus, Eq. (4.15) becomes

$$H_\rho = \frac{2}{e^{-\rho \Gamma(\xi, \eta, \zeta)} + 1} - 1 \tag{4.23}$$

The shape functions for the trilinear hexahedron element are

$$N_1(\xi,\eta,\zeta) = \frac{1}{8}(1+\xi)(1-\eta)(1-\zeta) \tag{4.24a}$$

$$N_2(\xi,\eta,\zeta) = \frac{1}{8}(1+\xi)(1+\eta)(1-\zeta) \tag{4.24b}$$

$$N_3(\xi,\eta,\zeta) = \frac{1}{8}(1-\xi)(1+\eta)(1-\zeta) \tag{4.24c}$$

$$N_4(\xi,\eta,\zeta) = \frac{1}{8}(1-\xi)(1-\eta)(1-\zeta) \tag{4.24d}$$

$$N_5(\xi,\eta,\zeta) = \frac{1}{8}(1+\xi)(1-\eta)(1+\zeta) \tag{4.24e}$$

$$N_6(\xi,\eta,\zeta) = \frac{1}{8}(1+\xi)(1+\eta)(1+\zeta) \tag{4.24f}$$

$$N_7(\xi,\eta,\zeta) = \frac{1}{8}(1-\xi)(1+\eta)(1+\zeta) \tag{4.24g}$$

$$N_8(\xi,\eta,\zeta) = \frac{1}{8}(1-\xi)(1-\eta)(1+\zeta) \tag{4.24h}$$

thus its stiffness matrix contains the following monomials

$$\begin{aligned}
\boldsymbol{m} = (1,\xi,\eta,\zeta,\xi^2,\eta^2,\zeta^2,\xi\eta,\xi\zeta,\eta\zeta, \\
\xi^2\eta,\eta^2\xi,\eta^2\zeta,\zeta^2\eta,\zeta^2\xi,\xi\eta\zeta, \\
\xi^2\eta\zeta,\eta^2\xi\zeta,\zeta^2\xi\eta,\xi^2\eta^2,\xi^2\zeta^2,\eta^2\zeta^2)
\end{aligned} \tag{4.25}$$

which are assumed as the equivalent polynomial terms [27] in Eq. (4.16) [27]. It is thus possible to obtain a closed form solution for the analysed problem and evaluate the equivalent polynomial $\tilde{H}$ for the linear hexahedron parent element. Since the equivalent polynomial coefficients expression are particularly long in this case, they will not be reported here. However, the details about their evaluation are extensively reported in [27]. It has to be stressed again that the coefficients defining $\tilde{H}$, consent to evaluate eqs. (4.2), (4.4) and (4.5), so that the integration is defined on the entire domain of the element and its splitting into Ω^- and Ω^+ is no longer required. However, since the integrand function in Eq. (4.2) has a higher polynomial degree than the one in Eq. (4.5), a higher-order Gauss quadrature is needed [22], requiring a bigger computational effort.

4.3.3 Non-polygonal elements: Circle and Sphere element case

The equivalent polynomials formulation hereby presented for the most common 2D and 3D finite element shapes can also be extended to non-polygonal element domains. The formulation has been, in fact, successfully implemented also to circular and spherical elements, following the procedure seen in the previous subsections. For the circle case, the parent element is a unit circle centred in $(0,0)$ in the parent coordinate system (ξ, η) (Figure 4.6a). For the sphere case, the parent element is a unit sphere centred in $(0,0,0)$ in the parent coordinate system (ξ, η, ζ) (Figure 4.6b). Let us assume that the aforesaid elements are cut by a discontinuity Γ, as seen previously in sections 4.3.1 and 4.3.2. For both elements, a coordinate translation has been defined, so that it is possible to extend the solution to any circular (or spherical element), however defined in a global coordinate system (x,y) (or (x,y,z)). In fact, knowing the centre and the radius, allow to define any point of the circle (or sphere) parent element, onto the global coordinate system by means of a simple transformation. Let $P(\xi, \eta) = (\xi_i, \eta_i)$ a point of the parent circle element defined in the parent coordinate system and having radius $r = 1$, and let $\bar{P}(x,y) = (x_i, y_i)$ a point of the circle element defined in the global coordinate system having radius $\bar{r}$, it is

$$\bar{P}(x,y) = (x_i, y_i) = (\bar{r}\xi_i + x_{\bar{C}}, \bar{r}\eta_i + y_{\bar{C}}) \tag{4.26}$$

where $(x_{\bar{C}}, y_{\bar{C}})$ are the coordinates of the centre of the circle element in the global coordinate system. For the sphere element, the relation in Eq. (4.26) becomes

$$\bar{P}(x,y) = (x_i, y_i, z_i) = (\bar{r}\xi_i + x_{\bar{C}}, \bar{r}\eta_i + y_{\bar{C}}, \bar{r}\zeta_i + z_{\bar{C}}) \tag{4.27}$$

where $(x_{\bar{C}}, y_{\bar{C}}, z_{\bar{C}})$ are the coordinates of the centre of the sphere element in the global coordinate system. As for the previous case, by means of the regularised expression in Eq. (4.15), a seamless integration throughout the parent element domain is allowed. Thus, defining the discontinuity Γ as in Eq. (4.22), it is straightforward to evaluate the equivalent polynomial $\tilde{H}$ also in such cases.

(a) Circle FE in the parent domain.   (b) Sphere FE in the parent domain.
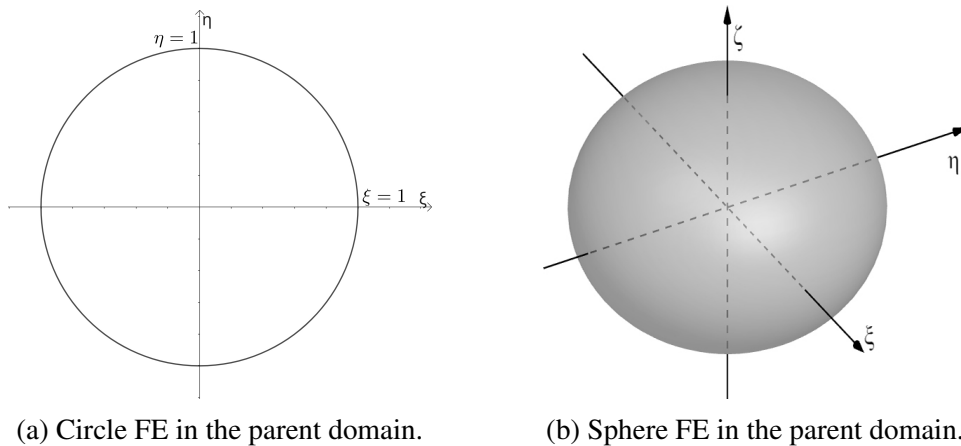
Fig. 4.6 Circle and sphere FE in the parent domain.

4.4 *EQP Library*: software implementation of equivalent polynomials formulation

As discussed in the previous Sections, the use of equivalent polynomials can be useful to overcome some of the limits of the conventional XFEM integration procedures presented in Section 3.7. Moreover, in many scientific and technical domains, as well as in computer graphics, it is necessary to numerically integrate polynomial functions in order to solve physical models and calculate data. A few representative examples are the computation of moments and products of inertia entering the inertia tensor of geometric shapes required for physics-based rigid body animations [136, 137]; the computation of a mechanical system stiffness matrix within the framework of the finite element method for the prediction of the mechanical behaviour of solids and structures [19, 37, 20]; and the computation of mass, total energy, angular momentum, and entropy to apply the conservation laws determining the atmosphere dynamics and thermodynamics [138]. Effective numerical quadrature techniques are available for polynomial integrands when the shape of the domain is an elementary geometry (triangle, parallelogram, parallelepiped), or can be reshaped back to an elementary geometry. A multiplying Heaviside step function is introduced when the polynomial presents a jump discontinuity or is required to be integrated over a subdomain (see Section 3.7). This might result in significant inaccuracies in the computation of the integral since numerical quadrature methods such as Gauss-Legendre implicitly embody a polynomial approximation of the integrand function. This scenario can be found in computer graphics when computing the geometrical

characteristics of complicated bodies, which may be considered as partition of a regular geometric shape [28]. Let us analyse the body Ω^+ in Figure 4.4b. This body is obtained by splitting the cubic domain Ω (Figure 4.4a) in two subdomains (Ω^- and Ω^+) using the discontinuity surface Γ. The integral in Eq. (4.28) may be used to calculate the geometrical characteristics of Ω^+, such as, for example, volume, moments, and products of inertia.

$$I = \int_{\Omega^+} \mathscr{P}_n(\boldsymbol{\xi}) \, d\Omega = \int_{\Omega} H(\boldsymbol{\xi}) \mathscr{P}_n(\boldsymbol{\xi}) \, d\Omega \qquad (4.28)$$

where $\mathscr{P}_n(\boldsymbol{\xi})$ is a n-degree polynomial function in the variables set $\boldsymbol{\xi} = (\xi, \eta, \zeta)$ required to compute the required geometrical properties of Ω^+ (e.g. $\mathscr{P}_n(\boldsymbol{\xi}) = 1$ to evaluate the volume, $\mathscr{P}_n(\boldsymbol{\xi}) = \eta^2 + \zeta^2$ to evaluate the second area moment with respect to the ξ-axis, etc.), and $H(\boldsymbol{\xi})$ is the standard Heaviside step function, as defined in Eq. (3.7). The body Ω^+ is defined by the normal vector $\boldsymbol{n}^+$ to the discontinuity surface Γ, pointing inwards Ω^+ (Figure 4.7). Vector $\boldsymbol{n}^+$ is orthogonal to Γ and its components are expressed by the Γ equation coefficients (a, b, c), as in Eq. (4.29).
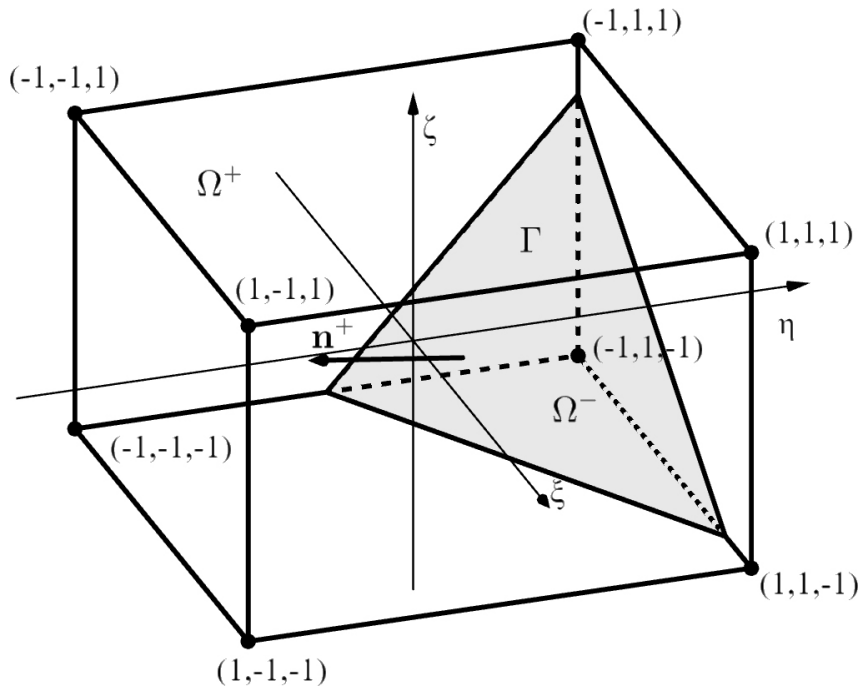
Fig. 4.7 Hexahedral FE in the parent domain, its intersection with a discontinuity Γ and the normal vector to the discontinuity $\boldsymbol{n}^+$.

$$\Gamma : a\xi + b\eta + c\zeta + d = 0 \tag{4.29}$$

The numerical integration problem stated in Eq. (4.28) is normally solved by partitioning the domain of integration to create quadrature subcells in which the integrals are polynomials [28]. The identification and cataloguing of all potential integration subdomain shapes, particularly for 3D geometries, is highly difficult. As discussed in the previous Sections of this Chapter, and also as presented in [22, 27, 15, 18] in the framework of the XFEM, an approach to avoid the subdivision of the quadrature domain has been proposed. Although the technique has been created for polynomial integrals, it could potentially be used to introduce discontinuities or trimmed domains into the piecewise polynomial representation of splines [28]. As presented in 4.3.2, the approach is based on substituting an equivalent polynomial function, $\tilde{H}(\boldsymbol{\xi})$, for the Heaviside function $H(\boldsymbol{\xi})$, such that:

$$\int_{\Omega} \tilde{H}(\boldsymbol{\xi}) \mathscr{P}_n(\boldsymbol{\xi}) \, \mathrm{d}\Omega = \int_{\Omega^-} H(\boldsymbol{\xi}) \mathscr{P}_n(\boldsymbol{\xi}) \, \mathrm{d}\Omega + \int_{\Omega^+} H(\boldsymbol{\xi}) \mathscr{P}_n(\boldsymbol{\xi}) \, \mathrm{d}\Omega \tag{4.30}$$

in which the equivalent polynomial $\tilde{H}(\boldsymbol{\xi})$ depends on Γ, is of the same degree of $\mathscr{P}_n(\boldsymbol{\xi})$ and can be written in vector notation as

$$\tilde{H}(\boldsymbol{\xi}) = \boldsymbol{c} \cdot \boldsymbol{m}(\boldsymbol{\xi}) \tag{4.31}$$

where $\boldsymbol{m}(\boldsymbol{\xi})$ is a collection of monomial basis (such as in Eq. (4.25)) and $\boldsymbol{c}$ is a vector of coefficients. By means of Eq. (4.30), is it possible to write Eq. (4.28) as

$$I = \int_{\Omega} \tilde{H}(\boldsymbol{\xi}) \mathscr{P}_n(\boldsymbol{\xi}) \, \mathrm{d}\Omega \tag{4.32}$$

Being $\tilde{H}(\boldsymbol{\xi}) \mathscr{P}_n(\boldsymbol{\xi})$ a polynomial function continuous over the entire domain Ω, it is possible to exactly integrate it using an appropriate quadrature rule [139]. It has to be noted that the integrand in Eq. (4.32) has doubled its degree, compared to the one in Eq. (4.28), since $\tilde{H}(\boldsymbol{\xi})$ has the same degree as $\mathscr{P}_n(\boldsymbol{\xi})$. The main advantage of the equivalent polynomial approach is allowing the integration over the entire standard domain Ω, instead of the non-standard partitioned subdomain Ω^+ [28]. In this Section the EQuivalent Polynomials (*EQP*) Library is presented. *EQP* has been developed as a first part of this PhD Thesis work in order to create a practical mathematical tool to easily evaluate the equivalent polynomial for various FE shapes, as well as exactly computing integrals such as the one defined in Eq. (4.32). Although

the main context for this Library is the XFEM and fracture mechanics in general, it could potentially be applied to successfully solve many other problems in various physical and engineering domains, such as computational geometry, computer graphics, physics-based animation of rigid bodies, etc. As it is illustrated in the following Subsections, the Library structure is straightforward. It is built in Fortran and it can be easily coupled with other existing libraries, programs or frameworks. The details for the mathematical procedure adopted to evaluate the expression of the equivalent polynomial have been presented in sections 4.3.1 to 4.3.2, as well as in [22, 27]. Some practical application to demonstrate the potential, precison and effectiveness of *EQP* are also carried out in this Section.

4.4.1 Software functionalities

As stated in Section 4.4, the main purpose of *EQP* is to provide the expression of the equivalent polynomial function $\tilde{H}(\boldsymbol{\xi})$. However, for a practical use, the library ought to be embedded in a algorithm that evaluates numerically the integral defined in Eq. (4.32) (i.e. applying standard Gauss quadrature rule, or any other quadrature algorithm to integrate polynomial functions non involving discontinuities). The Library functionalities are presented through a generic example. Let us consider a polynomial $\mathscr{P}_n(\boldsymbol{x})$ that is to be integrated over a subdomain $\bar{\Omega}^+$, obtained by dividing a parallelepiped domain $\bar{\Omega}$ with a plane $\bar{\Gamma}$ (Figure 4.8). The problem is
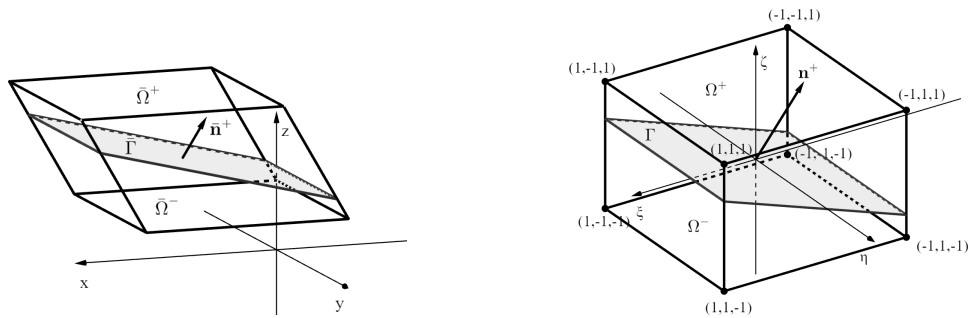
(a) Configuration of the parallelepiped element in the global coordinate system.

(b) Configuration of the parallelepiped element in the parent coordinate system.

Fig. 4.8 Configuration of the parallelepiped element in the global and parent coordinate system.

defined in the global reference system $\boldsymbol{x} = (x, y, z)$ and its solution can be obtained

through Eq. (4.32), once the equivalent polynomial function $\tilde{H}(\boldsymbol{\xi})$ is known, so that

$$I = \int_{\bar{\Omega}^+} \mathscr{P}_n(\boldsymbol{x}) \, \mathrm{d}\bar{\Omega} = \int_{\bar{\Omega}} \tilde{H}(\boldsymbol{x}) \mathscr{P}_n(\boldsymbol{x}) \, \mathrm{d}\bar{\Omega} \tag{4.33}$$

The problem is to be transformed to a quadrature on a standard domain in the first place. Thus, a variables change from the global reference system (x, y, z) to the parent reference system (ξ, η, ζ) is employed, in order to compute the integral over a standard regular geometrical shape (Figure 4.8). This transformation consent to deal with a variety of different cases, utilising a single parent geometry. In fact, parallelepipeds of any size and placed in any position in the global reference system can be brought back to the cubic parent geometry defined in the parent reference system $(\xi, \eta, \zeta) \in [-1, +1]$, as shown in 4.8 [28]. The change of variables is achieved by way of isoparametric mapping, which is normally used in FEM. Let $P(\xi, \eta, \zeta) \in \Omega$ be a generic point defined in the parent coordinate system and corresponding to the point $\bar{P}(x, y, z) \in \bar{\Omega}$ in the global coordinate system [28]. The isoparametric mapping of $P(\xi, \eta, \zeta) \in \Omega$ onto $\bar{P}(x, y, z) \in \bar{\Omega}$ can be written as

$$x = \sum_{i=1}^{n} N_i(\xi, \eta, \zeta) x_i \tag{4.34a}$$

$$y = \sum_{i=1}^{n} N_i(\xi, \eta, \zeta) y_i \tag{4.34b}$$

$$z = \sum_{i=1}^{n} N_i(\xi, \eta, \zeta) z_i \tag{4.34c}$$

in which n is the number of nodes of the element defined in the global coordinate system, having coordinates (x_i, y_i, z_i), and $N_i(\xi, \eta, \zeta)$ is the shape function, defined in terms of the parent coordinates for the i-th parent element node. As for the discontinuity $\bar{\Gamma}(\boldsymbol{x})$ equation, defined in the global coordinate system, it has to be mapped into $\Gamma(\boldsymbol{\xi})$, defined in the parent coordinate system. The procedure used in the library follows these steps:

- evaluating the signed distances D_i between $\bar{\Gamma}(\boldsymbol{x})$ and the integration domain nodes in the global coordinate system [28];

- writing the coefficients of $\bar{\Gamma}(\boldsymbol{x})$ (a, b, c, d) in terms of D_i, solving a system of linear equations [28];
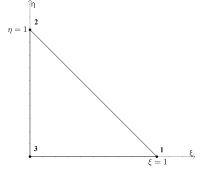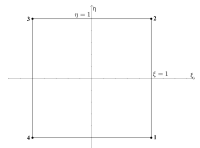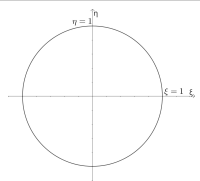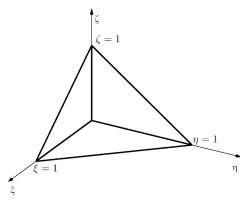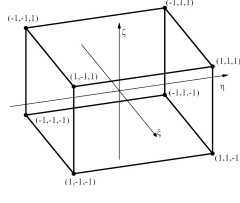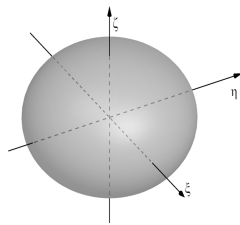
- replacing the variables of $\bar{\Gamma}(\boldsymbol{x})$ (x, y, z) by means of Eq. (4.34), obtaining $\Gamma(\boldsymbol{\xi})$, defined by the coefficients (a', b', c', d'), function of D_i [28].

Once $\bar{\Gamma}(\boldsymbol{x})$ is mapped onto $\Gamma(\boldsymbol{\xi})$, the expression of the equivalent polynomial function $\tilde{H}(\boldsymbol{\xi})$ can be evaluated by the library and it is provided in terms of the parent domain coordinate system. Consequently, the Jacobian matrix, which contains the partial derivatives of the interpolation functions N_i, differentiated with respect to the parent system variables (ξ, η, ζ), is then used to introduce the coordinate and integration domain transformation into the quadrature rule [140], so that

$$
\begin{aligned}
I &= \int_{\bar{\Omega}} \tilde{H}(\boldsymbol{x}) \mathscr{P}_n(\boldsymbol{x}) \, \mathrm{d}\bar{\Omega} = \int_{\Omega} \tilde{H}(\boldsymbol{\xi}) \mathscr{P}_n(\boldsymbol{\xi}) |\boldsymbol{J}| \, \mathrm{d}\Omega \\
&= \sum_{j=1}^{gp} w_j \tilde{H}(\xi_j, \eta_j, \zeta_j) \mathscr{P}_n(\xi_j, \eta_j, \zeta_j) |\boldsymbol{J}(\xi_j, \eta_j, \zeta_j)|
\end{aligned}
\tag{4.35}
$$

where $|\boldsymbol{J}|$ is the Jacobian matrix determinant, gp is the number of quadrature points, and w_j their weights. The integral in Eq. (4.33) is then computed in Eq. (4.35) by means of standard Gauss-Legendre quadrature rule [141]. It is important to emphasise once more that the library performs integral calculations over the entire domain $\bar{\Omega}$ and produces the $\bar{\Omega}^+$ subdomain integral result. In order to have the unit vector $\boldsymbol{n}^+$ pointing in the desired subdomain direction, the equation of the discontinuity must be properly defined. For instance, by simply changing the sign of all the discontinuity coefficients, the evaluation over the domain $\bar{\Omega}^-$ can be carried out. Also keep in mind that the discontinuity need not necessarily intersect $\bar{\Omega}$; instead, the quadrature result could be either zero (if $\bar{\Omega}^+ = \emptyset$) or the integral over $\bar{\Omega}$ (if $\bar{\Omega}^+ = \bar{\Omega}$) [28]. The degree and composition of the polynomial function that can be precisely integrated with the suggested approach depend on some conditions imposed to determine the equivalent polynomial, as can be deduced from [22, 27]. Table 4.1 lists the monomials that can make up the polynomial function to be integrated as well as the parent geometrical shapes that are present in the current library version. However, the Library can be extended to any polynomial degree in each of the listed domains [28].

Table 4.1 Integration domain, domain type, parent element domain and monomial basis included in the library.

Domain of Integration	*etype*	Parent Domain	Monomial Basis
Triangle	20		1
Parallelogram	21		$1, \xi, \xi^2, \eta, \xi\eta, \eta^2$
Circle	22		$1, \xi, \xi^2, \eta, \xi\eta, \eta^2$
Tetrahedron	30		1
Hexahedron	31		$1, \xi, \xi^2, \eta, \xi\eta, \xi^2\eta,$ $\eta^2, \xi\eta^2, \xi^2\eta^2, \zeta,$ $\xi\zeta, \xi^2\zeta, \eta\zeta, \xi\eta\zeta,$ $\xi^2\eta\zeta, \eta^2\zeta, \xi\eta^2\zeta,$ $\zeta^2, \xi\zeta^2, \xi^2\zeta^2, \eta\zeta^2,$ $\xi\eta\zeta^2, \eta^2\zeta^2$
Sphere	32		$1, \xi, \xi^2, \eta, \xi\eta, \xi^2\eta,$ $\eta^2, \xi\eta^2, \xi^2\eta^2, \zeta,$ $\xi\zeta, \xi^2\zeta, \eta\zeta, \xi\eta\zeta,$ $\xi^2\eta\zeta, \eta^2\zeta, \xi\eta^2\zeta,$ $\zeta^2, \xi\zeta^2, \xi^2\zeta^2, \eta\zeta^2,$ $\xi\eta\zeta^2, \eta^2\zeta^2$

4.4.2   Software architecture

The design of the software library is simple. *eqpol.f90* is the main library file. It includes the algorithms to map the equation of the discontinuity from the global to the parent coordinate system, to calculate the coefficients, and to compute the equivalent polynomial function $\tilde{H}(\boldsymbol{\xi})$. Other files that contain the mathematical expressions of the coefficients required to define the equivalent polynomial function round out the system [28]. A main programme file, *main.f90*, and a module file, *mapping_module.f90*, that are not strictly part of the library, but are added as an extra for the purpose of use demonstration allow the user to exactly compute the integral in Eq. (4.35) for the supported domain shapes. The following steps are required for the practical use of the library:

1. primal data preparation:

    - integration domain selection (as in Table 4.1);

    - definition of the nodal coordinates of the domain in the global coordinate system (or radius and centre for the circular and spherical domains);

    - definition of the coefficients of the discontinuity plane in the global coordinate system.

2. isoparametric mapping onto the parent element domain and computation of the coefficient vector for the equivalent polynomial function, by way of the subroutine *Heqpol_coefficients*;

3. quadrature by means of any chosen rule, as in Eq. (4.35). The values of the equivalent polynomial at the quadrature points are obtained by means of the function *HeqPol*, while the function *det_J* provides the determinant of the Jacobian matrix of the coordinate transformation.

The exact quadrature result is computed by the library if:

- the determinant of the Jacobian matrix in Eq. (4.35) for the coordinate transformation is constant (this is always true for triangular, circular, tetrahedral, spherical and for non-distorted quadrangular and hexahedral domains);

- $\mathscr{P}_n$ is a linear combination of the monomial presented in Table 4.1.

It should be noted that two calls must be planned in the event that users seek to directly incorporate the core of the library into their own quadrature algorithm: one call to the subroutine *Heqpol_coefficients* for each integration domain (step 2 above), and another to the function *HeqPol* for each quadrature point (step 3 above). Since the function *det_J* belongs in the quadrature algorithm, it is not a part of the library core functionality [28].

4.4.3   Numerical examples

The library usage file *main.f90* has been employed for the examples that follow. The library yields accurate outcomes up to machine precision for the examples hereby presented.

Parallelogram

A parallelogram is considered in this example (Figure 4.9). The dimensions are in
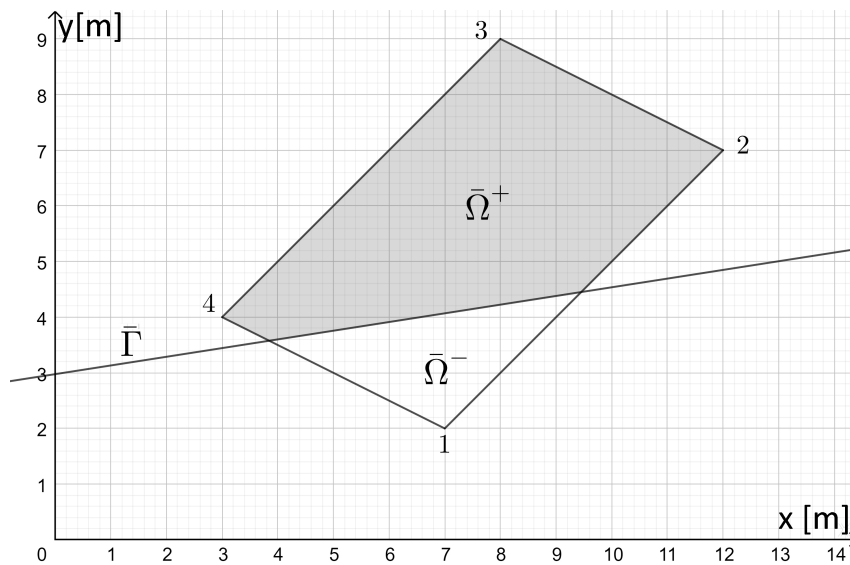
Fig. 4.9 Parallelogram split in two subdomains by a discontinuity $\bar{\Gamma}$.

meters and the element nodes in the global coordinate system are:

$$
\begin{aligned}
\mathbf{1} &\equiv (7,2) \\
\mathbf{2} &\equiv (12,7) \\
\mathbf{3} &\equiv (8,9) \\
\mathbf{4} &\equiv (3,4)
\end{aligned}
\tag{4.36}
$$

The element is split in two parts, $\bar{\Omega}^+$ and $\bar{\Omega}^-$, by the discontinuity line $\bar{\Gamma}: -\frac{39}{250}x + y - \frac{372}{125} = 0$. The aim of this example is to evaluate the inertia tensor and the area of the subdomain $\bar{\Omega}^+$. Once the library usage file *main.f90* is launched and nodal coordinates of the element and the discontinuity coefficients ($a = \frac{39}{250}, b = -1, c = \frac{372}{125}$) are inputted, the program maps the parallelogram onto the parent coordinate system, in which the equivalent polynomial $\tilde{H}(\boldsymbol{\xi})$ is evaluated and the integration is performed by means of standard Gauss quadrature, without splitting the domain. The monomials to integrate are $\mathscr{P} = 1$ to evaluate the area of $\bar{\Omega}^+$, and x^2, y^2, xy to compute its inertia tensor $\boldsymbol{I}$. The results obtained by the program output are

$$
Area = 24.207 m^2
\tag{4.37}
$$

$$
\boldsymbol{I} = \rho_s
\begin{bmatrix}
1517.185 & -1148.046 \\
-1148.046 & 913.802
\end{bmatrix}
(\text{units: kg } m^2)
\tag{4.38}
$$

where ρ_s is the surface density of the material (kg/m^2). To gauge the effectiveness of the results provided by the library, the subdomain $\bar{\Omega}^+$ has been defined and the following definite integrals have been exactly evaluated

$$
I_i = \int_{\bar{\Omega}^+} \mathscr{P}_i \, d\bar{\Omega}
\tag{4.39}
$$

where $\mathscr{P} = \{1, x^2, xy, y^2\}$.

The exact analytical result obtained coincide up to machine precision to the library output, demonstrating its exactness.

Parallelepiped

A 3D exemple is presented through a parallelepiped (Figure 4.10).
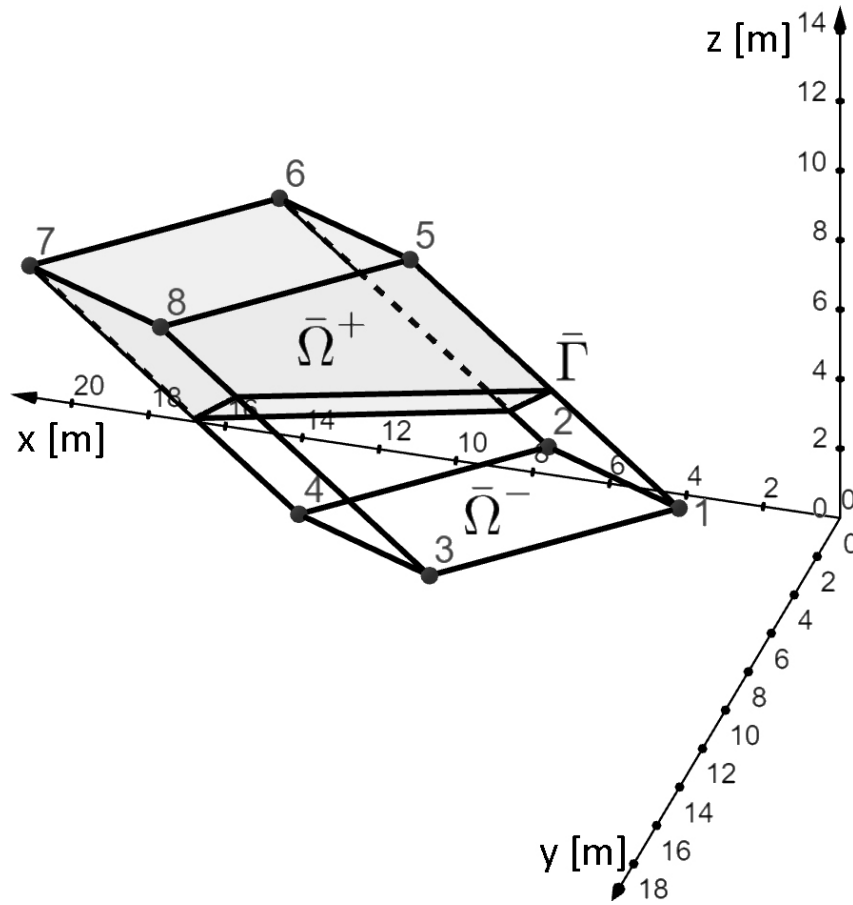
Fig. 4.10 Parallelepiped split in two subdomains by a discontinuity $\bar{\Gamma}$.

The dimensions are in meters and the element nodes in the global coordinate system are:

$$
\begin{array}{ll}
\mathbf{1} \equiv (3,4,2) & \mathbf{5} \equiv (10,4,8) \\
\mathbf{2} \equiv (7,2,2) & \mathbf{6} \equiv (14,2,8) \\
\mathbf{3} \equiv (12,7,2) & \mathbf{7} \equiv (19,7,8) \\
\mathbf{4} \equiv (8,9,2) & \mathbf{8} \equiv (15,9,8)
\end{array}
\tag{4.40}
$$

The element is split in two parts, $\bar{\Omega}^+$ and $\bar{\Omega}^-$, by the discontinuity plane $\bar{\Gamma} : \frac{71}{10}x - \frac{789}{50}y + \frac{543}{25}z - \frac{8757}{100} = 0$. The aim of this example is to evaluate the inertia tensor and the area of the subdomain $\bar{\Omega}^+$. The procedure is the same followed in the previous example and the results obtained by the program output are

$$
Volume = 102.339m^3
\tag{4.41}
$$

$$I = \rho_s \begin{bmatrix} 7118.221 & -6852.748 & -8062.194 \\ -6852.748 & 20438.215 & -3372.193 \\ -8062.194 & -3372.193 & 19388.499 \end{bmatrix} \text{(units: kg } \text{m}^3\text{)} \qquad (4.42)$$

where ρ_s is the volumetric density of the material (kg/m^3). Once again the effectiveness of the results provided by the library has been proved evaluating the same definite integrals computed by the library over the subdomain $\bar{\Omega}^+$. The exact analytical result obtained coincide up to machine precision to the library output, demonstrating again its exactness.

4.5   Conclusions

In this chapter the integration of polynomials times step functions by means of equivalent polynomials has been explored in the context of XFEM analysis. As discussed in Section 4.2, the problem of integrating polynomials multiplied by Heaviside step function arises commonly when the computation of the stiffness matrix of enriched elements containing cracks is required. The problem is commonly solved in XFEM analysis by defining integration subdomains in which the step function is continuous and differentiable, thus the exact integration by means of standard quadrature can be achieved. This technique results, though, in a discretisation requirement that somehow disrupts the elegance of the XFEM method. In this scope, the use of equivalent polynomials allow to perform the integration of polynomials times step function over the entire integration domain, avoiding the subdomain definition requirement. By leveraging the concept of equivalent polynomials presented in [22, 27], in fact, the exact integration of polynomials multiplied by the Heaviside step function by way of standard quadrature rules can be achieved. This approach ensures that the discontinuity is properly captured during the numerical integration process, leading to accurate results. The equivalent polynomial definition for standard 2D FE domains, such as a linear 3-node triangle element and a bilinear 4-node quadrangular element have been discussed and a closed form solution has been reported. The procedure has been applied as well for 3D FE domains, such as a linear 4-node tetrahedral element and a trilinear 8-node quadrangular element. A closed form solution has also been defined for non-polygonal element shapes, such as a circle element domain and a sphere element domain. Although these elements have very few practical applications in FEM/XFEM analysis, the fact that the formulation investigated in this chapter could

be extended also to non-canonical domain shapes has been considered an interesting aspect to explore. Moreover, still in this scope, a software library (*EQP*) to compute the equivalent polynomial for various 2D and 3D domain shapes has been developed and presented in Section 4.4. The library also includes an isoparametric mapping module in order to bring back the integration domain, defined by the user in the global coordinate system, to an elementary standard geometry, defined in a parent coordinate system where computations are made. An algorithm to map the discontinuity onto the parent coordinate system is also embedded in the library. For the sake of usage demonstration, the library is complemented by an executable programme that allow users to compute integrals of polynomials times step function over the domain shapes supported by the *EQP* library, however defined in a global coordinate system. The efficiency and exactness of the library has been demonstrated by way of practical usage examples carried out in section 4.4.3 and it can be considered a useful tool to compute integrals of discontinuous functions by means of any quadrature rule, without subdividing the domain of integration. Although the library main scope is XFEM analysis, it can be extended to other contexts in which the numerical integration of polynomial functions is a frequent problem, such as computational geometry, computer graphics and simulations in which a dynamic change in shape and position of object is involved. The proposed library could in fact be employed to evaluate geometrical characteristics of complex figures, generated by a standard shape cut by a plane or surface (as in the presented examples in section 4.4.3), or used in brittle fracture analysis, in which an object breaks into various pieces. The main advantage of the library, and the formulation behind it, is its versatility, the capability of eliminating complicated subdomains, the speed of computation, and the accuracy. The main limit is that this approach could manage only one discontinuity for each integration domain. This problem has been addressed and, in Chapter 5, an innovative approach for handling two discontinuities within an integration domain is presented. This approach also enhances the potentiality of the proposed library and it is a step towards the integration of an arbitrary number of discontinuities.

Chapter 5

Integration of XFEM Elements Containing Multiple Discontinuities[1]

5.1 Introduction

As discussed in the previous Chapters, the exact numerical integration of discontinuous functions using a common quadrature rule is a challenging subject that has been explored by a number of authors over the years. In particular, in the XFEM context, the problem is usually undertaken splitting the integration domain in subdomains in which the discontinuous function is continuous and differentiable. In Chapter 4, an efficient method by means of equivalent polynomials proposed by Ventura [22, 27] to overcome the problem has been investigated and a software implementation of the formulation has been carried out, delivering a library that is a practical tool to exactly evaluate integrals of polynomials times step functions over various 2D and 3D element shapes, without splitting the integration domain. The concept of equivalent polynomials has been investigated, and as a first step towards the integration of any number of discontinuities, it has been extended to the case of a double discontinuity within a single finite element. This situation frequently occurs when events like crack branching, kinking, or junction arise [11, 21, 29–32, 35, 36, 33, 34]. In this Chapter, the problem of 2D and 3D finite elements containing more than one discontinuity is investigated and an efficient formulation to exactly integrate polynomials times

---

[1]Part of the work described in this Chapter has been previously published in: S. Fichera, G. Mariggiò, M. Corrado, G. Ventura. Integration of Polynomials Times Double Step Function in Quadrilateral Domains for XFEM Analysis. Algorithms 16(6):290 (2023).

double step function over 2D and 3D domains is presented. The extension of the problem to an arbitrary number of discontinuities is also discussed and a closed form solution for quadrilateral elements has been carried out. The proposed formulation has been developed in order to address the integration problems involving more than one discontinuity in an enriched XFEM element, such as crack branching or multiple fractures, delivering an exact numerical solution without the need for domain subdivision. The importance of this work is much deeper, however, as it aims to provide a powerful integration technique that could be highly beneficial not just for problems in the context of XFEM/GFEM and fracture mechanics, but also in computational geometry and as a tool for easily and effortlessly solving integrals over complex domain shapes. The organisation of this Chapter is herein presented. In Section 5.2 the problem of the integration of double discontinuous functions in 2D quadrilateral elements is presented. The proposed formulation is introduced in Section 5.3, with mathematical demonstration and proof for each analysed domain. In order to practically employ the proposed formulation, as well as to prove its effectiveness and validate it, the presented integration technique has been implemented in a software library called *double discontinuity equivalent polynomials* (*DD_EQP*) which is illustrated in Section 5.3.2, along with some numerical examples. The extension of the proposed formulation is then carried out also for triangular, hexahedral and tetrahedral elements, respectively in sections 5.4 to 5.6, following the same pattern defined for the 2D quadrilateral element. Moreover, the effect of distortion on the accuracy of the results is analysed by means of numerical comparison with other integration techniques in Section 5.7. Finally, the extension of the proposed formulation for an arbitrary number of discontinuities is presented in Section 5.8 and a general discussion on the outcomes is carried out in Section 5.9.

5.2 Problem definition

Problems involving multiple discontinuities are common in numerous domains [142–154, 24, 155, 156]. In the context of fracture mechanics, such problems have been investigated by numerous authors [33, 157, 35, 36, 156, 30, 32]. Comparable problems arise also in other contexts, such as computer graphics, evaluation of geometric region properties and computer simulation in general. In fact, similar

integration problems have been recently addressed in different studies [158–160, 138, 161–165, 150, 166–169, 100, 170, 171, 156, 172–174, 11].

A noteworthy approach in the context of XFEM has been presented by Daux in [34], in which a method to model multiple branched cracks is carried out. A linear combination of Heaviside step functions (one for each discontinuity) is used together with a *junction function* that defines the solution behaviour on either side of the junction point of the crack [11]. The junction function is defined as a discontinuous step function dependent on the value of the Heaviside functions describing each discontinuity. With reference to the set of variables $\boldsymbol{x} = (x, y)$, the displacement approximation formulation for this method can be written as

$$
\begin{aligned}
\boldsymbol{u}^h(\boldsymbol{x}) \quad &= \sum_{I \in n} \boldsymbol{u}_I \phi_I(\boldsymbol{x}) + \sum_{J=1}^{N_c} \sum_{I \in L_J} \boldsymbol{a}_{I,J} \phi_I(\boldsymbol{x}) H_J(\boldsymbol{x}) \\
&+ \sum_{J=1}^{N_t} \sum_{I \in K_J} \phi_I(\boldsymbol{x}) \left(\sum_{L=1}^{4} \boldsymbol{b}_{I,J}^L F_J^L(\boldsymbol{x}) \right) + \sum_{J=1}^{N_x} \sum_{I \in J_J} \boldsymbol{c}_{I,J} \phi_I(\boldsymbol{x}) J_J(\boldsymbol{x})
\end{aligned}
\tag{5.1}
$$

in which:

- $L_J \subset I$ are the nodes to enrich for the *j*-th discontinuity, as such their support does not contain the ends of the discontinuity, and $\boldsymbol{a}_{I,J}$ are the respective enriched degrees of freedom [34];

- $K_J \subset I$ are the nodes to enrich for the *j*-th discontinuity extremity, as such their support contains the ends of the discontinuity, and $\boldsymbol{b}_{I,J}^L$, $L = 1, ..., 4$ are the respective enriched degrees of freedom [34];

- $J_J \subset I$ are the nodes to enrich for the *j*-th junction, as such their support contains the *j*-th junction, and $\boldsymbol{c}_{I,J}$ are the respective enriched degrees of freedom [34].

Although this technique allow to tackle the eventuality of an arbitrary number of discontinuities within an enriched element without remeshing, a subdivision of the integration domains is still required to evaluate the element stiffness matrix. In fact, as defined in Eq. (5.1), multiple discontinuous functions are introduced in the solution space of the enriched elements, affecting the reliability of the numerical integration process. In [34] the issue is addressed by way of the formulation proposed in [7], in which the integration domain Ω is subdivided into portions Ω_s, where the junction function and the enrichment functions are continuous and differentiable. Hence,

partitioning the integration domain is still necessary for the quadrature process [34]. The formulation proposed in [34] is illustrated also in [33], in which numerical tests are carried out. Although the approach presented in [34] offers an effective method to tackle down problems involving two or more discontinuities within an enriched element, the domain subdivision is needed in order to achieve exact integration results. Other comparable integration approaches are also found in [35, 36]. In this scope, the proposed formulation is an ideal fit, providing accurate results by means of an efficient numerical integration technique, without the need for splitting the domain. Moreover, the formulation can handle not only intersecting cracks but also cracks that cross an element without intersecting each other. This allows for various applications also in other domains such as computer graphics, computational geometry, or as an effective method for the evaluation of integrals over complex domain shapes, obtained by trimming a regular quadrilateral domain with one or two discontinuities (as investigated in [150]).

Let us consider a body $\mathscr{B}$ and let $\boldsymbol{u}$ be the displacement field so that the local partition of unity (PU) approximation field referred to the set of variables $\boldsymbol{x} = (x, y)$ is

$$\boldsymbol{u}(\boldsymbol{x}) = \sum_{I \in n} N_I(\boldsymbol{x})(\boldsymbol{u}_I + \boldsymbol{a}_I \Psi(\boldsymbol{x})) \tag{5.2}$$

in which n is the number of nodes of the finite element mesh, $N_I(\boldsymbol{x})$ are the finite elements shape functions, $\Psi(\boldsymbol{x})$ is the enrichment function and $\boldsymbol{u}_I$ and $\boldsymbol{a}_I$ are the standard and enriched nodal variables, respectively. Let us assume that $\boldsymbol{d}$ is an ensemble of m discontinuity surfaces, and let $s_i(\boldsymbol{x})$ be the signed distance of a point $\boldsymbol{x}$ to the i-th discontinuity surface d_i. In the case of a strong discontinuity (e.g., a crack), the discontinuity in the displacement field can be described considering the standard Heaviside step function as the enrichment function Ψ [33]:

$$\Psi(\boldsymbol{x}) = H(\boldsymbol{x}) = \text{sign}(s_i(\boldsymbol{x})) = \begin{cases} 1 & \text{if } s_i(\boldsymbol{x}) \geq 0 \\ 0 & \text{if } s_i(\boldsymbol{x}) < 0 \end{cases} \tag{5.3}$$

As discussed in 3.3, the enrichment function is to be applied to the nodes of the elements crossed by the discontinuity. Furthermore, the presence in the enriched elements of the enrichment function in (5.3) by way of (5.2) affects the precision of the standard Gauss quadrature method for calculating the element stiffness matrix,

which results ill-suited for this scenario. As stated in Section 5.1, the standard approach is to divide the element domain into quadrature subdomains, which are defined by the i-th discontinuity surface d_i [22]. In the following Subsections, the proposed formulation to circumvent the subdivision of the domain in the case of a double discontinuity is presented. In 5.3, the problem of a quadrilateral finite element cut by strong discontinuities will be illustrated. Starting from the assumption presented in 4.3, the proposed formulation is firstly introduced and validated for a 2D quadrilateral element, and then extended for other 2D and 3D element domains in the subsequent Sections.

5.3 Closed form solution for quadrilateral integration domains

The eventuality of multiple discontinuities in the same finite element is not unusual in the context of fracture mechanics [28], for instance when crack branching, kinking or junction occurs, both in linear and nonlinear materials [29, 21, 30–32]. Let us consider the body $\mathscr{B}$ defined in Section 5.2 and a quadrilateral element of its mesh, Ω, supposing it is divided into four portions by the discontinuity lines q and r, as showed in Figure 5.1. Let us define Ω_A as the portion obtained when the normal to each discontinuity points inwards. Starting from Ω_A, the remaining partitions (Ω_B, Ω_C and Ω_D) are defined counterclockwise by convention.
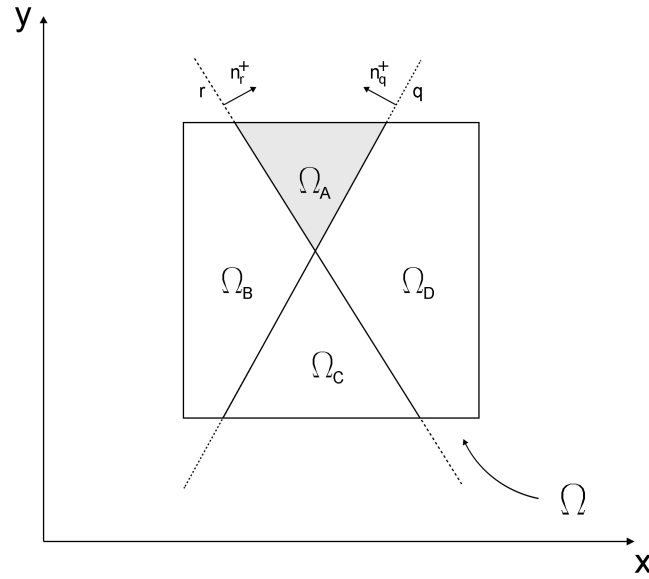
Fig. 5.1 A 2D quadrilateral domain Ω crossed by two discontinuity lines: *q* and *r*. Reproduced with permission from Integration of Polynomials Times Double Step Function in Quadrilateral Domains for XFEM Analysis, Fichera S., Mariggiò G., Corrado M., Ventura G., Algorithms; published by MDPI, 2023.

In the context of XFEM, the element stiffness matrix has to be evaluated on each of the four subdomains Ω_A, Ω_B, Ω_C or Ω_D. As seen in (3.33), discontinuous functions times polynomials that cannot be integrated using standard quadrature rules over the entire domain Ω will be contained in such a matrix.

It has to be noted that the Heaviside step function (5.3) is defined so that the integrand function is zeroed on the subdomains with negative signed distance, thus a proper definition of the normal vector of the discontinuities allows to perform the quadrature on each subdomain. This also grants a direct extension of the proposed formulation to the generalised Heaviside function, having values $+1$ and -1 on the two sides of the discontinuity instead of $+1$ and 0, as defined in (5.3).

Let us assume an *n*th-degree polynomial $\mathscr{P}_n(\boldsymbol{x})$ to be integrated across the subdomains Ω_A, Ω_B, Ω_C or Ω_D obtained by partitioning a regular 2×2 square centred in $(0,0)$ on the (x,y) reference system with two lines *q* and *r*, so it is

$$I_i = \int_{\Omega_i} \mathscr{P}_n(\boldsymbol{x}) \, \mathrm{d}\Omega \tag{5.4}$$

where: $i = \{A, B, C, D\}$ and $\mathscr{P}_n(\boldsymbol{x}) = k_0 + k_1 x + k_2 x^2 + k_3 xy + k_4 y + k_5 y^2 + \ldots + k_{m-1} x^n + k_m y^n$.

The definition of each integration subdomain Ω_i is needed in order to evaluate the integral in (5.4) for each value of i with standard quadrature rules. This is not always a straightforward task due to the eventuality of rather complex polygonal shapes generated by the integration domain, depending on the slope of the lines.

The main objective is to use the equivalent polynomials for the two discontinuities q and r in order to allow, for each subdomain Ω_i, the integration over the entire element domain Ω by means of the standard Gauss-Legendre quadrature rule, i.e., to compute (5.4) with integrations on the entire element domain Ω instead of Ω_i.

Let $\tilde{H}_{q+}$ and $\tilde{H}_{r+}$ be the equivalent polynomials related to the normals $\mathbf{n}_{q+}$ and $\mathbf{n}_{r+}$, and $\tilde{H}_{q-}$ and $\tilde{H}_{r-}$ be the equivalent polynomials related to the reversed normals $-\mathbf{n}_{q+}$ and $-\mathbf{n}_{r+}$. With reference to Figure 5.1, we have:

$$I_A + I_D = \int_{\Omega_A \cup \Omega_D} \mathscr{P}_n(\boldsymbol{x}) \, d\Omega = \int_{\Omega} \tilde{H}_{r+}(\boldsymbol{x}) \mathscr{P}_n(\boldsymbol{x}) \, d\Omega \tag{5.5}$$

$$I_A + I_B = \int_{\Omega_A \cup \Omega_B} \mathscr{P}_n(\boldsymbol{x}) \, d\Omega = \int_{\Omega} \tilde{H}_{q+}(\boldsymbol{x}) \mathscr{P}_n(\boldsymbol{x}) \, d\Omega \tag{5.6}$$

$$I_B + I_C = \int_{\Omega_B \cup \Omega_C} \mathscr{P}_n(\boldsymbol{x}) \, d\Omega = \int_{\Omega} \tilde{H}_{r-}(\boldsymbol{x}) \mathscr{P}_n(\boldsymbol{x}) \, d\Omega \tag{5.7}$$

$$I_C + I_D = \int_{\Omega_C \cup \Omega_D} \mathscr{P}_n(\boldsymbol{x}) \, d\Omega = \int_{\Omega} \tilde{H}_{q-}(\boldsymbol{x}) \mathscr{P}_n(\boldsymbol{x}) \, d\Omega \tag{5.8}$$

Equations (5.5) to (5.8) give a system of four equations in the four unknowns I_A, I_B, I_C and I_D that, in general, can be proved to be indeterminate. In particular, it can be observed that if the intersection point between the two discontinuities q and r is external to the element domain or is on its boundary, then the solution will be unique. If the intersection point lies inside the element domain, the system will be indeterminate, with the system coefficient matrix having rank three.

When the intersection point between the two discontinuities q and r is internal to the element domain, the above observation suggests the introduction of an auxiliary integration limit s along the abscissa axis of the element domain to eliminate indeterminacy. The line $x = s$ contains the discontinuities intersection point P and is parallel to the vertical axis of the reference system. It should be noted that the introduction of the auxiliary integration limit s keeps the reduced integration domain rectangular, so that standard quadrature rules can be applied.

Let $\tilde{H}_{q+}^{(s)}(\boldsymbol{x})$ and $\tilde{H}_{r+}^{(s)}(\boldsymbol{x})$ be the equivalent polynomial functions for the discontinuities q and r evaluated into the regular 2×2 square element (called the *parent element*), with respect to the domain bounded by s (Figure 5.2). Combining them together, it is possible to find the equivalent polynomial $\tilde{H}_i(\boldsymbol{x})$:

$$I_i = \int_{\Omega_i} \mathscr{P}_n(\boldsymbol{x}) \, \mathrm{d}\Omega = \int_{\Omega} \tilde{H}_i(\boldsymbol{x}) \mathscr{P}_n(\boldsymbol{x}) \, \mathrm{d}\Omega \tag{5.9}$$

(a)   (b)
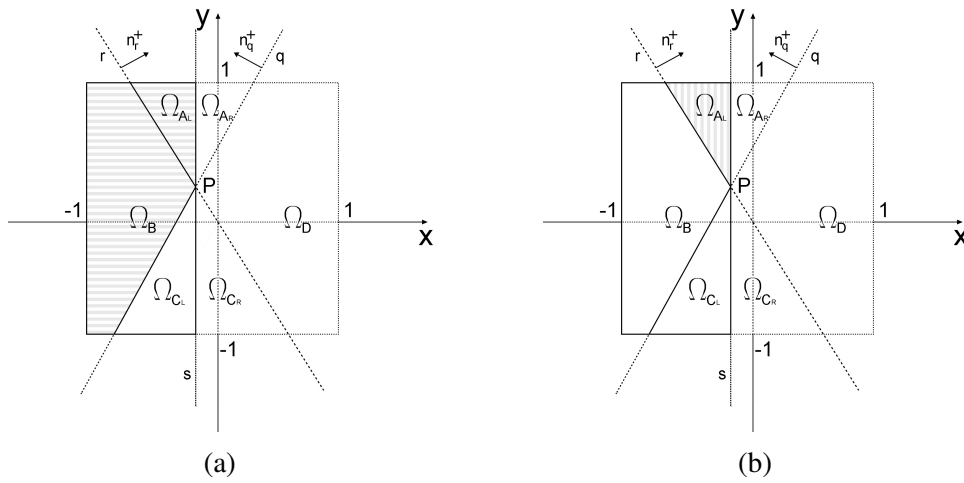
Fig. 5.2 Use of the auxiliary integration limit s to evaluate the equivalent polynomials $\tilde{H}_i(\boldsymbol{x})$. In the figure $\tilde{H}_B(\boldsymbol{x}) = \tilde{H}_{q+}^{(s)}(\boldsymbol{x}) - \tilde{H}_{r+}^{(s)}(\boldsymbol{x})$. (**a**) Integration domain evaluated by means of $\tilde{H}_{q+}(\boldsymbol{x})$ with respect to the discontinuity q and the auxiliary integration limit s. (**b**) Integration domain evaluated by means of $\tilde{H}_{r+}(\boldsymbol{x})$ with respect to the discontinuity r and the auxiliary integration limit s. Reproduced with permission from Integration of Polynomials Times Double Step Function in Quadrilateral Domains for XFEM Analysis, Fichera S., Mariggiò G., Corrado M., Ventura G., Algorithms; published by MDPI, 2023.

With reference to Figure 5.2, the equivalent polynomial functions to perform the integration on each of the four areas in (5.9) are

$$\tilde{H}_A(\boldsymbol{x}) = \tilde{H}_{q+}(\boldsymbol{x}) - \tilde{H}_B(\boldsymbol{x}) \tag{5.10}$$

$$\tilde{H}_B(\boldsymbol{x}) = \tilde{H}_{q+}^{(s)}(\boldsymbol{x}) - \tilde{H}_{r+}^{(s)}(\boldsymbol{x}) \tag{5.11}$$

$$\tilde{H}_C(\boldsymbol{x}) = \tilde{H}_{r-}(\boldsymbol{x}) - \tilde{H}_B(\boldsymbol{x}) \tag{5.12}$$

$$\tilde{H}_D(\boldsymbol{x}) = \tilde{H}_{r+}(\boldsymbol{x}) - \tilde{H}_{q+}(\boldsymbol{x}) + \tilde{H}_B(\boldsymbol{x}) \tag{5.13}$$

with the equivalent polynomial functions $\tilde{H}_A(\boldsymbol{x})\ldots\tilde{H}_D(\boldsymbol{x})$ representing linear combinations of equivalent polynomials for the single discontinuity lines q and r, they will depend on the equations of the two discontinuities and, according to [22, 27], will have the same degree of $\mathscr{P}_n(\boldsymbol{x})$ and the algebraic polynomial form:

$$\tilde{H}_i(\boldsymbol{x}) = \boldsymbol{c} \cdot \boldsymbol{m}(\boldsymbol{x}) \tag{5.14}$$

where the vector $\boldsymbol{m}(\boldsymbol{x})$ gather a monomial basis, i.e., $\boldsymbol{m}(\boldsymbol{x}) = (1, x, y, x^2, \ldots)$, and $\boldsymbol{c}$ is a vector of coefficients [28]. Since $\tilde{H}_i(\boldsymbol{x})\mathscr{P}_n(\boldsymbol{x})$ is a polynomial function that is continuous over the entire domain, Ω, it can be exactly integrated with a proper quadrature rule. It has to be noted that the integrand in (5.9) has doubled its degree, compared to the one in (5.4), thus slightly increasing the computational effort. The main advantage of this approach is that it allows integration over the standard domain Ω or its rectangular restriction defined by the line s, rather than the non-standard partitioned subdomains $\Omega_A \ldots \Omega_D$.

Analytical expressions of the equivalent polynomials $\tilde{H}_i(\boldsymbol{x})$ are excessively long and are not reported in this text. However, the analytical procedure to obtain the exact expressions by means of the software *Wolfram Mathematica* is reported in the Appendix (A.1.1).

5.3.1 Integration algorithm for quadrilateral domains

The purpose of the proposed integration technique is to deliver the expression for the equivalent polynomial function $\tilde{H}_i(\boldsymbol{x})$, in order to compute the integral in Equation (5.9) without splitting the integration domain. The usefulness of the proposed algorithm is presented by way of a generic example. Let us consider a polynomial $\mathscr{P}_n(\boldsymbol{x})$ to be integrated over a subdomain $\bar{\Omega}_A$, generated by dividing a parallelogram $\bar{\Omega}$ with two lines $\bar{q}$ and $\bar{r}$, as shown in Figure 5.3a. The problem is defined in the global coordinate system $\boldsymbol{x} = (x, y)$. Applying Equation (5.9) after the equivalent polynomial function $\tilde{H}_A(\boldsymbol{x})$ determines:

$$I = \int_{\bar{\Omega}_A} \mathscr{P}_n(\boldsymbol{x}) \, \mathrm{d}\bar{\Omega} = \int_{\bar{\Omega}} \tilde{H}_A(\boldsymbol{x}) \mathscr{P}_n(\boldsymbol{x}) \, \mathrm{d}\bar{\Omega} \tag{5.15}$$

Beforehand, the problem has to be mapped to a standard quadrature domain. Therefore, a change in variables from the (x, y) coordinate system to the parent

coordinate system (ξ, η) is employed in order to compute the integral over a standard and regular domain (see eq. (4.10)), as illustrated in Figure 5.3b. By means of such a procedure, single parent geometry can be used to address various scenarios. Thus, parallelograms having any position and size in the global coordinate system can be mapped to the square parent geometry in the local coordinate system $(\xi, \eta) \in [-1, +1]$ illustrated in Figure 5.3b.

(a)   (b)
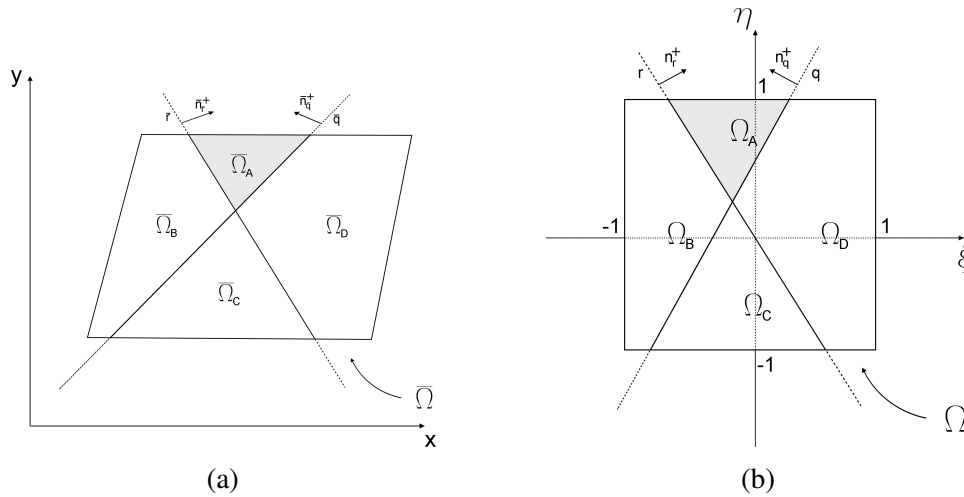
Fig. 5.3 Isoparametric mapping of a quadrilateral element. (**a**) Element configuration in the global coordinate system. (**b**) Element configuration in the parent coordinate system. Reproduced with permission from Integration of Polynomials Times Double Step Function in Quadrilateral Domains for XFEM Analysis, Fichera S., Mariggiò G., Corrado M., Ventura G., Algorithms; published by MDPI, 2023.

The mathematical concept used in the proposed algorithm (as well as in the *DD_EQP* library) for this purpose is *isoparametric mapping*, which is commonly employed in the FEM [37, 19]. Let $P(\xi, \eta) \in \Omega$ be a generic point in the parent reference system, corresponding to the point $\bar{P}(x, y) \in \bar{\Omega}$ in the global reference system. The mapping of $P(\xi, \eta)$ onto $\bar{P}(x, y)$ is described by:

$$x = \sum_{i=1}^{v} N_i(\xi, \eta) x_i \qquad (5.16a)$$

$$y = \sum_{i=1}^{v} N_i(\xi, \eta) y_i \qquad (5.16b)$$

where v is the number of nodes of the geometric element denoted by coordinates (x_i, y_i) in the global reference system, and $N_i(\xi, \eta)$ is the shape function in terms of local coordinates for the parent element i-th node [28].

Likewise, the discontinuities $\bar{q}(\boldsymbol{x})$ and $\bar{r}(\boldsymbol{x})$ equations, defined in the global reference system, have to be mapped onto $q(\boldsymbol{\xi})$ and $r(\boldsymbol{\xi})$, defined in the parent coordinate system (Figure 5.3). This is achieved, for each discontinuity, by:

- Calculating the signed distances (D_i) in the global coordinate system between each discontinuity and each node of the integration domain;

- Writing the discontinuity coefficients (a, b and c) in the parent coordinate system as a function of D_i by solving a linear equations system;

- Substituting the variables x and y in $\bar{q}(\boldsymbol{x})$ and $\bar{r}(\boldsymbol{x})$ by means of Equation (5.16), so that $q(\boldsymbol{\xi})$ and $r(\boldsymbol{\xi})$ are obtained in terms of the coefficients a', b' and c' dependent on D_i.

For a 2D square parent element, the coefficients are:

$$a' = \frac{D_2 - D_1}{2} \tag{5.17a}$$

$$b' = \frac{D_3 - D_1}{2} \tag{5.17b}$$

$$c' = \frac{D_2 + D_3}{2} \tag{5.17c}$$

After $\bar{q}(\boldsymbol{x})$ and $\bar{r}(\boldsymbol{x})$ are transformed into $q(\boldsymbol{\xi})$ and $r(\boldsymbol{\xi})$, the correct expression for the equivalent polynomial function $\tilde{H}_i(\boldsymbol{x})$ with respect to the parent domain coordinate system can be generated. The coordinates and integration domain transformation in the quadrature are then introduced using the Jacobian matrix, which contains the partial derivatives of the interpolation functions N_i that are differentiated with respect to the parent system variables (ξ, η) [140].

$$I = \int_{\bar{\Omega}} \tilde{H}_i(\boldsymbol{x}) \mathscr{P}_n(\boldsymbol{x}) \, d\bar{\Omega} = \int_{\Omega} \tilde{H}_i(\boldsymbol{\xi}) \mathscr{P}_n(\boldsymbol{\xi}) |\boldsymbol{J}| d\Omega =$$
$$= \sum_{j=1}^{gp} w_j \tilde{H}_i(\xi_j, \eta_j) \mathscr{P}_n(\xi_j, \eta_j) |\boldsymbol{J}(\xi_j, \eta_j)| \tag{5.18}$$

where $|\boldsymbol{J}|$ is the Jacobian matrix determinant. The integral in Equation (5.15) is calculated in (5.18), applying the standard scheme of the Gauss–Legendre numerical quadrature [175]. In (5.18), gp stands for the number of Gauss-Legendre quadrature points and w_j stands for each point weight. It needs to be emphasised that the proposed algorithm is intended for integration over the entire domain $\bar{\Omega}$ yielding the result of the integral over the subdomains $\bar{\Omega}_A$, $\bar{\Omega}_B$, $\bar{\Omega}_C$ and $\bar{\Omega}_D$. Thus, the discontinuities equations have to be accurately defined, so that the unit vectors $\boldsymbol{n_i}^+$ point inwards. Additionally, it has to be noted that the discontinuities do not necessarily have to intersect $\bar{\Omega}$ or one another (the proposed algorithm can handle all possible scenarios). The composition and the degree of the polynomials that can be precisely integrated using the suggested technique rely on specific requirements necessary to find the equivalent polynomial, as can be deduced from Refs. [22, 27].

The presented algorithm has been implemented into a Fortran library called *double discontinuity EQP, DD_EQP*, which provides the expressions of the equivalent polynomial functions $\tilde{H}_i(\boldsymbol{x})$ for 2D quadrilateral integration domains as a function of the position of two discontinuity lines. In this Section, the library is used to validate the proposed algorithm and prove its robustness by means of numerical testing. The equivalent polynomial functions $\tilde{H}_i(\boldsymbol{x})$ are evaluated into a regular square parent element. More details about the mathematical formulation employed to compute the equivalent polynomial $\tilde{H}_i(\boldsymbol{x})$ for each discontinuity have been presented in Chapter 4, and can be found in [22, 27]. It has to be noted that the proposed integration technique can be extended to a standard triangular parent element (which is described in Subsection 5.4.1), as well as to 3D parent elements, such as tetrahedrons and hexahedrons (wich is discussed in Section 5.5 and 5.6).
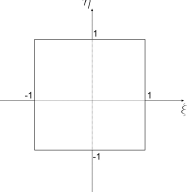
In the following subsections, the library architecture is presented and two numerical tests are carried out. The results obtained by means of the proposed algorithm are then compared with other integration methods and validated, in order to demonstrate the effectiveness and precision of the proposed formulation, as well as the usefulness of the library implementing it.

5.3.2   *DD_EQP* library architecture

The library source code is freely available and usable. The fundamental file of the library is *dd_eqpol.f90*, in which the algorithm to map the discontinuities from the

global coordinate system to the parent coordinate system (retrieving their coefficients) and the algorithm to evaluate the equivalent polynomial functions $\tilde{H}_i(\boldsymbol{x})$ are contained. Other files that include the coefficients' analytical expressions, required to evaluate the equivalent polynomial functions, complete the system. Table 4.1 contains a list of the monomials that the integrand polynomial function can be made up of. Nevertheless, in each of the analysed domains, the library may be extended to any polynomial degree. Note that the method provides exact results for constant Jacobian and approximate results for non-constant Jacobian [22, 27].

Table 5.1 Integration domain, domain type, parent element domain and monomial basis included in the library. Reproduced with permission from Integration of Polynomials Times Double Step Function in Quadrilateral Domains for XFEM Analysis, Fichera S., Mariggiò G., Corrado M., Ventura G., Algorithms; published by MDPI, 2023.

Domain of Integration	*etype*	Parent Domain	Monomial Basis
Parallelogram	21		$1, \xi, \xi^2, \eta, \xi\eta, \eta^2$

The library is completed by the module file *class_Quad.f90*, which contains the 2D square finite element Class and all the methods needed to perform the element isoparametric mapping and to evaluate the integral in (5.18). The module file *i_functions.f90*, containing the methods to handle the data input via text file, is also provided. A main program file, *main.f90*, which implements both the library and the 2D square element Class is provided for the purpose of usage demonstration. The practical use of the library follows these steps:

1. Primary data preparation:

   • Individuation of the domain nodal coordinates in the global coordinate system;

   • Individuation of the discontinuities coefficients in the global coordinate system;

- Selection of the domain portions to be evaluated.

2. Isoparametric mapping onto the parent element domain and computation of the coefficient vector of the equivalent polynomial by means of the *DD_Heqpol_coefficients* subroutine.

3. Quadrature by way of any chosen rule (i.e., (5.18)) in which the equivalent polynomial values at the quadrature points are provided by the function *HeqPol* and the Jacobian matrix determinant is given by the function *detJ*.

In order to obtain exact quadrature results by means of the current version of the library, the following conditions have to be met:

- The Jacobian of the transformation in (5.18) has to be constant;

- The polynomial $\mathscr{P}_n$ in (5.15) is a linear combination of the monomials presented in Table 4.1.

It should be noted that two calls are needed if users seek to directly incorporate the core of the library into their own quadrature algorithm: one call to the subroutine *Heqpol_coefficients* for each integration domain (step 2, mentioned previously), and one to the function *HeqPol* for each quadrature point (step 3, mentioned previously). Notice that users can add their own quadrature algorithm directly into the element Class. In this case, a new method has to be defined within the element Class and a call to this method in the *EvalQuad* and *EvalQuadFromFile* subroutines has to be foreseen.

5.3.3   Numerical testing and validation

In this Subsection the *DD_EQP* library has been used to test and validate the proposed formulation for 2D quadrilateral integration domains by means of two numerical examples. The results produced by the library are exact with machine precision.

Parallelogram partitioned by two discontinuities intersecting within the element

The parallelogram element $\bar{\Omega}$ shown in Figure 5.4a as a part of a bigger body discretisation is examined in the first example. All dimensions are in meters. The element nodal coordinates, with respect to the global reference system (x, y), are:

- $\mathbf{1} \equiv (0.5, 3.0)$;

- $\mathbf{2} \equiv (2.0, 1.5)$;

- $\mathbf{3} \equiv (6.0, 2.5)$;

- $\mathbf{4} \equiv (4.5, 4.0)$.

and it is crossed by two discontinuities, described by means of the lines q and r:

- $q : \frac{7}{4}x - y - \frac{7}{2} = 0$;

- $r : \frac{7}{4}x + y - \frac{21}{2} = 0$.

and split into the subdomains $\bar{\Omega}_A$, $\bar{\Omega}_B$, $\bar{\Omega}_C$ and $\bar{\Omega}_D$. The objective is to evaluate the inertia tensor and the area of $\bar{\Omega}_B$, namely solving the integral in (5.19) by means of the proposed formulation without subdividing the integration domain $\bar{\Omega}$.

$$\int_{\bar{\Omega}} \boldsymbol{m}(\boldsymbol{x}) H_q(\boldsymbol{x}) H_r(\boldsymbol{x}) \, \mathrm{d}\Omega \tag{5.19}$$

where vector $\boldsymbol{m}(\boldsymbol{x})$ contains the monomial basis for the examined finite element (listed in Table 4.1) and $H_q(\boldsymbol{x})$ and $H_r(\boldsymbol{x})$ are the step functions for each discontinuity line (see (5.3)). Note that the normal to each discontinuity line has to be accurately defined for the sake of obtaining the targeted domain portion (as discussed in Section 5.2).

The software maps the parallelogram $\bar{\Omega}$ onto the parent coordinate system, which is used to compute $\tilde{H}_B(\boldsymbol{x})$ and carry out the integration.

(a)   (b)
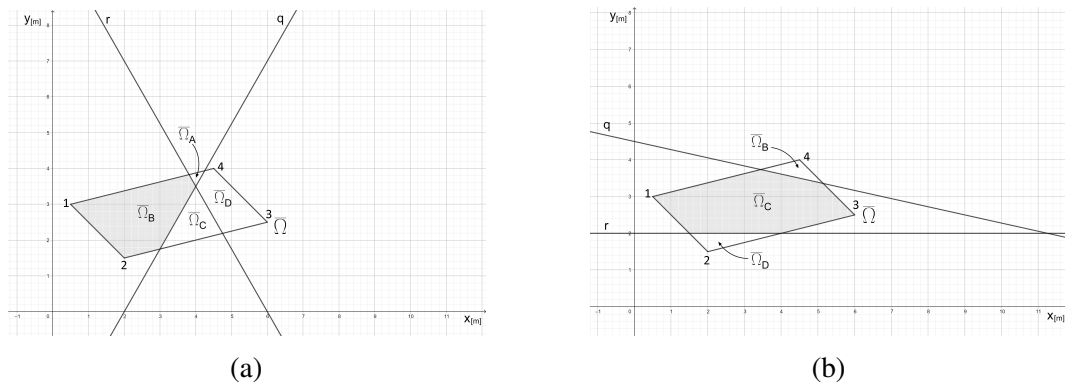
Fig. 5.4 *DD_EQP* illustrative examples. (**a**) Example 1: parallelogram domain cut by two discontinuities intersecting inside the domain. (**b**) Example 2: parallelogram domain cut by two discontinuities intersecting outside the domain. Reproduced with permission from Integration of Polynomials Times Double Step Function in Quadrilateral Domains for XFEM Analysis, Fichera S., Mariggiò G., Corrado M., Ventura G., Algorithms; published by MDPI, 2023.

After launching the library example program, the user has to choose whether to input the data manually as the program executes or select an input data file.

```
Input from file? (y/n): y
example_1.txt
```

For the first example, the input data is provided by the text file *example_1.txt*.

```
\\ DOUBLE DISCONTINUITY EQP LIBRARY
\\ EXAMPLE 1: DISCONTINUITIES INTERSECTING INSIDE THE DOMAIN
$ElementType
\\ 21 : Quad
21
$Coords
\\ Set the coordinates for the element
\\ 1st col : x
\\ 2nd col : y
\\ Coordinates Scheme :
\\  Quad Element :
\\  4-------------3
```

```
\\  |               |
\\  |               |
\\  |               |
\\  |               |
\\  |               |
\\  1-------------2
2.0 1.5
6.0 2.5
4.5 4.0
0.5 3.0
$NumOfDiscont
\\ Number of discontinuities crossing the element (1 or 2)
2
$DiscontCoefficients
\\ a,b,c coefficients for each discontinuity
\\ coefficients are separated by a blank
1.75 -1.0 -3.5
1.75 1.0 -10.5
$ElementPart
\\ In case of 2 discontinuities choose the element portion
\\ to integrate
\\ Part : A, B, C, D, all
\\  3-----4
\\  | \A /|
\\  |B \/D|
\\  | / \ |
\\  |/ C \|
\\  1-----2
B
```

where '\\' identifies a comment in the input section, while '$' identifies an input
command.

The program creates an output file containing the integration results for all the
monomials listed in Table 4.1, referred to as the selected domain part. The integration
result for the monomial $\mathscr{P}_n = 1$ corresponds to the area of the selected domain part,

while the results for the monomials y^2, x^2 and xy correspond to the elements of the inertia tensor I. The results produced by the library for the area A and the inertia tensor I of $\bar{\Omega}_B$, evaluated with respect to the global coordinate system (x, y), are:

$$A = 4.371 \text{ m}^2 \qquad (5.20)$$

$$I = \rho_s \begin{bmatrix} 33.200 & -28.814 \\ -28.814 & 27.670 \end{bmatrix} (\text{units: kg m}^2) \qquad (5.21)$$

where ρ_s is the material surface density (kg/m^2).

In order to estimate the performance and robustness of the proposed algorithm, the integration problem has been addressed by means of the method proposed in [34] (via the integration procedure defined in [7]). The domain $\bar{\Omega}$ has been split into $i = 4$ subdomains ($\bar{\Omega}_A, \bar{\Omega}_B, \bar{\Omega}_C, \bar{\Omega}_D$), in which the functions $H_q(x)$ and $H_r(x)$ are continuous and the integral for the portion of interest $\bar{\Omega}_B$ has been evaluated by means of Gauss quadrature. The integral in (5.19), computed above by way of the *DD_EQP* library, has also been evaluated numerically using the adaptive integration method "*NIntegrate*" of the software *Wolfram Mathematica*. Finally, the integration subdomain $\bar{\Omega}_B$ has been defined in the global reference system (x, y) by way of the intersections between the discontinuity lines q and r and the parallelogram domain $\bar{\Omega}$, and the definite integral at the left-hand side of Equation (5.9) has been exactly computed. The obtained results coincide up to machine precision for all evaluation methods. The error has been estimated as in Eq. (5.22) and the results are shown in Table 5.2.

$$err = \frac{\left| res_{comparison} - res_{proposed} \right|}{res_{comparison}} \qquad (5.22)$$

Table 5.2 Proposed formulation error (percentage) for each computed term compared to other integration methods.

Integrand	Quadrature over $\bar{\Omega}_B$ ([34, 7])	Adaptive integration	Definite integral over $\bar{\Omega}_B$ (5.9)
1	0.00%	0.00%	0.00%
xy	0.00%	0.00%	0.00%
x^2	0.00%	0.00%	0.00%
y^2	0.00%	0.00%	0.00%

Parallelogram partitioned by two discontinuities intersecting outside the element

The parallelogram element $\bar{\Omega}$ shown in Figure 5.4b as a part of a bigger body discretisation is examined in the second example. As before, all dimensions are in meters. The element nodal coordinates, with respect to the global reference system (x,y), are:

- $\mathbf{1} \equiv (0.5, 3.0)$;

- $\mathbf{2} \equiv (2.0, 1.5)$;

- $\mathbf{3} \equiv (6.0, 2.5)$;

- $\mathbf{4} \equiv (4.5, 4.0)$.

and it is crossed by two discontinuities, described by means of the lines q and r:

- $q : \frac{2}{9}x + y - \frac{9}{2} = 0$;

- $r : y - 2 = 0$.

and split into three subdomains: $\bar{\Omega}_A$, $\bar{\Omega}_B$ and $\bar{\Omega}_C$. The aim is to evaluate the inertia tensor and the area of $\bar{\Omega}_C$, namely solving the integral in (5.19) by means of the proposed formulation, without subdividing the integration domain $\bar{\Omega}$.

The input is analogous to the previous example in Figure 5.4a.

The results produced by the library for the area A and the inertia tensor I of $\bar{\Omega}_C$, evaluated with respect to the global coordinate system (x, y), are:

$$A = 6.450 \text{ m}^2 \tag{5.23}$$

$$I = \rho_s \begin{bmatrix} 50.817 & -58.396 \\ -58.396 & 78.392 \end{bmatrix} \text{(units: kg m}^2\text{)} \tag{5.24}$$

where ρ_s is the material surface density (kg/m^2). As in the example in Figure 5.4a, the integral in (5.19), computed above by means of the *DD_EQP* library, has also been evaluated numerically by means of the method proposed in [34], via the adaptive integration strategy *NIntegrate* of the software *Wolfram Mathematica*, and by way of definite integral computation after defining the integration subdomain $\bar{\Omega}_C$. Once again, the obtained results coincide to the level of machine precision for all evaluation methods. The error has been estimated as in Eq. (5.22) and the results are shown in Table 5.3.

Table 5.3 Proposed formulation error (percentage) for each computed term compared to other integration methods.

Integrand	Quadrature over $\bar{\Omega}_C$ ([34, 7])	Adaptive integration	Definite integral over $\bar{\Omega}_C$ (5.9)
1	0.00%	0.00%	0.00%
xy	0.00%	0.00%	0.00%
x^2	0.00%	0.00%	0.00%
y^2	0.00%	0.00%	0.00%

Outcomes

The outcomes of the examples presented in section 5.3.3 and section 5.3.3 validate both the algorithm and the *DD_EQP* library itself, demonstrating the precision, robustness and versatility of the proposed formulation. It has to be noted that, when equivalent polynomials are used, the integrand function doubles its degree, thus requiring a higher computational effort compared to other methods (such as in [34, 33, 7]) [22, 27]. On the other hand, the proposed formulation removes the necessity of defining subdomains, smoothing the overall integration process.

5.4   Closed form solution extension to triangular integration domains

The solution presented in Section 5.3 can be easily extended also to triangular elements. Let us consider the body $\mathscr{B}$ defined in Section 5.2 and a triangular element of its mesh, Ω, supposing it is divided into four portions by the discontinuity lines q and r, as showed in Figure 5.5. Let us define Ω_A as the portion obtained when the normal to each discontinuity points inwards. Starting from Ω_A, the remaining partitions (Ω_B, Ω_C and Ω_D) are defined counterclockwise by convention.
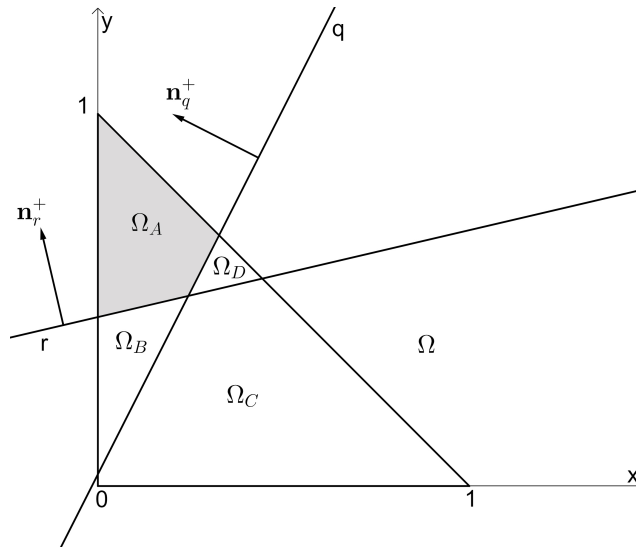
Fig. 5.5 A 2D triangular domain Ω crossed by two discontinuity lines: *q* and *r*.

As discussed before, in the XFEM context the element stiffness matrix has to be evaluated on each of the four subdomains Ω_A, Ω_B, Ω_C or Ω_D. As seen in (3.33), discontinuous functions times polynomials that cannot be integrated using standard quadrature rules over the entire domain Ω will be contained in such a matrix.

It has to be stressed again that the Heaviside step function (5.3) is defined so that the integrand function is zeroed on the subdomains with negative signed distance, thus a proper definition of the normal vector of the discontinuities allows to perform the quadrature on each subdomain. This also grants a direct extension of the proposed formulation to the generalised Heaviside function, having values $+1$ and -1 on the two sides of the discontinuity instead of $+1$ and 0, as defined in (5.3).

Let us assume an nth-degree polynomial $\mathscr{P}_n(\boldsymbol{x})$ to be integrated across the subdomains Ω_A, Ω_B, Ω_C or Ω_D obtained by partitioning a regular triangle element defined by the vertices $\{(0,0),(1,0),(0,1)\}$ on the (x,y) reference system with two lines q and r, as in Eq. (5.4).

The definition of each integration subdomain Ω_i is needed in order to evaluate the integral in (5.4) for each value of i with standard quadrature rules. This is not always a straightforward task due to the eventuality of rather complex polygonal shapes generated by the integration domain, depending on the slope of the lines.

The main objective is to use the equivalent polynomials for the two discontinuities q and r in order to allow, for each subdomain Ω_i, the integration over the entire element domain Ω by means of the standard Gauss-Legendre quadrature rule, i.e., to compute (5.4) with integrations on the entire element domain Ω instead of Ω_i.

As before, let $\tilde{H}_{q+}$ and $\tilde{H}_{r+}$ be the equivalent polynomials related to the normals $\mathbf{n}_{q+}$ and $\mathbf{n}_{r+}$, and $\tilde{H}_{q-}$ and $\tilde{H}_{r-}$ be the equivalent polynomials related to the reversed normals $-\mathbf{n}_{q+}$ and $-\mathbf{n}_{r+}$. With reference to Figure 5.5, is it possible to define again the equations (5.5) to (5.8), which give a system of four equations in the four unknowns I_A, I_B, I_C and I_D that, in general, can be proved to be indeterminate. In particular, it can be observed that if the intersection point between the two discontinuities q and r is external to the element domain or is on its boundary, then the solution will be unique. If the intersection point lies inside the element domain, the system will be indeterminate, with the system coefficient matrix having rank three.

The same mathematical approach presented in Section 5.3 is followed. In the case of intersection point between the two discontinuities q and r being internal to the element domain, the above observation suggests the introduction of an auxiliary integration limit s along the abscissa axis of the element domain to eliminate indeterminacy. As in the case of a qudrilateral domain, the line $s = x$ contains the discontinuities intersection point P and is parallel to the vertical axis of the reference system.

Let $\tilde{H}_{q+}^{(s)}(\boldsymbol{x})$ and $\tilde{H}_{r+}^{(s)}(\boldsymbol{x})$ be the equivalent polynomial functions for the discontinuities q and r evaluated into the regular triangular parent element, with respect to the domain bounded by s (Figure 5.6). Combining them together, it is possible to find the equivalent polynomial $\tilde{H}_i(\boldsymbol{x})$ (as defined in Eq. (5.9)).
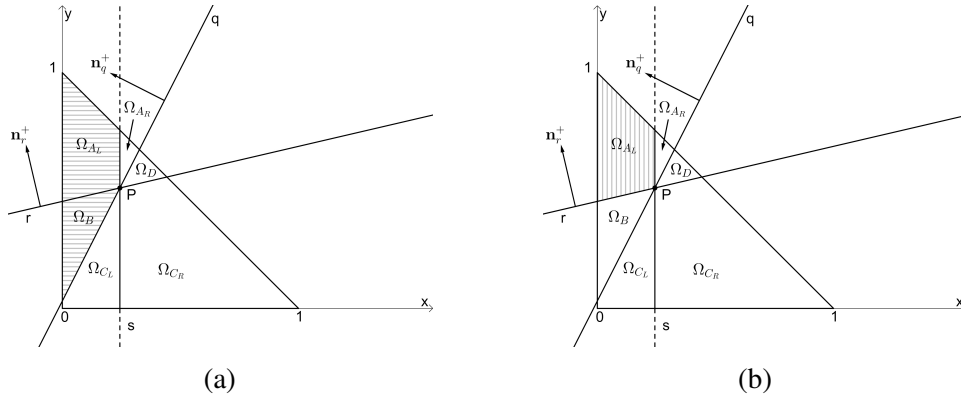
Fig. 5.6 Use of the auxiliary integration limit s to evaluate the equivalent polynomials $\tilde{H}_i(\boldsymbol{x})$. In the figure $\tilde{H}_B(\boldsymbol{x}) = \tilde{H}_{q^+}^{(s)}(\boldsymbol{x}) - \tilde{H}_{r^+}^{(s)}(\boldsymbol{x})$. (a) Integration domain evaluated by means of $\tilde{H}_{q^+}(\boldsymbol{x})$ with respect to the discontinuity q and the auxiliary integration limit s. (b) Integration domain evaluated by means of $\tilde{H}_{r^+}(\boldsymbol{x})$ with respect to the discontinuity r and the auxiliary integration limit s.

As for the quadrilateral element case, with reference to Figure 5.6, it is possible to define the equivalent polynomial functions to perform the integration on each of the four areas in (5.9), which coincide to the ones described in Eq. (5.10). Once again, the equivalent polynomial functions $\tilde{H}_A(\boldsymbol{x}) \ldots \tilde{H}_D(\boldsymbol{x})$ representing linear combinations of equivalent polynomials for the single discontinuity lines q and r, they will depend on the equations of the two discontinuities and, according to [22, 27], will have the same degree of $\mathscr{P}_n(\boldsymbol{x})$ and their algebraic polynomial form is the one described in Eq. (5.14).

Since the same considerations made for the linear triangular parent element discussed in section 4.3.1 can be extended also to the current scenario, the monomial basis constituting the equivalent polynomial for such element is $\boldsymbol{m}(\boldsymbol{x}) = (1)$.

As before, the polynomial function $\tilde{H}_i(\boldsymbol{x})\mathscr{P}_n(\boldsymbol{x})$ is continuous over the entire domain, Ω, thus can be exactly integrated with a proper quadrature rule. It is stressed again that the integrand in (5.9) has doubled its degree, compared to the one in (5.4). The principal advantage of this approach is allowing the exact integration over the standard domain Ω, rather than non-standard partitioned subdomains $(\Omega_A \ldots \Omega_D)$.

Analytical expressions of the equivalent polynomials $\tilde{H}_i(\boldsymbol{x})$ are excessively long and are not reported in this text. However, the analytical procedure to obtain the

exact expressions by means of the software *Wolfram Mathematica* is reported in the Appendix (A.1.2).

5.4.1   Integration algorithm for triangular domains

As for the single discontinuity case illustrated in Chapter 4, the proposed integration technique, presented and validated for quadrilateral domains in section 5.3.1, can be easily and directly extended to a triangular parent element. Once again, the demonstration is carried out by means of a generic example. Let us consider a polynomial $\mathscr{P}_n(\boldsymbol{x})$ to be integrated over a subdomain $\bar{\Omega}_A$, generated by dividing a generic triangle $\bar{\Omega}$ with two lines $\bar{q}$ and $\bar{r}$, as shown in Figure 5.7a. The problem is defined in the global coordinate system $\boldsymbol{x} = (x, y)$. The integration problem to be solved is obtained applying Equation (5.9) after the equivalent polynomial function $\tilde{H}_A(\boldsymbol{x})$ (Eq. (5.15)).

First, the problem has to be mapped to a standard quadrature domain. Therefore, a change in variables from the (x, y) coordinate system to the parent coordinate system (ξ, η) by way of isoparametric mapping is employed in order to compute the integral over a standard and regular domain (see eq. (4.6)), as illustrated in Figure 5.7b. By means of such a procedure, single parent geometry can be used to address various scenarios. Thus, triangles having any position and size in the global coordinate system can be mapped to the square parent geometry in the local coordinate system (ξ, η) illustrated in Figure 5.7b.

| (a) | (b) |
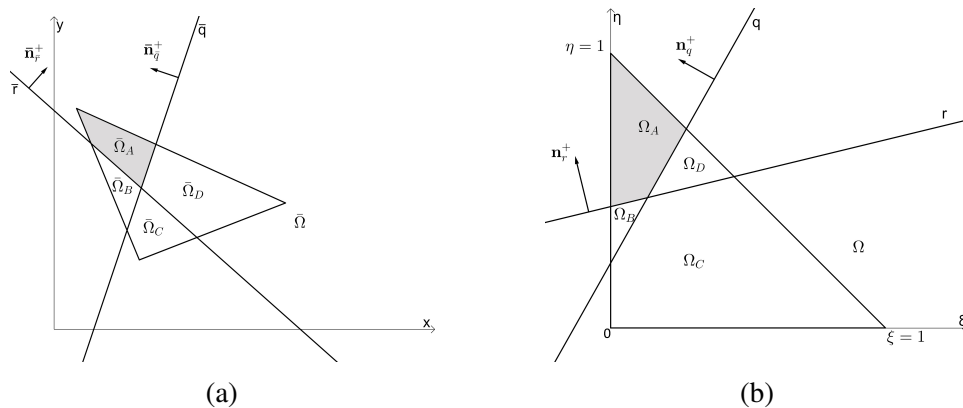
Fig. 5.7 Isoparametric mapping of a triangular element. (**a**) Element configuration in the global coordinate system. (**b**) Element configuration in the parent coordinate system.

Let $P(\xi, \eta) \in \Omega$ be a generic point in the parent reference system, corresponding to the point $\bar{P}(x, y) \in \bar{\Omega}$ in the global reference system. The mapping of $P(\xi, \eta)$ onto $\bar{P}(x, y)$, as before, is described by Eq. (5.16).

Likewise, the discontinuities $\bar{q}(\boldsymbol{x})$ and $\bar{r}(\boldsymbol{x})$ equations, defined in the global reference system, have to be mapped onto $q(\boldsymbol{\xi})$ and $r(\boldsymbol{\xi})$, defined in the parent coordinate system (Figure 5.7). This is achieved by:

- Calculating the signed distances (D_i) in the global coordinate system between each discontinuity and each node of the integration domain;

- Writing the discontinuity coefficients (a, b and c) in the parent coordinate system as a function of D_i by solving a linear equations system;

- Substituting the variables x and y in $\bar{q}(\boldsymbol{x})$ and $\bar{r}(\boldsymbol{x})$ by means of Equation (5.16), so that $q(\boldsymbol{\xi})$ and $r(\boldsymbol{\xi})$ are obtained in terms of the coefficients a', b' and c' dependent on D_i.

For a 2D triangular parent element, the coefficients are:

$$a' = D_2 - D_1 \tag{5.25a}$$

$$b' = D_3 - D_1 \tag{5.25b}$$

$$c' = D_1 \tag{5.25c}$$

As in section 5.3.1, $\bar{q}(\boldsymbol{x})$ and $\bar{r}(\boldsymbol{x})$ are transformed into $q(\boldsymbol{\xi})$ and $r(\boldsymbol{\xi})$, the correct expression for the equivalent polynomial function $\tilde{H}_i(\boldsymbol{x})$ with respect to the parent domain coordinate system can be generated. The coordinates and integration domain transformation in the quadrature are then introduced using the Jacobian matrix, which contains the partial derivatives of the interpolation functions N_i that are differentiated with respect to the parent system variables (ξ, η) [140].

The integral in Equation (5.15) is calculated by means of the standard Gauss-Legendre numerical quadrature rule defined in (5.18) [175]. It has to be highlighted once more that the proposed formulation is intended for integration over the entire domain $\bar{\Omega}$ yielding the result of the integral over the subdomains $\bar{\Omega}_A$, $\bar{\Omega}_B$, $\bar{\Omega}_C$ and $\bar{\Omega}_D$. Thus, the discontinuities equations have to be accurately defined, so that the unit vectors $\boldsymbol{n}_i{}^+$ point inwards. Additionally, it has to be noted that the discontinuities

do not necessarily have to intersect $\bar{\Omega}$ or one another (the presented formulation can handle all possible scenarios). The composition and the degree of the polynomials that can be precisely integrated using the suggested technique rely on specific requirements necessary to find the equivalent polynomial, as already discussed in 4 and as can be deduced from Refs. [22, 27].

In the following subsection, some numerical tests are performed in order to demonstrate the precision and efficacy of the presented formulation. The results are compared to other integration methods to validate the proposed technique.

5.4.2   Numerical testing and validation

The formulation presented in section 5.4 for 2D triangular domains has been tested and validated by way of two numerical examples. The results obtained by means of the proposed formulation are exact with machine precision.

Triangle partitioned by two discontinuities intersecting within the element

The triangular element $\bar{\Omega}$ shown in Figure 5.8a as a part of a bigger body discretisation is herein examined. All dimensions are in meters. The element nodal coordinates, with respect to the global reference system (x, y), are:

- $\mathbf{1} \equiv (0.195, 1.910)$;

- $\mathbf{2} \equiv (0.739, 0.599)$;

- $\mathbf{3} \equiv (2.007, 1.092)$.

and it is crossed by two discontinuities, described by way of the lines q and r:

- $q : -\frac{887}{1000}x - y + \frac{1891}{1000} = 0$;

- $r : \frac{297}{100}x - y - \frac{128}{125} = 0$.

and split into the subdomains $\bar{\Omega}_A$, $\bar{\Omega}_B$, $\bar{\Omega}_C$ and $\bar{\Omega}_D$. The objective is to evaluate the area of $\bar{\Omega}_D$, namely solving the integral in Eq. 5.19 by means of the proposed formulation without subdividing the integration domain $\bar{\Omega}$, in which the monomial

basis vector is $\boldsymbol{m}(\boldsymbol{x}) = (1)$, and $H_q(\boldsymbol{x})$ and $H_r(\boldsymbol{x})$ are the step functions for each discontinuity line (see (5.3)). Note that the normal to each discontinuity line has to be accurately defined in order to obtain the desired domain portion (as discussed in Section 5.3.1).

In order to set up the proposed integration technique, as described in section 5.4.1, the triangle $\bar{\Omega}$ has to be mapped onto the parent coordinate system, which is used to compute $\tilde{H}_B(\boldsymbol{x})$ and carry out the integration. This is performed by means of the shape functions defined in eq. (4.6), while the coefficients for the two discontinuities are brought back to the parent coordinate system by way of the expressions defined in eq. (5.25).

(a)   (b)
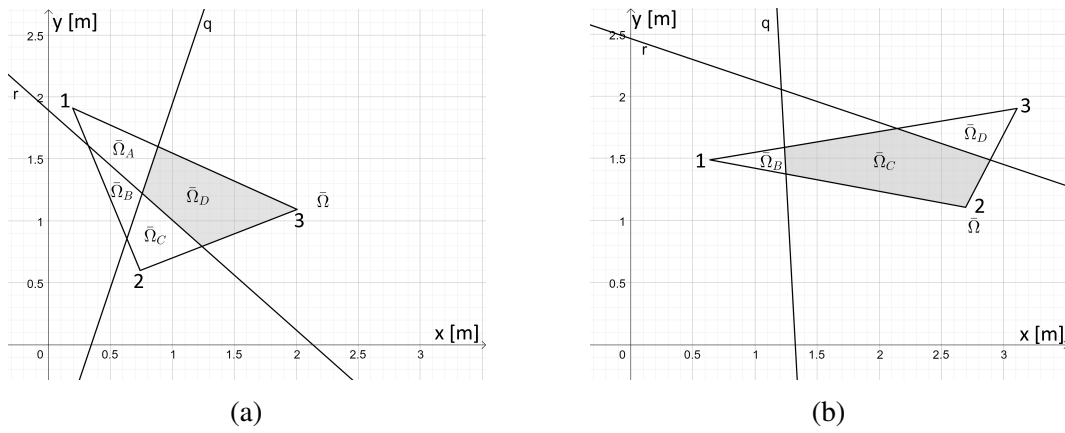
Fig. 5.8 Proposed formulation testing on triangular domains. (**a**) Example 1: triangle domain cut by two discontinuities intersecting inside the domain. (**b**) Example 2: triangle domain cut by two discontinuities intersecting outside the domain.

Since the equivalent polynomials $\tilde{H}_i(\boldsymbol{x})$ only depends on the values of the discontinuities coefficients, the exact computation is straightforward. It is then possible to move forward by applying the quadrature rule in eq. (5.18), in which the monomial $\mathscr{P}_n = 1$ corresponds to the area of the selected domain part. The results evaluated with respect to the global coordinate system (x, y), are:

$$A = 0.481 \text{ m}^2 \tag{5.26}$$

In order to estimate the performance and robustness of the proposed algorithm, the integration problem has been addressed by means of the method proposed in [34] (via the integration procedure defined in [7]). The domain $\bar{\Omega}$ has been split into

$i = 4$ subdomains $(\bar{\Omega}_A, \bar{\Omega}_B, \bar{\Omega}_C, \bar{\Omega}_D)$, in which the functions $H_q(x)$ and $H_r(x)$ are continuous and the integral for the portion of interest $\bar{\Omega}_B$ has been evaluated by means of Gauss quadrature. The integral for the portion of interest has also been evaluated numerically using the adaptive integration method "*NIntegrate*" of the software *Wolfram Mathematica*. Finally, the integration subdomain $\bar{\Omega}_B$ has been defined in the global reference system (x, y) by way of the intersections between the discontinuity lines q and r and the parallelogram domain $\bar{\Omega}$, and the definite integral at the left-hand side of Equation (5.9) has been exactly computed. The obtained results coincide up to machine precision for all evaluation methods. The error has been estimated as in Eq. (5.22) and the results are reported in Table 5.4.

Table 5.4 Proposed formulation error (percentage) for each computed term compared to other integration methods.

Integrand	Quadrature over $\bar{\Omega}_B$ ([34, 7])	Adaptive integration	Definite integral over $\bar{\Omega}_B$ (5.9)
1	0.00%	0.00%	0.00%

Triangle partitioned by two discontinuities intersecting outside the element

The triangle element $\bar{\Omega}$ shown in Figure 5.8b as a part of a bigger body discretisation is herein examined. As before, all dimensions are in meters. The element nodal coordinates, with respect to the global reference system (x, y), are:

- **1** $\equiv (0.637, 1.487)$;

- **2** $\equiv (2.695, 1.106)$;

- **3** $\equiv (3.109, 1.901)$.

and it is crossed by two discontinuities, described by means of the lines q and r:

- $q : -\frac{9147}{500}x - y + \frac{24227}{1000} = 0$;

- $r : -\frac{169}{500}x - y - \frac{2463}{1000} = 0$.

and split into three subdomains: $\bar{\Omega}_B$, $\bar{\Omega}_C$ and $\bar{\Omega}_D$. The aim is to evaluate the inertia tensor and the area of $\bar{\Omega}_C$, namely solving the integral in (5.19) by means of the proposed formulation, without subdividing the integration domain $\bar{\Omega}$.

The procedure is analogous to the previous case in Figure 5.8a.

The results obtained by means of the proposed formulation for the area of $\bar{\Omega}_C$, evaluated with respect to the global coordinate system (x,y), are:

$$A = 0.650 \text{ m}^2 \qquad\qquad (5.27)$$

As in the example in Figure 5.4a, the integral in (5.19), computed above by means of the proposed formulation, has also been evaluated numerically by means of the method proposed in [34], via the adaptive integration strategy *NIntegrate* of the software *Wolfram Mathematica*, and by way of definite integral computation after defining the integration subdomain $\bar{\Omega}_C$. Once again, the obtained results coincide to the level of machine precision for all evaluation methods. The error has been estimated as in Eq. (5.22) and the results are shown in Table 5.5.

Table 5.5 Proposed formulation error (percentage) for each computed term compared to other integration methods.

Integrand	Quadrature over $\bar{\Omega}_C$ ([34, 7])	Adaptive integration	Definite integral over $\bar{\Omega}_C$ (5.9)
1	0.00%	0.00%	0.00%

Outcomes

The outcomes for the tests presented in section 5.4.2 and section 5.4.2 validate proposed formulation, demonstrating its precision, robustness and versatility. As discussed in section 5.3.3, when equivalent polynomials are used, the integrand function doubles its degree, thus requiring a higher computational effort compared to other methods (such as in [34, 33, 7]) [22, 27]. On the other hand, the proposed formulation removes the necessity of defining subdomains, smoothing the overall integration process.

5.5 Closed form solution for hexahedral integration domains

In sections 5.3 and 5.4, a closed form solution for the problem of exactly integrating polynomials times double step function over quadrilateral and triangular domains by way of standard quadrature rules, without defining subdomains, has been presented. In this Section, the extension of the proposed formulation to three-dimensional hexahedral elements is demonstrated. The presence of multiple discontinuities in three-dimensional finite elements is common in certain fracture mechanics applications, for instance in problems involving hydraulic fracture and fracture analysis in rocks [176–181].

Let us consider a body $\mathscr{B}$ and let $\boldsymbol{u}$ be the displacement field so that the local partition of unity (PU) approximation field referred to the set of variables $\boldsymbol{x} = (x, y, z)$ is defined by Eq. (5.2). Let us consider a hexahedral element of its mesh, Ω, supposing it is divided into four portions by the discontinuity planes Q and R, as showed in Figure 5.9. Let us define Ω_A as the portion obtained when the normal to each discontinuity points inwards. Starting from Ω_A, the remaining partitions (Ω_B, Ω_C and Ω_D) are defined counterclockwise by convention.
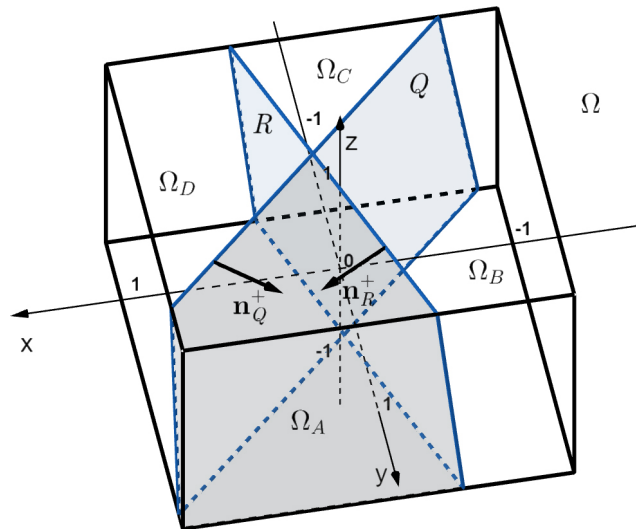
Fig. 5.9 A 3D hexahedral domain Ω crossed by two discontinuity planes: Q and R.

In the context of XFEM, the element stiffness matrix has to be evaluated on each of the four subdomains Ω_A, Ω_B, Ω_C or Ω_D. As seen in (3.33), discontinuous

functions times polynomials that cannot be integrated using standard quadrature rules over the entire domain Ω will be contained in such a matrix.

It has to be noted that the Heaviside step function (5.3) is defined so that the integrand function is zeroed on the subdomains with negative signed distance, thus a proper definition of the normal vector of the discontinuities allows to perform the quadrature on each subdomain. This also grants a direct extension of the proposed formulation to the generalised Heaviside function, having values $+1$ and -1 on the two sides of the discontinuity instead of $+1$ and 0, as defined in (5.3).

Let us assume an nth-degree polynomial $\mathscr{P}_n(\boldsymbol{x})$ to be integrated across the subdomains Ω_A, Ω_B, Ω_C or Ω_D obtained by partitioning a regular $2 \times 2 \times 2$ hexahedron centred in $(0,0,0)$ on the (x,y,z) reference system with two planes Q and R, so it is

$$I_i = \int_{\Omega_i} \mathscr{P}_n(\boldsymbol{x}) \, d\Omega \tag{5.28}$$

where: $i = \{A, B, C, D\}$ and $\mathscr{P}_n(\boldsymbol{x}) = k_0 + k_1 x + k_2 x^2 + k_3 xy + k_4 y + k_5 y^2 + \ldots + k_{m-2} x^n + k_{m-1} y^n + k_m z^n$.

The definition of each integration subdomain Ω_i is needed in order to evaluate the integral in (5.28) for each value of i with standard quadrature rules. This is not always a straightforward task due to the eventuality of rather complex three-dimensional shapes generated by the integration domain, depending on the slope of the discontinuity planes.

The main objective is to use the equivalent polynomials for the two discontinuity planes Q and R in order to allow, for each subdomain Ω_i, the integration over the entire element domain Ω by means of the standard Gauss-Legendre quadrature rule, i.e., to compute (5.28) with integrations on the entire element domain Ω instead of Ω_i.

Let $\tilde{H}_{Q^+}$ and $\tilde{H}_{R^+}$ be the equivalent polynomials related to the normals $\mathbf{n}_{Q^+}$ and $\mathbf{n}_{R^+}$, and $\tilde{H}_{Q^-}$ and $\tilde{H}_{R^-}$ be the equivalent polynomials related to the reversed normals $-\mathbf{n}_{Q^+}$ and $-\mathbf{n}_{R^+}$. With reference to Figure 5.9, we have:

$$I_A + I_D = \int_{\Omega_A \cup \Omega_D} \mathscr{P}_n(\boldsymbol{x}) \, d\Omega = \int_\Omega \tilde{H}_{R^+}(\boldsymbol{x}) \mathscr{P}_n(\boldsymbol{x}) \, d\Omega \tag{5.29}$$

$$I_A + I_B = \int_{\Omega_A \cup \Omega_B} \mathscr{P}_n(\boldsymbol{x}) \, d\Omega = \int_\Omega \tilde{H}_{Q^+}(\boldsymbol{x}) \mathscr{P}_n(\boldsymbol{x}) \, d\Omega \tag{5.30}$$

$$I_B + I_C = \int_{\Omega_B \cup \Omega_C} \mathscr{P}_n(\boldsymbol{x}) \, d\Omega = \int_\Omega \tilde{H}_{R^-}(\boldsymbol{x}) \mathscr{P}_n(\boldsymbol{x}) \, d\Omega \tag{5.31}$$

$$I_C + I_D = \int_{\Omega_C \cup \Omega_D} \mathscr{P}_n(\boldsymbol{x}) \, d\Omega = \int_\Omega \tilde{H}_{Q^-}(\boldsymbol{x}) \mathscr{P}_n(\boldsymbol{x}) \, d\Omega \tag{5.32}$$

Equations (5.29) to (5.32) give a system of four equations in the four unknowns I_A, I_B, I_C and I_D that, in general, can be proved to be indeterminate. In particular, it can be observed that if the intersection line between the two discontinuities Q and R is external to the element domain or is contained on its boundary, then the solution will be unique. If the intersection line lies inside the element domain, the system will be indeterminate, with the system coefficient matrix having rank three.

When the intersection line between the two discontinuities Q and R is internal to the element domain, the above observation suggests the introduction of an auxiliary integration limit S to eliminate indeterminacy.

The plane $S : x = mz + n$ is obtained such that it belongs to the sheaf of planes generated by the intersection line between Q and R and that its normal has null component with respect to the y-axis of the reference system. Being a_1, b_1, c_1, d_1 the coefficients for the plane Q, and a_2, b_2, c_2, d_2 the coefficients for the plane R, with respect to the (x, y, z) coordinate system, it is

$$m = \frac{c_1 + \left(-\frac{b_1}{b_2}\right) c_2}{a_1 + \left(-\frac{b_1}{b_2}\right) a_2} \quad n = \frac{d_1 + \left(-\frac{b_1}{b_2}\right) d_2}{a_1 + \left(-\frac{b_1}{b_2}\right) a_2} \tag{5.33}$$

In order to properly define the equivalent polynomials for all the integration portions, the auxiliary integration limit defined by means of the plane S should be coupled by integration limits also in the z-axis direction. In particular, the domain in which the equivalent polynomial functions for the discontinuities Q and R are evaluated has also to be bounded by planes Z_1 and Z_2. These planes have null components with respect to the x-axis and y-axis of the reference system and contain the intersection line between the plane S and the parent hexaheral domain limits along the x-axis: planes $x = -1$ and $x = 1$. Trivially, integration limits along the

z-axis will coincide to the actual parent domain limits in that direction if plane *S* intersects these bounds (as in the case shown in Figure 5.9).

It should be noted that the introduction of the auxiliary integration limit *S* (and also Z_1 and Z_2, when needed) keeps the reduced integration domain hexahedral, so that standard quadrature rules can be applied.

Let $\tilde{H}_{Q+}^{(S)}(\boldsymbol{x})$ and $\tilde{H}_{R+}^{(S)}(\boldsymbol{x})$ be the equivalent polynomial functions for the discontinuities *Q* and *R* evaluated into the regular $2 \times 2 \times 2$ hexahedral element (called the *parent element*), with respect to the domain bounded by *S* (Figure 5.10). Combining them together, it is possible to find the equivalent polynomial $\tilde{H}_i(\boldsymbol{x})$:

$$I_i = \int_{\Omega_i} \mathscr{P}_n(\boldsymbol{x}) \, d\Omega = \int_{\Omega} \tilde{H}_i(\boldsymbol{x}) \mathscr{P}_n(\boldsymbol{x}) \, d\Omega \qquad (5.34)$$

(a)   (b)
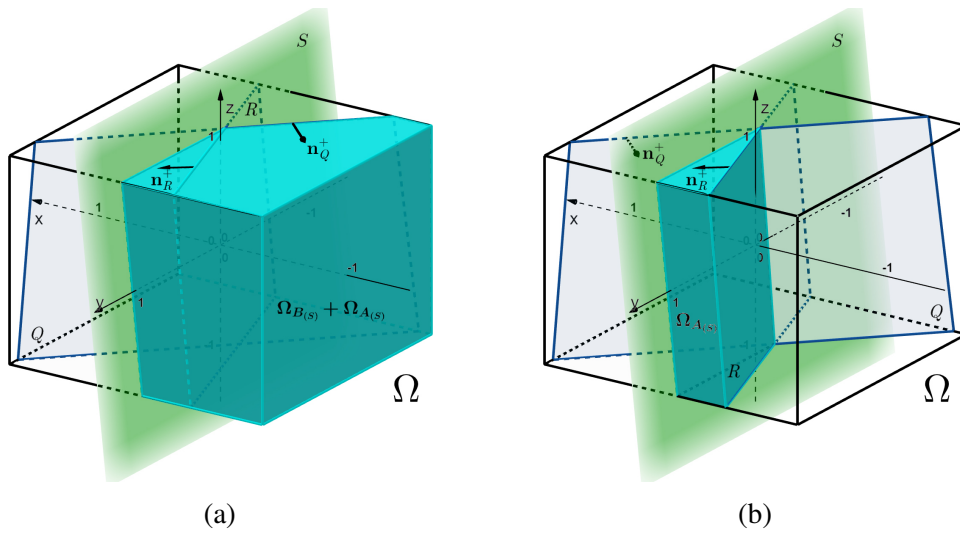
Fig. 5.10 Use of the auxiliary integration limit *S* to evaluate the equivalent polynomials $\tilde{H}_i(\boldsymbol{x})$. In the figure $\tilde{H}_B(\boldsymbol{x}) = \tilde{H}_{Q+}^{(S)}(\boldsymbol{x}) - \tilde{H}_{R+}^{(S)}(\boldsymbol{x})$. (a) Integration domain evaluated by means of $\tilde{H}_{Q+}(\boldsymbol{x})$ with respect to the discontinuity *Q* and the auxiliary integration limit *S*. (b) Integration domain evaluated by means of $\tilde{H}_{R+}(\boldsymbol{x})$ with respect to the discontinuity *R* and the auxiliary integration limit *S*.

With reference to Figure 5.10, the equivalent polynomial functions to perform the integration on each of the four areas in (5.34) are

$$\tilde{H}_A(\boldsymbol{x}) = \tilde{H}_{Q^+}(\boldsymbol{x}) - \tilde{H}_B(\boldsymbol{x}) \tag{5.35}$$

$$\tilde{H}_B(\boldsymbol{x}) = \tilde{H}_{Q^+}^{(S)}(\boldsymbol{x}) - \tilde{H}_{R^+}^{(S)}(\boldsymbol{x}) \tag{5.36}$$

$$\tilde{H}_C(\boldsymbol{x}) = \tilde{H}_{R^-}(\boldsymbol{x}) - \tilde{H}_B(\boldsymbol{x}) \tag{5.37}$$

$$\tilde{H}_D(\boldsymbol{x}) = \tilde{H}_{R^+}(\boldsymbol{x}) - \tilde{H}_{Q^+}(\boldsymbol{x}) + \tilde{H}_B(\boldsymbol{x}) \tag{5.38}$$

with the equivalent polynomial functions $\tilde{H}_A(\boldsymbol{x})\ldots\tilde{H}_D(\boldsymbol{x})$ representing linear combinations of equivalent polynomials for the single discontinuity planes Q and R, they will depend on the equations of the two discontinuities and, according to [22, 27], will have the same degree of $\mathscr{P}_n(\boldsymbol{x})$ and the algebraic polynomial form:

$$\tilde{H}_i(\boldsymbol{x}) = \boldsymbol{c} \cdot \boldsymbol{m}(\boldsymbol{x}) \tag{5.39}$$

where the vector $\boldsymbol{m}(\boldsymbol{x})$ gather a monomial basis, i.e., $\boldsymbol{m}(\boldsymbol{x}) = (1, x, y, x^2, \ldots)$, and $\boldsymbol{c}$ is a vector of coefficients [28]. Since $\tilde{H}_i(\boldsymbol{x})\mathscr{P}_n(\boldsymbol{x})$ is a polynomial function that is continuous over the entire domain, Ω, it can be exactly integrated with a proper quadrature rule. It has to be noted that the integrand in (5.34) has doubled its degree, compared to the one in (5.28), thus slightly increasing the computational effort. The main advantage of this approach is that it allows integration over the standard domain Ω or its hexahedral restriction defined by the auxiliary plane S, rather than the non-standard partitioned subdomains $\Omega_A \ldots \Omega_D$.

Analytical expressions of the equivalent polynomials $\tilde{H}_i(\boldsymbol{x})$ are excessively long and are not reported in this text. However, the analytical procedure to obtain the exact expressions by means of the software *Wolfram Mathematica* is reported in the Appendix (A.1.3).

5.5.1   Integration algorithm for hexahedral domains

The purpose of the proposed integration technique is to deliver the expression for the equivalent polynomial function $\tilde{H}_i(\boldsymbol{x})$, in order to compute the integral in Equation (5.34) without splitting the integration domain. The usefulness of the proposed algorithm is presented by way of a generic example. Let us consider a polynomial $\mathscr{P}_n(\boldsymbol{x})$ to be integrated over a subdomain $\bar{\Omega}_A$, generated by dividing a hexahedron $\bar{\Omega}$ with two planes $\bar{Q}$ and $\bar{R}$, as shown in Figure 5.11a. The problem is defined in the global coordinate system $\boldsymbol{x} = (x, y, z)$. Applying Equation (5.34) after

the equivalent polynomial function $\tilde{H}_A(\boldsymbol{x})$ determines:

$$I = \int_{\bar{\Omega}_A} \mathscr{P}_n(\boldsymbol{x}) \, \mathrm{d}\bar{\Omega} = \int_{\bar{\Omega}} \tilde{H}_A(\boldsymbol{x}) \mathscr{P}_n(\boldsymbol{x}) \, \mathrm{d}\bar{\Omega} \tag{5.40}$$

Beforehand, the problem has to be mapped to a standard quadrature domain. Therefore, a change in variables from the (x, y, z) coordinate system to the parent coordinate system (ξ, η, ζ) is employed in order to compute the integral over a standard and regular domain (see eq. (4.24)), as illustrated in Figure 5.11b. By means of such a procedure, single parent geometry can be used to address various scenarios. Thus, hexahedrons having any position and size in the global coordinate system can be mapped to the hexahedral parent geometry in the local coordinate system $(\xi, \eta, \zeta) \in [-1, +1]$ illustrated in Figure 5.11b.
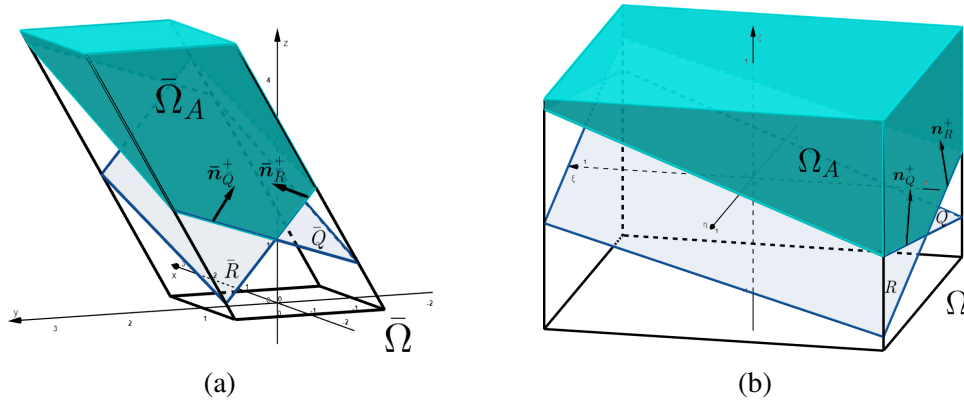
Fig. 5.11 Isoparametric mapping of a hexahedral element. (**a**) Element configuration in the global coordinate system. (**b**) Element configuration in the parent coordinate system.

The mathematical concept used in the proposed technique for this purpose is *isoparametric mapping*, which is commonly employed in the FEM [37, 19]. Let $P(\xi, \eta, \zeta) \in \Omega$ be a generic point in the parent reference system, corresponding to the point $\bar{P}(x, y, z) \in \bar{\Omega}$ in the global reference system. The mapping of $P(\xi, \eta, \zeta)$ onto $\bar{P}(x, y, z)$ is described by:

$$x = \sum_{i=1}^{v} N_i(\xi, \eta, \zeta) x_i \tag{5.41a}$$

$$y = \sum_{i=1}^{v} N_i(\xi, \eta, \zeta) y_i \tag{5.41b}$$

$$z = \sum_{i=1}^{v} N_i(\xi, \eta, \zeta) z_i \tag{5.41c}$$

where v is the number of nodes of the geometric element denoted by coordinates (x_i, y_i, z_i) in the global reference system, and $N_i(\xi, \eta, \zeta)$ is the shape function in terms of local coordinates for the parent element i-th node [28].

Similarly, the discontinuities $\bar{Q}(x)$ and $\bar{R}(x)$ equations, defined in the global reference system, have to be mapped onto $Q(\xi)$ and $R(\xi)$, defined in the parent coordinate system (Figure 5.11). This is achieved, for each discontinuity, by:

- Calculating the signed distances (D_i) in the global coordinate system between each discontinuity and each node of the integration domain;

- Writing the discontinuity coefficients (a, b, c, and d) in the parent coordinate system as a function of D_i by solving a linear equations system;

- Substituting the variables x, y, and z in $\bar{Q}(x)$ and $\bar{R}(x)$ by means of Equation (5.41), so that $Q(\xi)$ and $R(\xi)$ are obtained in terms of the coefficients a', b', c', and d' dependent on D_i.

For a 3D hexahedral parent element, the coefficients are:

$$a' = \frac{D_2 - D_1}{2} \tag{5.42a}$$

$$b' = \frac{D_3 - D_1}{2} \tag{5.42b}$$

$$c' = \frac{D_4 - D_1}{2} \tag{5.42c}$$

$$d' = \frac{D_4 + D_3 + D_2 - D_1}{2} \tag{5.42d}$$

After $\bar{Q}(x)$ and $\bar{R}(x)$ are transformed into $Q(\xi)$ and $R(\xi)$, the correct expression for the equivalent polynomial function $\tilde{H}_i(x)$ with respect to the parent domain coordinate system can be generated. The coordinates and integration domain transformation in the quadrature are then introduced using the Jacobian matrix, which

contains the partial derivatives of the interpolation functions N_i that are differentiated with respect to the parent system variables (ξ, η, ζ) [140].

$$
\begin{aligned}
I &= \int_{\bar{\Omega}} \tilde{H}_i(\boldsymbol{x}) \mathscr{P}_n(\boldsymbol{x}) \, d\bar{\Omega} = \int_{\Omega} \tilde{H}_i(\boldsymbol{\xi}) \mathscr{P}_n(\boldsymbol{\xi}) |\boldsymbol{J}| d\Omega = \\
&= \sum_{j=1}^{gp} w_j \tilde{H}_i(\xi_j, \eta_j, \zeta_j) \mathscr{P}_n(\xi_j, \eta_j, \zeta_j) |\boldsymbol{J}(\xi_j, \eta_j, \zeta_j)|
\end{aligned}
\tag{5.43}
$$

where $|\boldsymbol{J}|$ is the Jacobian matrix determinant. The integral in Equation (5.40) is calculated in (5.43), applying the standard scheme of the Gauss–Legendre numerical quadrature [175]. In (5.43), gp stands for the number of Gauss-Legendre quadrature points and w_j stands for each point weight. It needs to be emphasised that the proposed algorithm is intended for integration over the entire domain $\bar{\Omega}$ yielding the result of the integral over the subdomains $\bar{\Omega}_A$, $\bar{\Omega}_B$, $\bar{\Omega}_C$ and $\bar{\Omega}_D$. Thus, the discontinuities equations have to be accurately defined, so that the unit vectors $\boldsymbol{n_i}^+$ point inwards. Additionally, it has to be noted that the discontinuities do not necessarily have to intersect $\bar{\Omega}$ or one another (the proposed algorithm can handle all possible scenarios). The composition and the degree of the polynomials that can be precisely integrated using the suggested technique rely on specific requirements necessary to find the equivalent polynomial, as can be deduced from Refs. [22, 27].

The equivalent polynomial functions $\tilde{H}_i(\boldsymbol{x})$ are evaluated into a regular hexahedral parent element. As for the previous Sections, more details about the mathematical formulation employed to compute the equivalent polynomial $\tilde{H}_i(\boldsymbol{x})$ for each discontinuity have been presented in Chapter 4, and can be found in [22, 27]. It has to be noted that the proposed integration technique can be extended to a standard tetrahedral parent element (which is described in Subsection 5.6.1).

In the following subsection, some numerical tests are performed in order to demonstrate the precision and efficacy of the proposed formulation. The results are then compared to other integration methods to validate the presented technique.

5.5.2 Numerical testing and validation

The formulation presented in section 5.5 for 3D hexahedral domains has been tested and validated by way of two numerical examples. The results obtained by means of the proposed formulation are exact with machine precision.

Hexahedron partitioned by two discontinuities intersecting within the element

The hexahedral element $\bar{\Omega}$ shown in Figure 5.12a as a part of a bigger body discretisation is herein examined. All dimensions are in meters. The element nodal coordinates, with respect to the global reference system (x, y, z), are:

- **1** $\equiv (-1.0, -1.0, 0.0)$;

- **2** $\equiv (1.0, -1.0, 0.0)$;

- **3** $\equiv (-1.0, 1.0, 0.0)$;

- **4** $\equiv (1.0, 1.0, 0.0)$.

- **5** $\equiv (-1.0, 1.0, 5.0)$

- **6** $\equiv (1.0, 1.0, 5.0)$

- **7** $\equiv (-1.0, 3.0, 5.0)$

- **8** $\equiv (1.0, 3.0, 5.0)$

and it is crossed by two discontinuities, described by way of the planes $\bar{Q}$ and $\bar{R}$:

- $\bar{Q}: -\frac{109}{20}x - \frac{47}{20}y + \frac{247}{50}z - \frac{113}{10} = 0$;

- $\bar{R}: -\frac{11}{5}x + \frac{11}{5}y + \frac{33}{25}z + \frac{507}{100} = 0$;

and split into four subdomains. The objective is to evaluate the inertia tensor and the volume of the highlighted portion $\bar{\Omega}_A$, namely solving the integral in Eq. 5.44 by means of the proposed formulation without subdividing the integration domain $\bar{\Omega}$.

$$\int_{\bar{\Omega}} \boldsymbol{m}(\boldsymbol{x}) H_Q(\boldsymbol{x}) H_R(\boldsymbol{x}) \, \mathrm{d}\Omega \qquad (5.44)$$

where vector $\boldsymbol{m}(\boldsymbol{x})$ contains the monomial basis for the examined finite element (listed in Eq. (4.25)) and $H_Q(\boldsymbol{x})$ and $H_R(\boldsymbol{x})$ are the step functions for each discontinuity line (see (5.3)). Note that the normal to each discontinuity plane has to be accurately defined for the sake of obtaining the targeted domain portion (as discussed in Section 5.3).

In order to set up the proposed integration technique, as described in section 5.5.1, the hexahedron $\bar{\Omega}$ has to be mapped onto the parent coordinate system, which is used to compute $\tilde{H}_A(\boldsymbol{x})$ and carry out the integration. This is performed by means of the shape functions defined in eq. (4.24), while the coefficients for the two discontinuities are brought back to the parent coordinate system by way of the expressions defined in eq. (5.42).
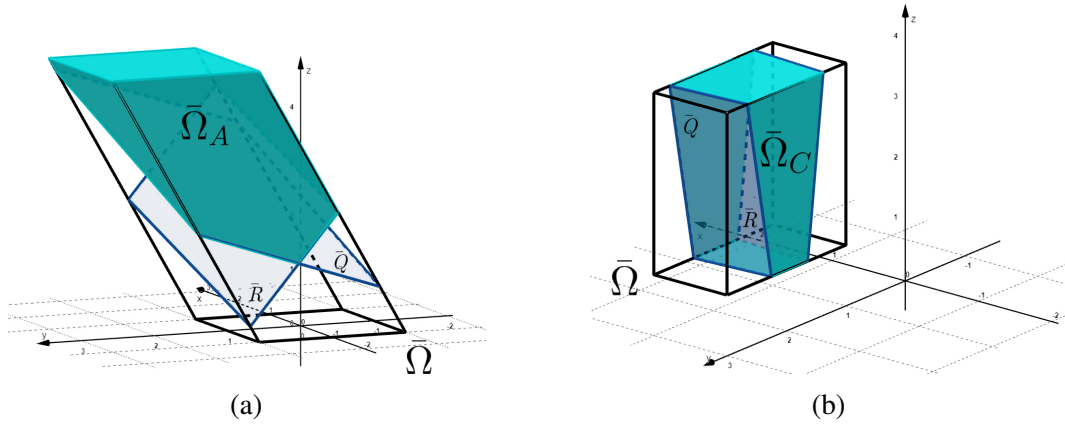
Fig. 5.12 Proposed formulation testing on hexahedral domains. (**a**) Example 1: hexahedron element cut by two discontinuities intersecting inside the domain. (**b**) Example 2: hexahedron element cut by two discontinuities intersecting outside the domain.

Since the equivalent polynomials $\tilde{H}_i(\boldsymbol{x})$ only depends on the values of the discontinuities coefficients, the exact computation is straightforward. It is then possible to apply the quadrature rule in eq. (5.43), in which the monomial $\mathscr{P}_n = 1$ corresponds to the volume of the selected domain part, while the monomials constituting the inertia tensor $\boldsymbol{I}$ are defined in Eq. (5.45).

$$I = \rho_s \begin{bmatrix} y^2 + z^2 & -xy & -xz \\ -yx & x^2 + z^2 & -yz \\ -zx & -zy & x^2 + y^2 \end{bmatrix} \tag{5.45}$$

where ρ_s is the material volumetric density (kg/m^3).

The results evaluated with respect to the global coordinate system (x, y, z) are

$$Volume = 7.947 \text{ m}^3 \tag{5.46}$$

$$I = \rho_s \begin{bmatrix} 144.820 & 2.110 & 5.010 \\ 2.110 & 125.962 & -48.480 \\ 5.010 & -48.480 & 24.141 \end{bmatrix} \text{(units: kg m}^3) \qquad (5.47)$$

In order to estimate the performance and robustness of the proposed algorithm, the integration problem has been addressed by means of the method proposed in [34] (via the integration procedure defined in [7]). The domain $\bar{\Omega}$ has been split into $i = 4$ subdomains, knowing the exact equations for the discontinuity planes $\bar{Q}$ and $\bar{R}$, in which the functions $H_{\bar{Q}}(x)$ and $H_{\bar{R}}(x)$ are continuous. The portion of interest, $\bar{\Omega}_A$, can thus be analytically defined and the integral has been evaluated by means of Gauss quadrature. The integral for the portion of interest has also been evaluated numerically using the adaptive integration method "*NIntegrate*" of the software *Wolfram Mathematica*. Finally, the integration subdomain $\bar{\Omega}_A$ has been analytically defined in the global reference system (x, y, z) by way of the intersections between the discontinuity planes $\bar{Q}$ and $\bar{R}$ and the hexahedral domain $\bar{\Omega}$, and the definite integral at the left-hand side of Eq. (5.34) has been computed. Results coincide, in general, up to the third decimal. The error in the computations of each integrand has been estimated as in Eq. (5.22) and the results are reported in Table 5.6.

Table 5.6 Proposed formulation error (percentage) for each computed term compared to other integration methods.

Integrand	Quadrature over $\bar{\Omega}_A$ ([34, 7])	Adaptive integration	Definite integral over $\bar{\Omega}_A$ (5.34)
1	2.34%	0.24%	2.34%
$y^2 + z^2$	1.40%	0.26%	1.40%
xy	1.53%	0.09%	1.53%
xz	6.26%	0.16%	6.26%
$x^2 + z^2$	1.68%	0.28%	1.68%
yz	0.41%	0.25%	0.41%
$x^2 + y^2$	0.28%	0.21%	0.28%

Although a slight error is present in this case, this is mainly due to the difficulty of exactly defining the integration region. In particular, this is more evident for the integration procedure defined in [7], and for the definite integral over the portion $\bar{\Omega}_A$, in which the partitioned domain has to be described thoroughly in order to obtain

precise results. In fact, being $\bar{\Omega}_A$ a complex and irregular polyhedron, its exact definition as an integration domain is not trivial. In the case analysed in this example, the integration subdomain $\bar{\Omega}_A$ has been defined by means of a Delaunay triangulation, once obtained the polyhedron vertices (Figure 5.13). Despite the Delaunay mesh being properly refined in order to maximise the accuracy, a small error still persists (Table 5.6).
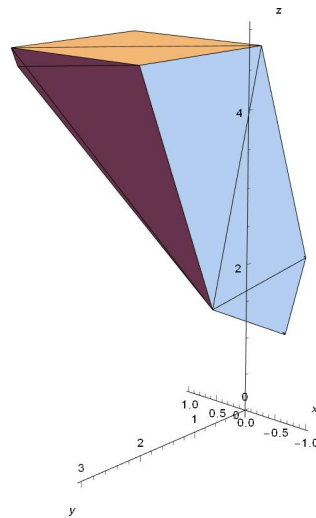
Fig. 5.13 $\bar{\Omega}_A$ integration domain discretised by way of Delaunay triangulation.

The numerical integral computation by means of the adaptive integration method "*NIntegrate*" of the software *Wolfram Mathematica*, however, produces an output that is closer to the proposed formulation.

Hexahedron partitioned by two discontinuities intersecting outside the element

The hexahedral element $\bar{\Omega}$ shown in Figure 5.12b as a part of a bigger body discretisation is herein examined. All dimensions are in meters. The element nodal coordinates, with respect to the global reference system (x, y, z), are:

- **1** $\equiv (0.0, 1.0, 1.0)$;

- **2** $\equiv (1.0, 1.0, 1.0)$;

- **3** $\equiv (0.0, 3.0, 1.0)$;

- $4 \equiv (1.0, 3.0, 1.0)$.

- $5 \equiv (0.0, 1.0, 4.0)$

- $6 \equiv (1.0, 1.0, 4.0)$

- $7 \equiv (0.0, 3.0, 4.0)$

- $8 \equiv (1.0, 3.0, 4.0)$

and it is crossed by two discontinuities, described by way of the planes $\bar{Q}$ and $\bar{R}$:

- $\bar{Q}: -\frac{11}{50}x + 3y - \frac{41}{100}z - \frac{159}{25} = 0$;

- $\bar{R}: \frac{1}{5}x + 3y + \frac{13}{50}z - \frac{26}{5} = 0$;

and split into three subdomains. The objective is to evaluate the inertia tensor and the volume of the highlighted portion $\bar{\Omega}_C$, namely solving the integral in Eq. 5.44 by means of the proposed formulation without subdividing the integration domain $\bar{\Omega}$. Note that the normal to each discontinuity plane has to be accurately defined for the sake of obtaining the targeted domain portion (as discussed in Section 5.3).

As in the previous example, the hexahedron $\bar{\Omega}$ and the discontinuities have to be mapped onto the parent coordinate system (by way of eqs. (4.24) and (5.42)) in order to set up the proposed integration technique to compute $\tilde{H}_C(\boldsymbol{x})$ and carry out the integration.

Since the equivalent polynomials $\tilde{H}_i(\boldsymbol{x})$ only depends on the values of the discontinuities coefficients, the exact computation is straightforward. It is then possible to apply the quadrature rule in eq. (5.43), in which the monomial $\mathscr{P}_n = 1$ corresponds to the volume of the selected domain part, while the monomials constituting the inertia tensor $\boldsymbol{I}$ are defined in Eq. (5.45).

The results evaluated with respect to the global coordinate system (x, y, z) are

$$Volume = 3.045 \text{ m}^3 \tag{5.48}$$

$$I = \rho_s \begin{bmatrix} 36.239 & -3.108 & -4.145 \\ -3.108 & 24.878 & -16.245 \\ -4.145 & -16.245 & 13.462 \end{bmatrix} \text{ (units: kg m}^3) \tag{5.49}$$

where ρ_s is the material volumetric density (kg/m^3).

As before, in order to estimate the performance and robustness of the proposed algorithm, the integration problem has been addressed by means of the method proposed in [34] (via the integration procedure defined in [7]). The domain $\bar{\Omega}$ has been split into $i = 3$ subdomains, knowing the exact equations for the discontinuity planes $\bar{Q}$ and $\bar{R}$, in which the functions $H_{\bar{Q}}(x)$ and $H_{\bar{R}}(x)$ are continuous. The portion of interest, $\bar{\Omega}_C$, can thus be analytically defined and the integral has been evaluated by means of Gauss quadrature. The integral for the portion of interest has also been evaluated numerically using the adaptive integration method "*NIntegrate*" of the software *Wolfram Mathematica*. Finally, the integration subdomain $\bar{\Omega}_C$ has been analytically defined in the global reference system (x, y, z) by way of the intersections between the discontinuity planes $\bar{Q}$ and $\bar{R}$ and the hexahedral domain $\bar{\Omega}$, and the definite integral at the left-hand side of Eq. (5.34) has been computed. The obtained results are almost coincident. The error in the computations of each integrand has been estimated as in Eq. (5.22) and the results are reported in Table 5.7.

Table 5.7 Proposed formulation error (percentage) for each computed term compared to other integration methods.

Integrand	Quadrature over $\bar{\Omega}_C$ ([34, 7])	Adaptive integration	Definite integral over $\bar{\Omega}_C$ (5.34)
1	0.33%	0.00%	0.33%
$y^2 + z^2$	0.44%	0.04%	0.44%
xy	0.49%	0.00%	0.49%
xz	0.34%	0.00%	0.34%
$x^2 + z^2$	0.30%	0.00%	0.30%
yz	0.51%	0.00%	0.51%
$x^2 + y^2$	0.67%	0.12%	0.67%

The slight error present in this case is even smaller compared to the results obtained in the previous example. In this case, in fact, the integration domain has a much regular shape and its analytical definition is amply easier. This leads to almost identical results for all the integration methods.

Outcomes

In general, the outcomes for the tests presented in section 5.5.2 and section 5.5.2 validate the proposed formulation, demonstrating its potential, precision, robustness and versatility also for three-dimensional elements. Moreover, it has to be noted that the solution evaluated by way of the presented formulation should be considered exact, due to the methodology employed to compute the equivalent polynomials $\tilde{H}_i(\boldsymbol{x})$ (see section 4.3.2 and [22, 27]). It has still to be stressed that, when equivalent polynomials are used, the integrand function in (5.28) doubles its degree, thus requiring a higher computational effort compared to other methods (such as in [34, 33, 7]) [22, 27]. On the other hand, the proposed formulation removes the necessity of defining complex three-dimensional subdomains, smoothing the overall integration process.

5.6 Closed form solution for tetrahedral integration domains

In this Section, the extension of the proposed formulation for 3D hexahedral elements (discussed in 5.5) to 3D tetrahedral elements is carried out.

Let us consider a body $\mathscr{B}$ and let $\boldsymbol{u}$ be the displacement field so that the local partition of unity (PU) approximation field referred to the set of variables $\boldsymbol{x} = (x, y, z)$ is defined by Eq. (5.2). Let us consider a tetrahedral element of its mesh, Ω, supposing it is divided into four portions by the discontinuity planes Q and R, as showed in Figure 5.14. Let us define Ω_A as the portion obtained when the normal to each discontinuity points inwards. Starting from Ω_A, the remaining partitions (Ω_B, Ω_C and Ω_D) are defined counterclockwise by convention.
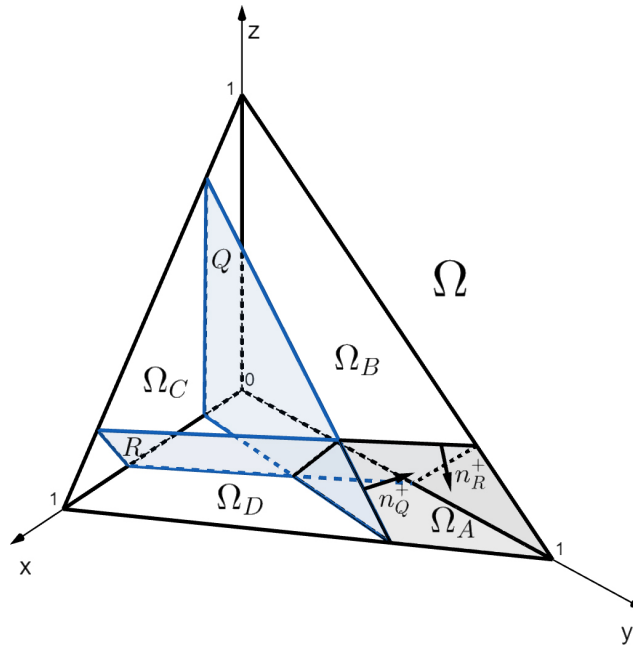
Fig. 5.14 A 3D tetrahedral domain Ω crossed by two discontinuity planes: Q and R.

In the context of XFEM, the element stiffness matrix has to be evaluated on each of the four subdomains Ω_A, Ω_B, Ω_C or Ω_D. As seen in (3.33), discontinuous functions times polynomials that cannot be integrated using standard quadrature rules over the entire domain Ω will be contained in such a matrix.

It has to be noted once again that the Heaviside step function (5.3) is defined so that the integrand function is zeroed on the subdomains with negative signed distance, thus a proper definition of the normal vector of the discontinuities allows to perform the quadrature on each subdomain. This also grants a direct extension of the proposed formulation to the generalised Heaviside function, having values $+1$ and -1 on the two sides of the discontinuity instead of $+1$ and 0, as defined in (5.3).

Let us assume an nth-degree polynomial $\mathscr{P}_n(\boldsymbol{x})$ to be integrated across the subdomains Ω_A, Ω_B, Ω_C or Ω_D obtained by partitioning a regular tetrahedron centred in $(0,0,0)$ on the (x,y,z) reference system with two planes Q and R (Eq. (5.28)).

The definition of each integration subdomain Ω_i is needed in order to evaluate the integral in (5.28) for each value of i with standard quadrature rules. This is not always a straightforward task due to the eventuality of rather complex three-dimensional shapes generated by the integration domain, depending on the slope of the discontinuity planes.

The main objective is to use the equivalent polynomials for the two discontinuity planes Q and R in order to allow, for each subdomain Ω_i, the integration over the entire element domain Ω by means of the standard Gauss-Legendre quadrature rule, i.e., to compute (5.28) with integrations on the entire element domain Ω instead of Ω_i.

Let $\tilde{H}_{Q^+}$ and $\tilde{H}_{R^+}$ be the equivalent polynomials related to the normals $\mathbf{n}_{Q^+}$ and $\mathbf{n}_{R^+}$, and $\tilde{H}_{Q^-}$ and $\tilde{H}_{R^-}$ be the equivalent polynomials related to the reversed normals $-\mathbf{n}_{Q^+}$ and $-\mathbf{n}_{R^+}$. With reference to Figure 5.14, equations (5.29) to (5.32) give a system of four equations in the four unknowns I_A, I_B, I_C and I_D that, in general, can be proved to be indeterminate. In particular, it can be observed that if the intersection line between the two discontinuities Q and R is external to the element domain or is contained on its boundary, then the solution will be unique. If the intersection line lies inside the element domain, the system will be indeterminate, with the system coefficient matrix having rank three.

When the intersection line between the two discontinuities Q and R is internal to the element domain, the above observation suggests the introduction of an auxiliary integration limit S to eliminate indeterminacy.

The plane $S : x = mz + n$ (defined in Eq. (5.33)) is obtained such that it belongs to the sheaf of planes generated by the intersection line between Q and R and that its normal has null component with respect to the y-axis of the reference system.

In order to properly define the equivalent polynomials for all the integration portions, the auxiliary integration limit defined by means of the plane S should be coupled by integration limits also in the z-axis direction. In particular, the domain in which the equivalent polynomial functions for the discontinuities Q and R are evaluated has also to be bounded by planes Z_1 and Z_2. These planes have null components with respect to the x-axis and y-axis of the reference system and contain the intersection line between the plane S and the parent tetrahedral domain limits along the x-axis: planes $x = 0$ and $y = 0$.

Let $\tilde{H}_{Q^+}^{(S)}(\boldsymbol{x})$ and $\tilde{H}_{R^+}^{(S)}(\boldsymbol{x})$ be the equivalent polynomial functions for the discontinuities Q and R evaluated into the regular tetrahedral element (called the *parent element*), with respect to the domain bounded by S (Figure 5.15). Combining them together, it is possible to find the equivalent polynomial $\tilde{H}_i(\boldsymbol{x})$ (see Eq. (5.28)).
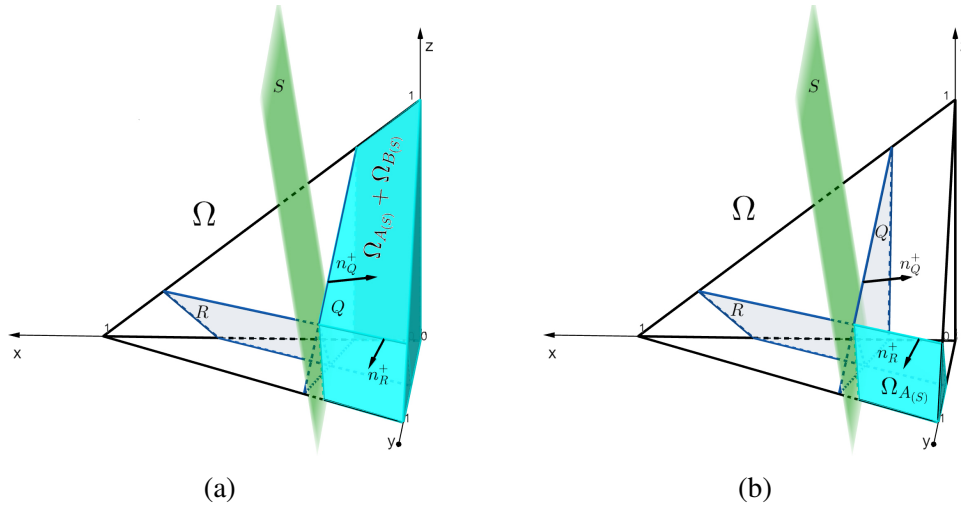
Fig. 5.15 Use of the auxiliary integration limit S to evaluate the equivalent polynomials $\tilde{H}_i(\boldsymbol{x})$. In the figure $\tilde{H}_B(\boldsymbol{x}) = \tilde{H}^{(S)}_{Q^+}(\boldsymbol{x}) - \tilde{H}^{(S)}_{R^+}(\boldsymbol{x})$. **(a)** Integration domain evaluated by means of $\tilde{H}_{Q^+}(\boldsymbol{x})$ with respect to the discontinuity Q and the auxiliary integration limit S. **(b)** Integration domain evaluated by means of $\tilde{H}_{R^+}(\boldsymbol{x})$ with respect to the discontinuity R and the auxiliary integration limit S.

With reference to Figure 5.15, the equivalent polynomial functions to perform the integration on each of the four areas in (5.34) are described in Eq. (5.35).

The equivalent polynomial functions $\tilde{H}_A(\boldsymbol{x}) \ldots \tilde{H}_D(\boldsymbol{x})$, being linear combinations of equivalent polynomials for the single discontinuity planes Q and R, will depend on the equations of the two discontinuities and, according to [22, 27], will have the same degree of $\mathscr{P}_n(\boldsymbol{x})$ and the algebraic polynomial form defined in Eq. (5.39).

Since $\tilde{H}_i(\boldsymbol{x})\mathscr{P}_n(\boldsymbol{x})$ is a polynomial function that is continuous over the entire domain, Ω, it can be exactly integrated with a proper quadrature rule. It has to be noted that the integrand in (5.34) has doubled its degree, compared to the one in (5.28), thus slightly increasing the computational effort. The main advantage of this approach is that it allows integration over the standard domain Ω rather than the non-standard partitioned subdomains $\Omega_A \ldots \Omega_D$.

The analytical procedure to obtain the exact expressions of the equivalent polynomials $\tilde{H}_i(\boldsymbol{x})$ by means of the software *Wolfram Mathematica* is reported in the Appendix (A.1.4).

5.6.1   Integration algorithm for tetrahedral domains

The purpose of the proposed integration technique is to deliver the expression for the equivalent polynomial function $\tilde{H}_i(\boldsymbol{x})$, in order to compute the integral in Equation (5.34) without splitting the integration domain. The usefulness of the proposed algorithm is again presented by way of a generic example. Let us consider a polynomial $\mathscr{P}_n(\boldsymbol{x})$ to be integrated over a subdomain $\bar{\Omega}_A$, generated by dividing a tetrahedron $\bar{\Omega}$ with two planes $\bar{Q}$ and $\bar{R}$, as shown in Figure 5.16a. The problem is defined in the global coordinate system $\boldsymbol{x} = (x, y, z)$. Applying Equation (5.34) after the equivalent polynomial function $\tilde{H}_A(\boldsymbol{x})$ let us define Eq. (5.40).

Beforehand, the problem has to be mapped to a standard quadrature domain. Therefore, a change in variables from the (x, y, z) coordinate system to the parent coordinate system (ξ, η, ζ) is employed in order to compute the integral over a standard and regular domain (see eq. (4.13)), as illustrated in Figure 5.16b. By means of such a procedure, single parent geometry can be used to address various scenarios. Thus, tetrahedrons having any position and size in the global coordinate system can be mapped to the tetrahedral parent geometry in the local coordinate system (ξ, η, ζ) illustrated in Figure 5.16b.

(a)	(b)
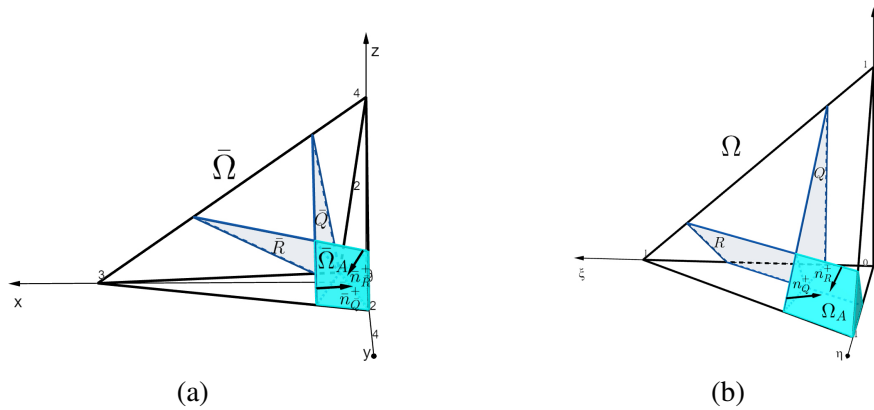
Fig. 5.16 Isoparametric mapping of a tetrahedral element. (**a**) Element configuration in the global coordinate system. (**b**) Element configuration in the parent coordinate system.

The mathematical concept used in the proposed technique for this purpose is *isoparametric mapping*, which is commonly employed in the FEM [37, 19]. Let $P(\xi, \eta, \zeta) \in \Omega$ be a generic point in the parent reference system, corresponding to

the point $\bar{P}(x,y,z) \in \bar{\Omega}$ in the global reference system. The mapping of $P(\xi,\eta,\zeta)$ onto $\bar{P}(x,y,z)$ is described by Eq. (5.41).

Similarly, the discontinuities $\bar{Q}(x)$ and $\bar{R}(x)$ equations, defined in the global reference system, have to be mapped onto $Q(\xi)$ and $R(\xi)$, defined in the parent coordinate system (Figure 5.16). This is achieved, for each discontinuity, by:

- Calculating the signed distances (D_i) in the global coordinate system between each discontinuity and each node of the integration domain;

- Writing the discontinuity coefficients (a, b, c, and d) in the parent coordinate system as a function of D_i by solving a linear equations system;

- Substituting the variables x, y, and z in $\bar{Q}(x)$ and $\bar{R}(x)$ by means of Equation (5.41), so that $Q(\xi)$ and $R(\xi)$ are obtained in terms of the coefficients a', b', c', and d' dependent on D_i.

For a 3D tetrahedral parent element, the coefficients are:

$$a' = D_2 - D_1 \tag{5.50a}$$

$$b' = D_3 - D_1 \tag{5.50b}$$

$$c' = D_4 - D_1 \tag{5.50c}$$

$$d' = D_1 \tag{5.50d}$$

After $\bar{Q}(x)$ and $\bar{R}(x)$ are transformed into $Q(\xi)$ and $R(\xi)$, the correct expression for the equivalent polynomial function $\tilde{H}_i(x)$ with respect to the parent domain coordinate system can be generated. The coordinates and integration domain transformation in the quadrature are then introduced using the Jacobian matrix, which contains the partial derivatives of the interpolation functions N_i that are differentiated with respect to the parent system variables (ξ,η,ζ) [140].

The integral in Eq. (5.40) is evaluated in (5.43), applying the standard scheme of the Gauss-Legendre numerical quadrature [175].

It needs to be emphasised that the proposed algorithm is intended for integration over the entire domain $\bar{\Omega}$ yielding the result of the integral over the subdomains $\bar{\Omega}_A$, $\bar{\Omega}_B$, $\bar{\Omega}_C$ and $\bar{\Omega}_D$. Thus, the discontinuities equations have to be accurately defined,

so that the unit vectors $\boldsymbol{n_i}^+$ point inwards. Additionally, it has to be noted that the discontinuities do not necessarily have to intersect $\bar{\Omega}$ or one another (the proposed algorithm can handle all possible scenarios). The composition and the degree of the polynomials that can be precisely integrated using the suggested technique rely on specific requirements necessary to find the equivalent polynomial, as can be deduced from Refs. [22, 27].

The equivalent polynomial functions $\tilde{H}_i(\boldsymbol{x})$ are evaluated into a regular tetrahedral parent element. As for the previous Sections, more details about the mathematical formulation employed to compute the equivalent polynomial $\tilde{H}_i(\boldsymbol{x})$ for each discontinuity have been presented in Chapter 4, and can be found in [22, 27]. It has to be noted that the proposed integration technique can be extended to a standard tetrahedral parent element (which is described in Subsection 5.6.1).

In the following subsection, some numerical tests are performed in order to demonstrate the precision and efficacy of the proposed formulation. The results are then compared to other integration methods to validate the presented technique.

5.6.2   Numerical testing and validation

The formulation presented in section 5.6 for 3D tetrahedral domains has been tested and validated by way of two numerical examples. The results obtained by means of the proposed formulation are exact with machine precision.

Tetrahedron partitioned by two discontinuities intersecting within the element

The tetrahedral element $\bar{\Omega}$ shown in Figure 5.17a as a part of a bigger body discretisation is herein examined. All dimensions are in meters. The element nodal coordinates, with respect to the global reference system (x, y, z), are

- $\mathbf{1} \equiv (1.0, 1.0, 0.0)$;

- $\mathbf{2} \equiv (4.0, 2.0, 0.0)$;

- $\mathbf{3} \equiv (1.0, 5.0, 0.0)$;

- $\mathbf{4} \equiv (0.0, 0.0, 3.0)$.

and it is crossed by two discontinuities, described by way of the planes $\bar{Q}$ and $\bar{R}$:

- $\bar{Q} : \frac{8}{5}x - \frac{33}{100}y + \frac{19}{50}z - \frac{189}{100} = 0$;

- $\bar{R} : -\frac{91}{50}x - \frac{189}{100}y - \frac{89}{100}z + \frac{167}{20} = 0$;

and split into four subdomains. The objective is to evaluate the volume of the highlighted portion $\bar{\Omega}_A$, namely solving the integral in Eq. 5.44 by means of the proposed formulation without subdividing the integration domain $\bar{\Omega}$.

Note that the normal to each discontinuity plane has to be accurately defined for the sake of obtaining the targeted domain portion (as discussed in Section 5.3).

In order to set up the proposed integration technique, as described in section 5.6.1, the tetrahedron $\bar{\Omega}$ has to be mapped onto the parent coordinate system, which is used to compute $\tilde{H}_B(\boldsymbol{x})$ and carry out the integration. This is performed by means of the shape functions defined in eq. (4.13), while the coefficients for the two discontinuities are brought back to the parent coordinate system by way of the expressions defined in eq. (5.50).

(a)   (b)
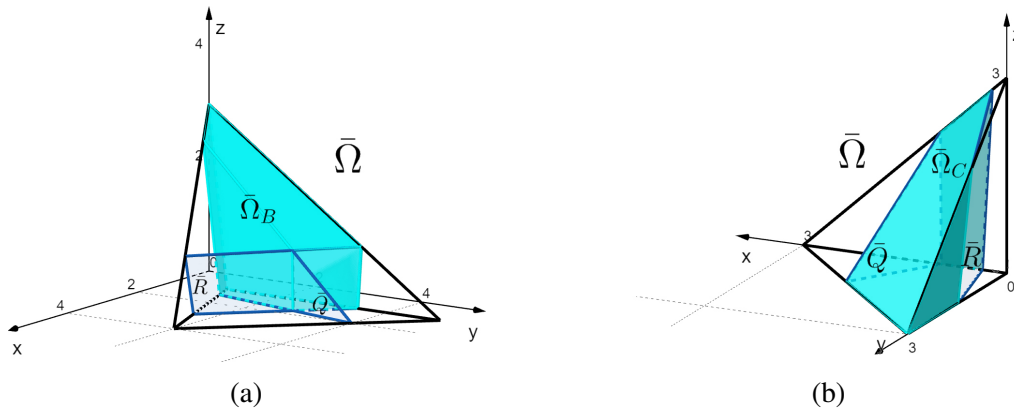
Fig. 5.17 Proposed formulation testing on tetrahedral domains. (**a**) Example 1: tetrahedron element cut by two discontinuities intersecting inside the domain. (**b**) Example 2: tetrahedron element cut by two discontinuities intersecting outside the domain.

Since the equivalent polynomials $\tilde{H}_i(\boldsymbol{x})$ only depends on the values of the discontinuities coefficients, the exact computation is straightforward. It is then possible to apply the quadrature rule in eq. (5.43), in which the monomial $\mathcal{P}_n = 1$ corresponds to the volume of the selected domain part.

The results evaluated with respect to the global coordinate system (x, y, z) for the subdomain $\bar{\Omega}_B$ are

$$Volume = 2.446 \text{ m}^3 \tag{5.51}$$

In order to estimate the performance and robustness of the proposed algorithm, the integration problem has been addressed by means of the method proposed in [34] (via the integration procedure defined in [7]). The domain $\bar{\Omega}$ has been split into $i = 4$ subdomains, knowing the exact equations for the discontinuity planes $\bar{Q}$ and $\bar{R}$, in which the functions $H_{\bar{Q}}(x)$ and $H_{\bar{R}}(x)$ are continuous. The portion of interest, $\bar{\Omega}_B$, can thus be analytically defined and the integral has been evaluated by means of Gauss quadrature. The integral for the portion of interest has also been evaluated numerically using the adaptive integration method "*NIntegrate*" of the software *Wolfram Mathematica*. Finally, the integration subdomain $\bar{\Omega}_B$ has been analytically defined in the global reference system (x, y, z) by way of the intersections between the discontinuity planes $\bar{Q}$ and $\bar{R}$ and the tetrahedral domain $\bar{\Omega}$, and the definite integral at the left-hand side of Eq. (5.34) has been computed. Results coincide, in general, up to the third decimal. The error in the computations of each integrand has been estimated as in Eq. (5.22) and the results are reported in Table 5.8.

Table 5.8 Proposed formulation error (percentage) for each computed term compared to other integration methods.

Integrand	Quadrature over $\bar{\Omega}_B$ ([34, 7])	Adaptive integration	Definite integral over $\bar{\Omega}_B$ (5.34)
1	0.42%	0.50%	0.42%

As reported in table 5.8, the proposed formulation delivers very precise results and the error compared to the other integration methods is almost null. Moreover, it has to be noted that the slight difference in the comparative results using the standard integration techniques in table 5.8 is mostly due to the irregular shape of the targeted integration region, $\bar{\Omega}_B$, and to the rounding introduced while defining its boundaries. The results obtained by means of equivalent polynomials, in fact, should be considered exact by definition, as highlighted in 4.3.

Tetrahedron partitioned by two discontinuities intersecting outside the element

The tetrahedral element $\bar{\Omega}$ shown in Figure 5.17b as a part of a bigger body discretisation is herein examined. All dimensions are in meters. The element nodal coordinates, with respect to the global reference system (x, y, z), are:

- $\mathbf{1} \equiv (0.0, 0.0, 0.0)$;

- $\mathbf{2} \equiv (3.0, 0.0, 0.0)$;

- $\mathbf{3} \equiv (0.0, 3.0, 0.0)$;

- $\mathbf{4} \equiv (0.0, 0.0, 3.0)$.

and it is crossed by two discontinuities, described by way of the planes $\bar{Q}$ and $\bar{R}$:

- $\bar{Q} : \frac{119}{20}x - \frac{77}{20}y - \frac{3}{100}z - \frac{23}{4} = 0$;

- $\bar{R} : \frac{401}{100}x + \frac{97}{100}y + \frac{21}{100}z - \frac{36}{25} = 0$;

and split into three subdomains. The objective is to evaluate the inertia tensor and the volume of the highlighted portion $\bar{\Omega}_C$, namely solving the integral in Eq. 5.44 by means of the proposed formulation without subdividing the integration domain $\bar{\Omega}$. Note that the normal to each discontinuity plane has to be accurately defined for the sake of obtaining the targeted domain portion (as discussed in Section 5.3).

As in the previous example, the tetrahedron $\bar{\Omega}$ and the discontinuities have to be mapped onto the parent coordinate system (by way of eqs. (4.24) and (5.42)) in order to set up the proposed integration technique to compute $\tilde{H}_C(\boldsymbol{x})$ and carry out the integration.

Since the equivalent polynomials $\tilde{H}_i(\boldsymbol{x})$ only depends on the values of the discontinuities coefficients, the exact computation is straightforward. It is then possible to apply the quadrature rule in eq. (5.43), in which the monomial $\mathscr{P}_n = 1$ corresponds to the volume of the selected domain part.

The results evaluated with respect to the global coordinate system (x, y, z) are

$$Volume = 3.150 \text{ m}^3 \tag{5.52}$$

As before, in order to estimate the performance and robustness of the proposed algorithm, the integration problem has been addressed by means of the method proposed in [34] (via the integration procedure defined in [7]). The domain $\bar{\Omega}$ has been split into $i = 3$ subdomains, knowing the exact equations for the discontinuity planes $\bar{Q}$ and $\bar{R}$, in which the functions $H_{\bar{Q}}(x)$ and $H_{\bar{R}}(x)$ are continuous. The portion of interest, $\bar{\Omega}_C$, can thus be analytically defined and the integral has been evaluated by means of Gauss quadrature. The integral for the portion of interest has also been evaluated numerically using the adaptive integration method "*NIntegrate*" of the software *Wolfram Mathematica*. Finally, the integration subdomain $\bar{\Omega}_C$ has been analytically defined in the global reference system (x, y, z) by way of the intersections between the discontinuity planes $\bar{Q}$ and $\bar{R}$ and the tetrahedral domain $\bar{\Omega}$, and the definite integral at the left-hand side of Eq. (5.34) has been computed. The obtained results are almost coincident. The error in the computations of each integrand has been estimated as in Eq. (5.22) and the results are reported in Table 5.9.

Table 5.9 Proposed formulation error (percentage) for each computed term compared to other integration methods.

Integrand	Quadrature over $\bar{\Omega}_C$ ([34, 7])	Adaptive integration	Definite integral over $\bar{\Omega}_C$ (5.34)
1	1.56%	0.55%	1.56%
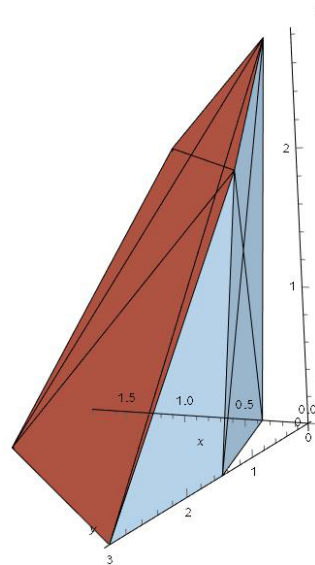
Fig. 5.18 $\bar{\Omega}_C$ integration domain discretised by way of Delaunay triangulation.

Once again, as reported in table 5.9, the results obtained by means of the proposed formulation are accurate, whith a almost null error compared to the standard integration methods. The slight error in table 5.9 is, again, mostly due to the irregular shape of the targeted integration region, $\bar{\Omega}_C$, and to the rounding introduced while defining its boundaries (a definition for $\bar{\Omega}_C$ by means of Delaunay triangulation is illustrated in Figure 5.18).

However, the results for all the integration methods are almost identical.

Outcomes

As in the previous cases, the results for the tests presented in section 5.6.2 validate the proposed formulation, demonstrating its precision, robustness and versatility also for tetrahedral finite elements. It has to be stressed again that the solution evaluated by way of the presented formulation should be considered exact, due to the methodology employed to compute the equivalent polynomials $\tilde{H}_i(\boldsymbol{x})$ (see section 4.3.2 and [22, 27]). It should be also noted that the integrand function in (5.28) doubles its degree when equivalent polynomials are employed, thus requiring a higher computational effort compared to other methods (such as in [34, 33, 7]) [22, 27]. On the other hand, the proposed formulation removes the necessity of defining complex three-dimensional subdomains, easing the overall integration process.

5.7 Distorted element domains and loss of accuracy

Distortions in the finite element mesh can arise due to various reasons, such as geometric complexities, element distortion during deformation, and sub-optimal mesh generation strategies. These distortions can significantly compromise the accuracy of the stiffness matrix, leading to unreliable numerical results. In this Section, the impact of distortions on the accuracy of the results obtained by means of the proposed formulation is discussed.

5.7.1 Distorted elements

The parent domain of the elements served as the foundation for all of the earlier results discussed in this Chapter. The correspondence between the parent domain

and the global domain is guaranteed by the isoparametric mapping process, in which the derivatives of the element shape function are multiplied by the inverse of the Jacobian matrix, and the integrand function is multiplied by the determinant of the Jacobian matrix. The Jacobian matrix for a quadrilateral element can be defined as

$$\boldsymbol{J} = \begin{bmatrix} \frac{\delta N_1}{\delta \xi} & \frac{\delta N_2}{\delta \xi} & \frac{\delta N_3}{\delta \xi} & \frac{\delta N_4}{\delta \xi} \\ \frac{\delta N_1}{\delta \eta} & \frac{\delta N_2}{\delta \eta} & \frac{\delta N_3}{\delta \eta} & \frac{\delta N_4}{\delta \eta} \end{bmatrix} \tag{5.53}$$

in which, $N_1...N_4$ are the element shape functions (see Eq. (4.10)).

Therefore, only when the Jacobian matrix, $\boldsymbol{J}$, contains constant terms the equivalent polynomials strategy is accurate [22]. Since the terms in the Jacobian matrix are the derivatives of the shape functions, this is always true for elements with linear shape functions (i.e. the triangular and tetrahedral elements presented in sections 5.4 and 5.6). As for the bilinear quadrilateral element and the trilinear hexahedral element, the entries of the Jacobian matrix are constant only when the element opposite sides are parallel [22]. In the general case, however, both the determinant of $\boldsymbol{J}$ and its elements are linear functions, leading to a rational integrand function when evaluating the element stiffness matrix. This brings to approximate results when using the standard Gauss quadrature, due to the additional polynomial degree introduced by the non-constant determinant of $\boldsymbol{J}$ and by the rational integrand function. Approximate results are, however, generally allowed im such situations [22, 19].

When dealing with PU finite elements containing discontinuities, on the other hand, a new source of approximation is introduced. The element distortion, in fact, makes discontinuity lines in the parent element domain map onto curves in the global reference system (as shown in Figure 5.19) and *vice versa* [22]. This not only makes the standard Gauss quadrature ill-suited for an exact computation, but also the proposed formulation generates approximations in the results that are dependent on the magnitude of the distortion. In the next subsection, numerical tests has been conducted in order to estimate the error produced by the proposed formulation when it is employed on distorted elements.
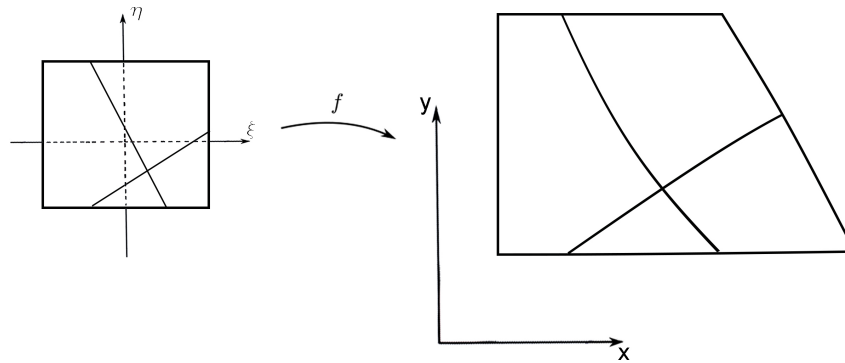
Fig. 5.19 Mapping of a standard parent element into a distorted element on the global reference system (x, y). The line discontinuities contained into the parent element are mapped onto curves on the distorted element (and *vice versa*).

5.7.2 Accuracy testing

A comparative study on quadrature errors in distorted elements containing a single linear discontinuity has been conducted in [22], demonstrating that the error in the results computed by means of equivalent polynomials are of the same order of magnitude of other standard quadrature methods commonly used in XFEM analysis (such as the domain splitting into quadrature subcells) [22]. This analysis has been replicated for the proposed formulation, in order to estimate the size of the error introduced in such situations. For this purpose, a distorted quadrilateral element containing two discontinuities is herein considered (Figure 5.20a) and the discontinuous part of its stiffnesss matrix, $I = \int_{\Omega} H \boldsymbol{B}^T \boldsymbol{E} \boldsymbol{B} \, d\Omega$, (see Eq. (4.2)) is computed by means of the proposed formulation and using the standard Gauss quadrature over integration subdomains. The nodal coordinates for the considered quadrilateral element are

$$\begin{aligned} \mathbf{1} &\equiv (1,1) \\ \mathbf{2} &\equiv (3,1) \\ \mathbf{3} &\equiv (6,5) \\ \mathbf{4} &\equiv (1,4) \end{aligned} \tag{5.54}$$

and it is cut by two discontinuity lines, q and r, at points $\boldsymbol{P1}_q, \boldsymbol{P2}_q$ and $\boldsymbol{P1}_r, \boldsymbol{P2}_r$ respectively.

(a)   (b)
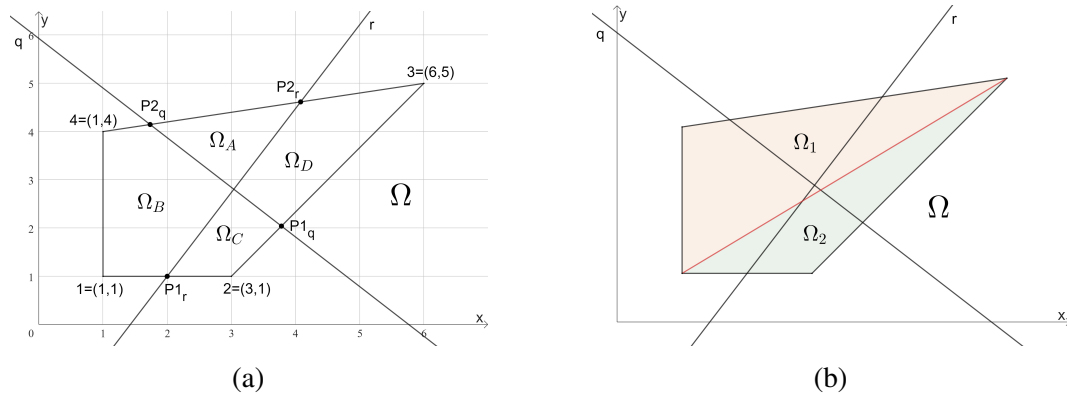
Fig. 5.20 Proposed formulation testing on distorted domains. (**a**) Distorted quadrilateral element cut by two discontinuities intersecting inside the domain. (**b**) Distorted quadrilateral domain splitting in two triangular domains (Ω_1 and Ω_2) to improve the solution accuracy.

$$err = \frac{\left|I_{adaptive} - I_{numerical}\right|}{I_{adaptive}} \tag{5.55}$$

The outcomes are then compared to the results obtained by way of the adaptive integration method "*NIntegrate*" of the software *Wolfram Mathematica*. The error is evaluated as in Eq. (5.55) and the results are reported in Table 5.10.

Table 5.10 Error (percentage) for distorted quadrilateral elements containing double discontinuities.

Integral	Proposed formulation error	Quadrature over each subdomain error
$I = \int_\Omega H \boldsymbol{B}^T \boldsymbol{E} \boldsymbol{B} \, d\Omega$	97.17%	97.16%

Although it is not negligible, the error introduced by way of the proposed formulation is of the same order of magnitude of the standard technique of splitting the domain into quadrature subcells, thus confirming the trend highlighted in [22].

The more effective and rapid strategy to null the error when using the proposed formulation on quadrilateral distorted elements is to diagonally split the distorted element Ω into two triangular subdomains (Ω_1 and Ω_2), which, by definition, are not affected by the distortion (Figure 5.20b). The proposed formulation is thus to be employed on each triangular subdomain separately, and then sum the obtained

results. This technique, however, involves a loss of information on the element domain, since a transition from a bilinear element to a linear element is made, thus could not be a perfect fit for every scenario.

The use of alternative techniques such as *subparametric mapping*, in which the number of nodes used for defining the element geometry is less than the number of nodes used for defining the element displacements, or the definition of a specific equivalent polynomial for distorted geometries (such as trapezoid elements) have been explored, but an extensive solution was not yet defined. Thus, this could be a subject to study and analyse in further researches in this context, in order to contribute to the advancement of computational analysis methods by enabling more accurate and reliable simulations, with broad applications in fracture mechanics, and other fields reliant on XFEM analysis.

5.8 A closed form solution for an arbitrary number of discontinuities

The effectiveness of the solution discussed in this Chapter has been demonstrated by way of numerical testing on various 2D and 3D finite elements. Although the case of two discontinuities within a single finite element has been explored, in order to simplify the analysed scenarios, the proposed formulation could be scaled and extended towards an arbitrary number of discontinuities.

5.8.1 Multiple discontinuities intersecting at a single point

Let us analyse the quadrilateral finite element shown in Figure 5.21a, in which a plurality of discontinuities stems from the same intersection point. This is a common scenario in fracture mechanics problems involving rock masses and hydraulic fracture [177, 179, 178, 180], and also in simulations concerning impacts on brittle objects that shatter into *n* multiple pieces. The standard XFEM integration procedure would require the definition of each integration subdomain, which in such cases could be rather laborious. However, the overall integration process could be smoothed by way of the proposed formulation.

As demonstrated in Section 5.3, a closed form solution by means of equivalent polynomials providing exact integration results over quadrilateral domains containing two discontinuities exists. Thus, the idea is to recursively employ the proposed formulation on a different couple of discontinuities at each step, in order to evaluate the equivalent polynomials $\tilde{H}_i(\boldsymbol{x})$ (where $i = 1, ..., n+1$) for each portion of the domain Ω.

The solution provided in Section 5.3, in fact, can be straightforwardly extended to an arbitrary number of discontinuities. Let us define a regular 2×2 quadrilateral element Ω, centred in $(0,0)$, and crossed by n discontinuities intersecting a point $\boldsymbol{P} \in \Omega$. Let s be the abscissa of $\boldsymbol{P}$, so that $n+1$ domain portions $(\Omega_1, ..., \Omega_{n+1})$ are defined in the Ω domain restriction from $x = -1$ to $x = s$, as well as in the domain restriction from $x = s$ to $x = 1$, as shown in Figure 5.21.

Let us define $n - 1$ sets of two discontinuity lines of equation $d_i : y = m_i x + n_i$, which are ordered depending on the value of their first derivative with respect to x, (namely the line slope, m_i). For the domain restriction to the left of s, the discontinuities are arranged starting from the lowest value of $\frac{\delta d_i}{\delta x}$ to the highest. Meanwhile, for the domain restriction to the right of s, the discontinuities are numbered starting from the highest value of $\frac{\delta d_i}{\delta x}$ to lowest.

It is then possible to define, for each rectangular restriction of Ω (namely $[-1, s]$ $\vee$ $[s, 1]$), a linear system of equations (Eq. (5.56) to Eq. (5.60)), whose solution is the equivalent polynomials equations, $\tilde{H}_i(\boldsymbol{x})$, for the domain portions bounded by the considered discontinuities.

$$I_1 \qquad = \int_{\Omega_1} \mathscr{P}_N(\boldsymbol{x})\,d\Omega \qquad = \int_\Omega \tilde{H}_{d_1^+} \mathscr{P}_N(\boldsymbol{x})\,d\Omega \qquad (5.56)$$

$$I_1 + I_2 \quad = \int_{\Omega_1 \bigcup \Omega_2} \mathscr{P}_N(\boldsymbol{x})\,d\Omega \ = \int_\Omega \tilde{H}_{d_2^+} \mathscr{P}_N(\boldsymbol{x})\,d\Omega \qquad (5.57)$$

$$\vdots$$

$$I_{i-1} + I_i = \int_{\Omega_{i-1} \bigcup \Omega_i} \mathscr{P}_N(\boldsymbol{x})\,d\Omega = \int_\Omega \tilde{H}_{d_i^+} \mathscr{P}_N(\boldsymbol{x})\,d\Omega \qquad (5.58)$$

$$\vdots$$

$$I_{n-1} + I_n = \int_{\Omega_{n-1} \bigcup \Omega_n} \mathscr{P}_N(\boldsymbol{x})\,d\Omega = \int_\Omega \tilde{H}_{d_n^+} \mathscr{P}_N(\boldsymbol{x})\,d\Omega \qquad (5.59)$$

$$I_{n+1} \qquad = \int_{\Omega_{n+1}} \mathscr{P}_N(\boldsymbol{x})\,d\Omega \qquad = \int_\Omega \tilde{H}_{d_n^-} \mathscr{P}_N(\boldsymbol{x})\,d\Omega \qquad (5.60)$$

in which $\mathscr{P}_N(\boldsymbol{x})$ is a N-th degree polynomial (see eq. (5.4)).

Such linear system of $n+1$ equations in $n+1$ unknowns has a unique solution only if the intersection point between the n discontinuities is external to the element domain or is on its boundary.

The extension of the proposed formulation to an arbitrary number, n, of discontinuities can then be analytically defined as

$$\tilde{H}_1^{(\alpha)}(\boldsymbol{x}) = \tilde{H}_{d_1^+}^{(s)}(\boldsymbol{x}) \tag{5.61}$$

$$\tilde{H}_2(\boldsymbol{x}) \quad = \tilde{H}_{d_2^+}^{(s)}(\boldsymbol{x}) - \tilde{H}_{d_1^+}^{(s)}(\boldsymbol{x}) \tag{5.62}$$

$$\vdots$$

$$\tilde{H}_i(\boldsymbol{x}) \quad = \tilde{H}_{d_i^+}^{(s)}(\boldsymbol{x}) - \tilde{H}_{d_{i-1}^+}^{(s)}(\boldsymbol{x}) \tag{5.63}$$

$$\vdots$$

$$\tilde{H}_n(\boldsymbol{x}) \quad = \tilde{H}_{d_n^+}^{(s)}(\boldsymbol{x}) - \tilde{H}_{d_{n-1}^+}^{(s)}(\boldsymbol{x}) \tag{5.64}$$

$$\tilde{H}_{n+1}^{(\alpha)}(\boldsymbol{x}) = \tilde{H}_{d_n^-}^{(s)}(\boldsymbol{x}) \tag{5.65}$$

where $\alpha = left, right$ and the superscript sign ($+$ or $-$) indicates the direction pointed the normal, $\boldsymbol{n} = (a,b)$, to the discontinuity: $+$ if its b component is positive; $-$ if its b component is negative (see Figure 5.21).

For the domain restriction $[-1,s]$, the discontinuities are grouped so that $\frac{\delta d_1}{\delta x} <$ ...$\frac{\delta d_i}{\delta x}$... $< \frac{\delta d_n}{\delta x}$. Meanwhile, for the domain restriction $[s,1]$, the discontinuities are grouped so that $\frac{\delta d_1}{\delta x} >$ ...$\frac{\delta d_i}{\delta x}$... $> \frac{\delta d_n}{\delta x}$.

It has to be noted that, in the case of $\boldsymbol{P} \in \Omega$, the values of the equivalent polynomials for the first domain portion, $\tilde{H}_1^{(left)}(\boldsymbol{x})$ and for the last domain portion, $\tilde{H}_{n+1}^{(left)}(\boldsymbol{x})$, obtained with respect to Ω restriction $[-1,s]$, have to be summed, respectively, to the values obtained for $\tilde{H}_1^{(right)}(\boldsymbol{x})$ and $\tilde{H}_{n+1}^{(right)}(\boldsymbol{x})$ with respect to Ω restriction $[s,1]$.

In the case of the intersection point $\boldsymbol{P} \notin \Omega$, or if $\boldsymbol{P}$ abscissa, s, is equal to ± 1, the auxiliary bound $x = s$ is to be adjusted to $x = sign(s)$, so that equations (5.61) to (5.65) remain valid. Clearly, in this last scenario, no domain restriction exists, since $[-1,s] \equiv \Omega \vee [s,1] \equiv \Omega$. This also implies that equations (5.61) to (5.65) can be directly evaluated over the entire domain Ω, obtaining all the equivalent polynomials values, $\tilde{H}_i(\boldsymbol{x}) \quad i = 1,...,n+1$.

(a)   (b)

Fig. 5.21 Extension of the proposed formulation for an arbitrary number n of discontinuities intersecting on a point $\boldsymbol{P}$. (**a**) Definition of the discontinuities and the portions of Ω for the domain restriction $[-1, s]$. (**b**) Definition of the discontinuities and the portions of Ω for the domain restriction $[s, 1]$.

In Table 5.11, the proposed formulation has been employed on a standard 2×2 quadrilateral parent element domain Ω, centred in $(0,0)$ and cut by $n = 5$ discontinuities (as in Figure 5.21) to compute the integral in Eq. (5.4) in which $\mathscr{P} = x^2 + y^2$. (The data used for this example is reported in the Appendix A.3.1). For each domain portion the integral results obtained by means of the proposed formulation are compared to the results obtained by way of the adaptive integration method "*NIntegrate*" of the software *Wolfram Mathematica*, as well as the numerical results by means of the method proposed in [34] and by way of definite integral computation over each subdomain. The error is evaluated as in Eq. (5.55).

Table 5.11 Proposed formulation error (percentage) for a quadrilateral element crossed by $n = 5$ discontinuities compared to other integration methods.

i-th portion	Quadrature over Ω_i ([34, 7])	Adaptive integration	Definite integral over Ω_i (5.9)
1	0.00%	0.00%	0.00%
2	0.00%	0.00%	0.00%
3	0.00%	0.00%	0.00%
4	0.00%	0.00%	0.00%
5	0.00%	0.00%	0.00%
6	0.00%	0.00%	0.00%

5.8.2   Multiple discontinuities intersecting at different points

As for a more generic scenario, in which the discontinuities are not stemming from a single point, but instead have multiple intersection points (both inside and/or outside the element domain), the problem of defining the equivalent polynomials, $\tilde{H}_i(\boldsymbol{x})$, for all the domain partitions is, unquestionably, more complex.

A solution by means of the proposed formulation can be set off using the definition of *junction points* presented by Daux in [34]. Let us suppose that the same 2×2 regular quadrilateral element Ω, centred in $(0,0)$, previously described, is now crossed by an arbitrary number n of discontinuities, which intersects each other in M different points $\boldsymbol{P}_i$, both inside and outside the domain Ω, defining N domain partitions(see Figure 5.22).
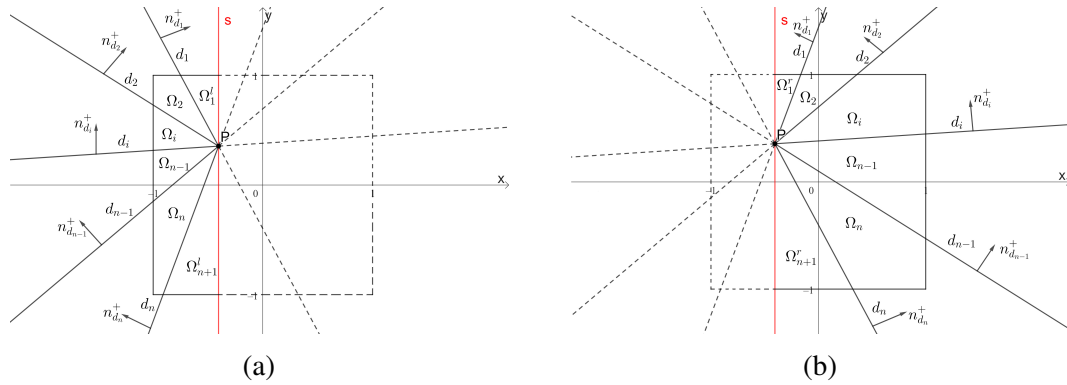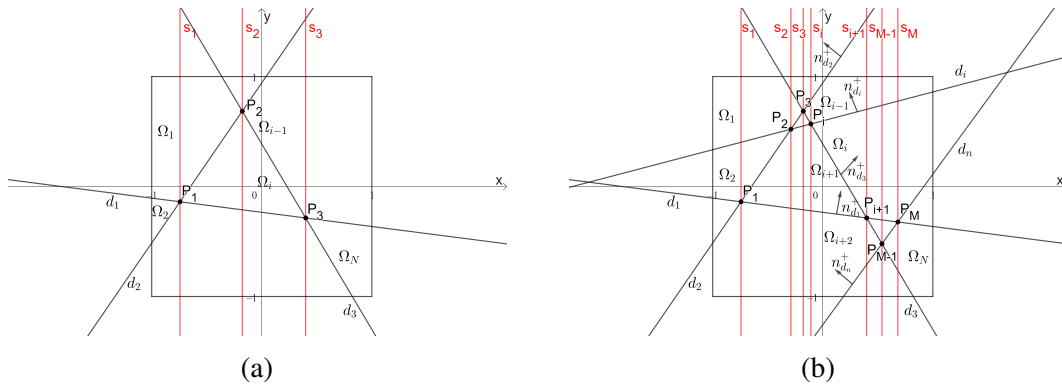

Fig. 5.22 Extension of the proposed formulation for an arbitrary number n of discontinuities intersecting on multiple junction points $\boldsymbol{P}_i$. (**a**) Definition of the discontinuities and the portions of Ω in the case of junction points within the domain. (**b**) Definition of the discontinuities and the portions of Ω in the case of junction points both inside and outside the domain.

As in [34], let us define the junction points, $\boldsymbol{P}_i$, as the points at which two (or more) discontinuities intersect each other and let s_i the abscissa of each junction point $\boldsymbol{P}_i$. It is then possible to describe M domain bounds, $x = s_i$, in order to define $M + 1$ domain restrictions: $[-1, s_1], [s_1, s_2], ..., [s_{i-1}, s_i], ..., [s_M, 1]$.

The idea is to recursively employ, at each domain restriction, the proposed formulation for an arbitrary number of discontinuities stemming from a single point (equations (5.61) to (5.65)). In this scenario, in fact, the i-th junction point will stand on the boundary $x = s_i$ of the i-th domain restriction, satisfying the conditions to

apply equations (5.61) to (5.65) over the entire i-th restriction, in order to obtain the expressions of the equivalent polynomials for all the domain portions contained in the i-th restriction.

Simply iterating the proposed technique $M + 1$ times, will allow to obtain the equivalent polynomials expressions for all the N domain portions contained in Ω.

Note that, in section 5.3, the proposed formulation has been initially defined for rectangular restrictions of Ω, in which only one arbitrary bound, $x = s$, has been defined, due to the presence of a single intersection point. The proposed formulation, however, maintains its validity also for rectangular restrictions of Ω defined by two successive arbitrary bounds, $x = s_1$ and $x = s_2$, namely any Ω restriction between two consecutive intersection points. The absence of intersection points within the domain restriction is, in fact, the necessary condition in order for the linear system in equations (5.56) to (5.60) to have a unique solution (defined in equations (5.61) to (5.65)).

It should be pointed out that the formulation presented in section 5.8.1 can be employed not only when the discontinuities stem from a unique point, but also in the case of arbitrary discontinuities not sharing the same intersection point, as long as none of their intersection points are contained in Ω, or in its restriction bounded by s_i. This leads to the possibility of employing the proposed formulation also in cases that require special attention, such as the presence of junction points both inside and outside the domain (see Figure 5.22b). Such scenario, in fact, can still be solved by means of the presented formulation (equations (5.61) to (5.65)) employed recursively at each domain restriction, as already described at the beginning of this Subsection for the case in Figure 5.22a. In order to better visualise this, in Figure 5.22b, the normals to the discontinuities crossing the central domain restriction between the bounds $x = s_i$ and $x = s_{i+1}$ have been highlighted, together with the domain portions defined by these discontinuities. Employing the proposed formulation by means of equations (5.61) to (5.65), it is possible to define the equivalent polynomials equations for each portion.

The general procedure to exactly integrate an arbitrary number of discontinuities over an element domain Ω by means of equivalent polynomials is outlined in the following steps:

1. Problem definition:

- Definition of the element nodal coordinates in the global coordinates system;

- Definition of the number of discontinuities crossing the element;

- Definition of the discontinuities coefficients in the global coordinates system;

2. Isoparametric mapping onto the parent element domain and definition of the discontinuities coefficients in the parent coordinates system;

3. Identification of all the junction points as the intersections of two, or more, discontinuities;

4. Definition of the Ω domain restrictions in the $x \in [-1,1]$ range ($[-1,s_1]$, ..., $[s_{i-1},s_i]$, ..., $[s_M,1]$);

5. Employing the proposed formulation recursively, by way of equations (5.61) to (5.65), on each domain restriction in order to evaluate the coefficient vectors of the equivalent polynomials for each Ω domain portion defined by the discontinuities;

6. Quadrature by way of any chosen rule (i.e., eq. (5.18)).

As a test, the proposed formulation described above has been employed on a standard 2×2 quadrilateral parent element domain Ω, centred in $(0,0)$ and cut by $n = 3$ discontinuities not sharing the same intersection point (as in Figure 5.21) to compute the integral in Eq. (5.4) in which $\mathscr{P} = xy$ and the targeted domain portion is Ω_1. (The data used for this example is reported in the Appendix A.3.2). The integral results obtained by means of the proposed formulation are compared to the results obtained by way of the adaptive integration method "*NIntegrate*" of the software *Wolfram Mathematica*, as well as the numerical results by means of the method proposed in [34] and by way of definite integral computation over each subdomain. The error is evaluated as in Eq. (5.55) and results are reported in Table 5.12.

Table 5.12 Proposed formulation error (percentage) for a quadrilateral element crossed by $n = 3$ discontinuities not sharing the same intersection point compared to other integration methods.

$\mathscr{P}$	Quadrature over Ω_1 ([34, 7])	Adaptive integration	Definite integral over Ω_1 (5.9)
xy	0.00%	0.00%	0.00%

As outlined in section 5.7, in order to obtain exact quadrature results by means of the proposed formulation the following requirements must be satisfied:

- The determinant of the Jacobian transformation matrix has to be constant;

- The N-th degree polynomial $\mathscr{P}_N$ to be integrated (see eq. (5.4)) has to be a linear combination of the monomials in Table 5.1.

As discussed in sections 5.3 and 5.4, the formulation herein presented for a standard 2×2 quadrilateral parent element, can be directly extended to a standard triangular parent element. The formulation can also be applied to 3-dimensional tetrahedral and hexahedral parent elements, as demonstrated in sections 5.5 and 5.6. Moreover, by means of isoparametric mapping, the proposed formulation can be employed on any 2D or 3D element in a global coordinates system, which can be brought back to a regular geometry in a parent coordinate system.

Thus, the proposed formulation delivers a direct yet simple approach for integrating multiple discontinuities within a single finite element by means of equivalent polynomials. The main problem in this approach could be the partition definition in the case of multiple discontinuities crossing in various points, both inside and outside the element domain (see Figure 5.22b).

Even though obtaining the equivalent polynomials equation for each partition defined within each restriction of the domain by means of the proposed formulation is straightforward, coupling equivalent polynomials values for a single partition which lies across multiple restrictions can be challenging (see partition Ω_1 in Figure 5.22b, bounded by $x = -1$ and $x = s_3$).

Although various methodologies have been explored, an efficient solution for this issue is yet to be defined and could be set as the objective of a future work aiming to improve the proposed formulation and extend its usefulness.

5.9   Outcomes and Discussion

The integration technique presented in Chapter, is a useful tool to evaluate the integral of multiple discontinuous functions by means of any numerical quadrature strategy, removing the need for dividing the domain of integration. The scope for the proposed formulation is mainly XFEM analysis of cracked bodies, in which scenarios involving crossing discontinuities are common [157, 35, 36, 181–183]. Additionally, the existing methods for dealing with problems involving multiple discontinuities rely on integration strategies that necessitate domain partitioning. In this situation, the proposed formulation is an ideal fit because it provides a resolution for the problem at hand and does not require domain splitting. Thus, it may be used in a variety of real-world XFEM applications where multiple discontinuities cross the domain, such as hydraulic fractures and multiple cracking in rocks [179, 178, 180, 177], brittle cracking and fracture propagation in brittle and quasi brittle materials [184, 102, 185], and also fracture behaviour in bones and bones-inspired bio-materials [186, 187], where crack branching, junction and kinking is frequent. However, the presented method can be expanded to a variety of fields, such as computational geometry, where it is possible to use the method to compute the geometrical properties of complex figures created by repeatedly cutting a simple shape (such as a parallelogram) with multiple lines. The suggested approach could fit problems brought up by different authors in this field such in [188, 189, 167, 190–192, 171]. The proposed formulation can be employed in simulations where the objects shapes and locations vary dynamically, such, for instance, an object that shatters into fragments or computer graphics in general [193–196]. Since numerical integration of polynomial functions with jump discontinuities is a common issue in various fields, the effectiveness of the proposed method, its ease of use, and the simplicity of implementation into any computational framework make it a well-suited mean for a broad variety of potential applications [142–154, 24, 155, 156, 174, 11]. However, it has to be noted that the use of equivalent polynomials lead to a higher computational effort during quadrature than splitting the integration domain, since the integrand function doubles its degree [22, 27]. This aspect can be especially onerous in analyses with a multitude of enriched elements. A possible enhancement could be accelerate and optimise the computation process. Future developments for the proposed formulation may include the improvement of the general solution for the case of an arbitrary number of discontinuities and junction points, as well as

the implementation of the proposed method into computational frameworks for a more widespread application in the context of computational geometry and fracture mechanics.

5.10   Conclusions

A formulation to exactly integrate multiple discontinuities in 2D and 3D finite element domains using equivalent polynomials has been presented in this Chapter. The integration of multiple discontinuities represents an arduous work, principally because of the the piecewise nature of the Heaviside step functions, which are commonly employed to reproduce discontinuities in XFEM analysis. The Chapter has been focused on investigating the behaviour and properties of integrals of discontinuous functions and their applications in fracture mechanics and XFEM analysis. An integration technique to efficiently and exactly perform these computations by way of equivalent polynomials without subdividing the integration domain has been developed. The concept of equivalent polynomials allowed for the seamless transition across discontinuities and preserved the continuity of the solution, while effectively capturing the physics of the problem. The proposed formulation represents also a useful tool for the numerical computation of integrals of polynomial functions across generic subdomains generated by two, or more, discontinuities partitioning a regular integration domain. In this Chapter, the implementation of the proposed integration technique for various 2D and 3D finite element shapes (such as triangle, quadrilateral, tetrahedral and hexahedral) cut by two discontinuities has been carried out and its accuracy and ease of calculation have been demonstrated by means of various practical examples. Moreover, a comparison with other integration methods has been performed in order to validate the proposed formulation. Additionally, a software implementation of the proposed formulation (*DD_EQP* Library) for quadrilateral domains crossed by two discontinuities has been developed and some numerical tests have been performed in order to demonstrate the precision in the results, the ease of implementation for the presented technique, as well as the extensibility and generality of the mathematical framework that underlies the proposed method. Also, an analysis on the accuracy of the results obtained by means of the proposed formulation in the case of distorted elements, and an extension for the presented methodology to an arbitrary number of discontinuities has been carried out. The integration of

polynomials times multiple step functions in 2D and 3D domains exhibited promising applications in various fields, such as numerical simulations, computational geometry and engineering problems that involve modelling phenomena with sharp transitions or abrupt changes. Overall, the presented method can be considered as a significant contributions to the field of numerical analysis by providing a technique for integrating multiple discontinuities in 2D and 3D finite element, without defining subdomains. The capability to accurately integrate discontinuities within various domain shapes without splitting the integration domain could define pathways for more precise calculations in various contexts. Future research can further explore optimisation approaches and advanced numerical techniques to enhance the accuracy and effectiveness, as well as to optimise the general solution for handling an arbitrary number of discontinuities.

Chapter 6

Conclusions and further research

6.1   Main conclusions

The integration of multiple discontinuities over various 2D and 3D domain shapes using equivalent polynomials has been explored in this PhD Thesis, and a technique to exactly integrate polynomials times multiple step functions without the need for splitting the integration domain has been proposed. The outcomes of the present work demonstrated that the use of equivalent polynomials offers a promising approach for the exact integration of multiple discontinuities by means of standard quadrature rules. This eliminates the necessity for complex numerical techniques and significantly simplifies the integration procedure.

The formulation has been firstly defined for a standard 2×2 bilinear quadrilateral parent element crossed by two discontinuities (namely as a closed form solution for the problem of numerically integrating polynomials times double step function over quadrilateral domains), describing the precision and rigour of the mathematical methods underlying the proposed solution. Moreover, a software implementation of the presented technique into a Fortran library, *DD_EQP*, has been carried out in order to prove the ease of implementation of the proposed method and to deliver a practical application of it. The library implements the closed form solution for a standard 2×2 bilinear quadrilateral parent element crossed by two discontinuities, as well as isoparametric mapping methods to extend the solution to any quadrilateral element, however defined in a global reference system. *DD_EQP* has been used to perform numerical tests on the proposed formulation comparing the results with

standard integration methods, demonstrating its accuracy, being the outcomes exact up to machine precision. The presented formulation has then been extended to a standard linear triangular parent element, demonstrating the adaptability of the proposed method.

The problem of defining an integration technique for three-dimensional parent elements crossed by multiple discontinuities has also been tackled. The case of a standard trilinear hexahedral parent element crossed by two discontinuities has been explored and a closed form solution for the exact integration of polynomials times double step function in hexahedral domains has been proposed, demonstrating once again its precision and the rigour of the mathematical methods underlying it. The presented method has been extended also to a linear tetrahedral parent element, showing the versatility of the proposed formulation. Moreover, by means of isoparametric mapping, the proposed formulation can be extended to elements, however defined in a global coordinate system, which can be brought back to a regular parent geometry. Numerical tests have been performed for each analysed element. The outcomes have been compared with the results obtained by way of standard integration methods, which validated the proposed formulation also for three-dimensional elements. Still in the isoparametric mapping context, the effect of distorted elements on the accuracy of the results obtained by means of the proposed formulation has been explored and numerical tests pointed out a non-negligible loss of precision in the case of distorted quadrilateral and hexahedral elements. The order of magnitude of the error, however, is comparable to the one obtained by way of standard integration techniques, such as splitting the domain of integration. On the other hand, triangular and tetrahedral elements are not affected by the distortion due to their linearity, always delivering precise results. Strategies to mitigate the problem exploiting this feature of linear elements, (i.e., the subdivision of a distorted quadrilateral domain by means of triangular elements) have been analysed. However, the transition from bilinear (or trilinear) elements to linear ones involves a loss of information in the results. Finally, the extension of the proposed formulation to problems involving an arbitrary number of discontinuities has been presented, demonstrating the scalability of the method. The presented technique has a straightforward adaptability to problems in which an arbitrary number of discontinuities stems from a single intersection point (inside or outside the element). Issues may arise in the case of discontinuities intersecting in various points, both inside and outside the element. These problems are mainly related to the complexity,

in some cases, to correctly identify element portions defined by the discontinuities when evaluating the equivalent polynomials equations. Particularly when a portion lies over multiple domain restrictions. The formulation has been proposed for quadrilateral domains, however, its extension to other bi-dimensional and three-dimensional domain shapes is straightforward.

In conclusion, the proposed formulation offers a method to exactly integrate polynomials times multiple discontinuities, handling diverse domain shapes. By employing equivalent polynomials, the behaviour of integrand functions embedding discontinuities can be accurately captured, allowing to precisely evaluate the overall integration result. The ability to handle multiple discontinuities simultaneously is a significant advantage, as it allows for a more comprehensive analysis of complex problems involving diverse physical phenomena. This feature is particularly valuable in various scientific and engineering applications where irregular domain shapes are common, especially in fracture mechanics and in the XFEM analysis context. The proposed formulation provides, however, an integration technique that could be exceptionally useful not only in the context of XFEM and fracture mechanics, but also in the field of computational geometry and as a mathematical tool to easily solve integrals over domains of non-trivial shape. Nonetheless, potential issues associated with the integration of multiple discontinuities using equivalent polynomials have been highlighted, such as the non-negligible effect of distortions on the results, and the complexity on correctly defining the domain portions in the case of discontinuities intersecting on various points, both inside and outside the element domain. Additionally, it must be noted that the introduction of equivalent polynomials into the integrand function increases its degree, thus requiring a higher computational effort. Despite the issues, the proposed formulation is a useful method for the integration of multiple discontinuities over various 2D and 3D domain shapes, which offers a promising alternative to traditional methods that rely on domain splitting. This approach allows for seamless integration by means of standard quadrature rules without sacrificing accuracy.

Further research is advised below to address the unresolved issues regarding some aspects of the proposed formulation since the presented results are undoubtedly not exhaustive.

6.2   Further research

On the basis of the unresolved issues for the proposed formulation, the following study directions are recommended:

Higher computational effort: While the use of equivalent polynomials ensures a seamless integration for problems involving discontinuities, it also involves the increment of the integrand function degree, thus leading to a higher computational demand (see [22, 27, 11]). Although the issue could be irrelevant when analysing a single element crossed by two (or more) discontinuities, it may become burdensome in the case of analysis in which numerous elements contains discontinuities (i.e., XFEM analysis on multi-fractured bodies or fracture branching problems). Exploring advanced numerical techniques and optimisation approaches to improve the efficiency of the proposed formulation, thus, is among the key aspect to address in further research.

Distorted elements: Integration results accuracy may be heavily affected when using the proposed formulation on distorted domains, particularly in the case of bilinear and trilinear parent elements. The non-constant determinant of the Jacobian matrix in such scenarios, as well as the effect of the distortion on the discontinuities (see section 5.7), are the main causes of unreliable results in the case of distorted elements. Possible workarounds to this problem, such as splitting the distorted element by means of linear elements, which are not affected by distortions, have been proposed. However, a general solution that ensures adequate accuracy on results, avoiding loss of information due to the use of different element types, has yet to be explored and should be tackled in further research.

Arbitrary number of intersection points: As analysed in section 5.8, the definition of the equivalent polynomials $\tilde{H}_i(\boldsymbol{x})$ for all the domain portions in the case of an indefinite number of discontinuities intersecting in various points, both inside and outside the element domain, could be challenging. A general procedure based on the technique presented in this Thesis, applying some concepts proposed in [34], has been illustrated, although criticalities may arise if a domain portion lies over several domain restrictions (see section 5.8.2). In fact, in such situations (see portion Ω_1 in Figure 5.22b), special attention is required on defining the normals of each discontinuity, in order to correct identify all the quantities that define the equivalent polynomials for the i-th portion. This process may result burdensome and

require additional computational effort in the case of domains containing numerous intersection points. Further research should address this issue, exploring a general (yet computational unheavy) method to precisely define domain portions that lies over various restrictions, in order to unambiguously determine the equivalent polynomial equation for the entire partition.

References

[1] T.J.R. Hughes. *The Finite Element Method: Linear Static and Dynamic Finite Element Analysis*. Dover Publications, 2000.

[2] I. Babuška and M. Suri. The p-version of the finite element method. *SIAM Journal on Numerical Analysis*, 29(2):864–893, 1992.

[3] T. Belytschko, Y.Y. Lu, and L. Gu. Element-free galerkin methods. *International Journal for Numerical Methods in Engineering*, 37(2):229–256, 1994.

[4] Carlos Duarte, Ivo Babuška, and John Oden. Generalized finite element method for three-dimensional structural mechanics problems. *Comput Struct*, 77:219–232, 2000.

[5] J.M. Melenk and I. Babuška. The partition of unity finite element method: Basic theory and applications. *Computer Methods in Applied Mechanics and Engineering*, 139(1):289–314, 1996.

[6] Natarajan Sukumar, Nicolas Moës, Brian Moran, and Ted Belytschko. Extended finite element method for three-dimensional crack modelling. *International journal for numerical methods in engineering*, 48(11):1549–1570, 2000.

[7] Nicolas Moës, John Dolbow, and Ted Belytschko. A finite element method for crack growth without remeshing. *International journal for numerical methods in engineering*, 46(1):131–150, 1999.

[8] Thomas-Peter Fries and Ted Belytschko. The extended/generalized finite element method: an overview of the method and its applications. *International journal for numerical methods in engineering*, 84(3):253–304, 2010.

[9] Amir R Khoei. *Extended finite element method: theory and applications*. John Wiley & Sons, 2014.

[10] K Rege and HG Lemu. A review of fatigue crack propagation modelling techniques using fem and xfem. In *IOP Conference Series: Materials Science and Engineering*, volume 276, page 012027. IOP Publishing, 2017.

[11] Sebastiano Fichera, Gregorio Mariggiò, Mauro Corrado, and Giulio Ventura. Integration of polynomials times double step function in quadrilateral domains for xfem analysis. *Algorithms*, 16(6), 2023.

[12] Timon Rabczuk, Stéphane Bordas, and Goangseup Zi. On three-dimensional modelling of crack growth using partition of unity methods. *Computers & structures*, 88(23-24):1391–1411, 2010.

[13] GR Liu. An overview on meshfree methods: for computational solid mechanics. *International Journal of Computational Methods*, 13(05):1630001, 2016.

[14] I Babushka and JM Melenk. The partition of unity method. *Int. J. Numer. Methods Eng*, 40:727–758, 1997.

[15] Ted Belytschko, Robert Gracie, and Giulio Ventura. A review of extended/generalized finite element methods for material modeling. *Modelling and Simulation in Materials Science and Engineering*, 17(4):043001, 2009.

[16] Theofanis Strouboulis, Ivo Babuška, and Kevin Copps. The design and analysis of the generalized finite element method. *Computer methods in applied mechanics and engineering*, 181(1-3):43–69, 2000.

[17] Theofanis Strouboulis, Kevin Copps, and Ivo Babuška. The generalized finite element method. *Computer methods in applied mechanics and engineering*, 190(32-33):4081–4193, 2001.

[18] Ted Belytschko and Tom Black. Elastic crack growth in finite elements with minimal remeshing. *International journal for numerical methods in engineering*, 45(5):601–620, 1999.

[19] Klaus-Jürgen Bathe. *Finite element procedures*. Klaus-Jurgen Bathe, 2006.

[20] Ted Belytschko, Wing Kam Liu, Brian Moran, and Khalil Elkhodary. *Nonlinear finite elements for continua and structures*. John wiley & sons, 2014.

[21] Timon Rabczuk, Jeong-Hoon Song, Xiaoying Zhuang, and Cosmin Anitescu. *Extended finite element and meshfree methods*. Academic Press, 2019.

[22] Giulio Ventura. On the elimination of quadrature subcells for discontinuous functions in the extended finite-element method. *International Journal for Numerical Methods in Engineering*, 66(5):761–795, 2006.

[23] SE Mousavi, JE Pask, and N Sukumar. Efficient adaptive integration of functions with sharp gradients and cusps in n-dimensional parallelepipeds. *International journal for numerical methods in engineering*, 91(4):343–357, 2012.

[24] E.B. Chin, J.B. Lasserre, and N. Sukumar. Modeling crack discontinuities without element-partitioning in the extended finite element method. *International Journal for Numerical Methods in Engineering*, 110(11):1021–1048, 2017.

[25] E Benvenuti, A Tralli, and Giulio Ventura. A regularized xfem model for the transition from continuous to discontinuous displacements. *International Journal for Numerical Methods in Engineering*, 74(6):911–944, 2008.

[26] Elena Benvenuti, Giulio Ventura, and Nicola Ponara. Finite element quadrature of regularized discontinuous and singular level set functions in 3d problems. *Algorithms*, 5(4):529–544, 2012.

[27] G Ventura and E Benvenuti. Equivalent polynomials for quadrature in heaviside function enriched elements. *International Journal for Numerical Methods in Engineering*, 102(3-4):688–710, 2015.

[28] Gregorio Mariggiò, Sebastiano Fichera, Mauro Corrado, and Giulio Ventura. Eqp-a 2d/3d library for integration of polynomials times step function. *SoftwareX*, 12:100636, 2020.

[29] Kyungsu Ha, Hyunil Baek, and Kyoungsoo Park. Convergence of fracture process zone size in cohesive zone modeling. *Applied Mathematical Modelling*, 39(19):5828–5836, 2015.

[30] Stéphane Bordas, Timon Rabczuk, and Goangseup Zi. Three-dimensional crack initiation, propagation, branching and junction in non-linear materials by an extended meshfree method without asymptotic enrichment. *Engineering Fracture Mechanics*, 75(5):943–960, 2008.

[31] Timon Rabczuk, Goangseup Zi, Stephane Bordas, and Hung Nguyen-Xuan. A simple and robust three-dimensional cracking-particle method without enrichment. *Computer Methods in Applied Mechanics and Engineering*, 199(37-40):2437–2455, 2010.

[32] Timon Rabczuk, Stéphane Bordas, and Goangseup Zi. A three-dimensional meshfree method for continuous multiple-crack initiation, propagation and junction in statics and dynamics. *Computational mechanics*, 40:473–495, 2007.

[33] Ted Belytschko, Nicolas Moës, Shuji Usui, and Chandu Parimi. Arbitrary discontinuities in finite elements. *International Journal for Numerical Methods in Engineering*, 50(4):993–1013, 2001.

[34] Christophe Daux, Nicolas Moës, John Dolbow, Natarajan Sukumar, and Ted Belytschko. Arbitrary branched and intersecting cracks with the extended finite element method. *International journal for numerical methods in engineering*, 48(12):1741–1760, 2000.

[35] Indra Vir Singh, G Bhardwaj, and BK Mishra. A new criterion for modeling multiple discontinuities passing through an element using xiga. *Journal of Mechanical Science and Technology*, 29(3):1131, 2015.

[36] Long-Fei Wen, Rong Tian, Li-Xiang Wang, and Chun Feng. Improved xfem for multiple crack analysis: Accurate and efficient implementations for stress intensity factors. *Computer Methods in Applied Mechanics and Engineering*, 411:116045, 2023.

[37] O. C. Zienkiewicz, R. L. Taylor, and J. Z. Zhu. *The Finite Element Method: Its Basis and Fundamentals, Sixth Edition*. Butterworth-Heinemann, 6 edition, May 2005.

[38] Yazid Abdelaziz and Abdelmadjid Hamouine. A survey of the extended finite element. *Computers & structures*, 86(11-12):1141–1151, 2008.

[39] Ted Belytschko, Jacob Fish, and Bruce E Engelmann. A finite element with embedded localization zones. *Computer methods in applied mechanics and engineering*, 70(1):59–89, 1988.

[40] Michael Ortiz, Yves Leroy, and Alan Needleman. A finite element method for localized failure analysis. *Computer methods in applied mechanics and engineering*, 61(2):189–214, 1987.

[41] Eduardo N Dvorkin, Alberto M Cuitino, and Gustavo Gioia. Finite elements with displacement interpolated embedded localization lines insensitive to mesh size and distortions. *International journal for numerical methods in engineering*, 30(3):541–564, 1990.

[42] Juan Carlos Simo, Javier Oliver, and Francisco Armero. An analysis of strong discontinuities induced by strain-softening in rate-independent inelastic solids. *Computational mechanics*, 12(5):277–296, 1993.

[43] John Everett Dolbow. *An extended finite element method with discontinuous enrichment for applied mechanics*. Northwestern university, 1999.

[44] Theofanis Strouboulis, Ivo Babuška, and Kevin Copps. The design and analysis of the generalized finite element method. *Computer methods in applied mechanics and engineering*, 181(1-3):43–69, 2000.

[45] T Strouboulis, K Copps, and Ivo Babuška. The generalized finite element method: an example of its implementation and illustration of its performance. *International Journal for Numerical Methods in Engineering*, 47(8):1401–1417, 2000.

[46] Theofanis Strouboulis, Kevin Copps, and Ivo Babuška. The generalized finite element method. *Computer methods in applied mechanics and engineering*, 190(32-33):4081–4193, 2001.

[47] Ivo Babuška, Gabriel Caloz, and John E Osborn. Special finite element methods for a class of second order elliptic problems with rough coefficients. *SIAM Journal on Numerical Analysis*, 31(4):945–981, 1994.

[48] Bhushan Lal Karihaloo and QZ Xiao. Modelling of stationary and growing cracks in fe framework without remeshing: a state-of-the-art review. *Computers & Structures*, 81(3):119–129, 2003.

[49] Stanley Osher and James A Sethian. Fronts propagating with curvature-dependent speed: Algorithms based on hamilton-jacobi formulations. *Journal of computational physics*, 79(1):12–49, 1988.

[50] M Stolarska, David L Chopp, Nicolas Moës, and Ted Belytschko. Modelling crack growth by level sets in the extended finite element method. *International journal for numerical methods in Engineering*, 51(8):943–960, 2001.

[51] M Stolarska and DL Chopp. Modeling thermal fatigue cracking in integrated circuits by level sets and the extended finite element method. *International Journal of Engineering Science*, 41(20):2381–2410, 2003.

[52] Anthony Gravouil, Nicolas Moës, and Ted Belytschko. Non-planar 3d crack growth by the extended finite element and level sets—part ii: Level set update. *International journal for numerical methods in engineering*, 53(11):2569–2586, 2002.

[53] Nicolas Moës, Anthony Gravouil, and Ted Belytschko. Non-planar 3d crack growth by the extended finite element and level sets—part i: Mechanical model. *International journal for numerical methods in engineering*, 53(11):2549–2568, 2002.

[54] N Sukumar, David L Chopp, and B Moran. Extended finite element method and fast marching method for three-dimensional fatigue crack propagation. *Engineering Fracture Mechanics*, 70(1):29–48, 2003.

[55] Thomas-Peter Fries and Malak Baydoun. Crack propagation with the extended finite element method and a hybrid explicit–implicit crack description. *International Journal for numerical methods in engineering*, 89(12):1527–1558, 2012.

[56] Natarajan Sukumar, David L Chopp, Nicolas Moës, and Ted Belytschko. Modeling holes and inclusions by level sets in the extended finite-element method. *Computer methods in applied mechanics and engineering*, 190(46-47):6183–6200, 2001.

[57] Giulio Ventura, JX Xu, and T Belytschko. A vector level set method and new discontinuity approximations for crack growth by efg. *International Journal for numerical methods in engineering*, 54(6):923–944, 2002.

[58] Jack Chessa and Ted Belytschko. An enriched finite element method and level sets for axisymmetric two-phase flow with surface tension. *International journal for numerical methods in engineering*, 58(13):2041–2064, 2003.

[59] Jack Chessa and Ted Belytschko. An extended finite element method for two-phase fluids. *J. Appl. Mech.*, 70(1):10–17, 2003.

[60] Jack Chessa and Ted Belytschko. Arbitrary discontinuities in space–time finite elements by level sets and x-fem. *International Journal for Numerical Methods in Engineering*, 61(15):2595–2614, 2004.

[61] Antoine Legay, Jack Chessa, and Ted Belytschko. An eulerian–lagrangian method for fluid–structure interaction based on level sets. *Computer Methods in Applied Mechanics and Engineering*, 195(17-18):2070–2087, 2006.

[62] James A Sethian. A fast marching level set method for monotonically advancing fronts. *Proceedings of the National Academy of Sciences*, 93(4):1591–1595, 1996.

[63] DL Chopp and N Sukumar. Fatigue crack propagation of multiple coplanar cracks with the coupled extended finite element/fast marching method. *International journal of engineering science*, 41(8):845–869, 2003.

[64] Nsu Sukumar, David L Chopp, Eric Béchet, and N Moës. Three-dimensional non-planar crack growth by a coupled extended finite element and fast marching method. *International journal for numerical methods in engineering*, 76(5):727–748, 2008.

[65] Ali Osman Ayhan and HF Nied. Stress intensity factors for three-dimensional surface cracks using enriched finite elements. *International journal for numerical methods in engineering*, 54(6):899–921, 2002.

[66] FL Stazi, Elisa Budyn, Jack Chessa, and Ted Belytschko. An extended finite element method with higher-order elements for curved cracks. *Computational Mechanics*, 31(1):38–48, 2003.

[67] Sang-Ho Lee, Jeong-Hoon Song, Young-Cheol Yoon, Goangseup Zi, and Ted Belytschko. Combined extended and superimposed finite element method for cracks. *International Journal for Numerical Methods in Engineering*, 59(8):1119–1136, 2004.

[68] E Budyn, Goangseup Zi, Nicolas Moës, and Ted Belytschko. A method for multiple crack growth in brittle materials without remeshing. *International journal for numerical methods in engineering*, 61(10):1741–1770, 2004.

[69] Goangseup Zi, Jeong-Hoon Song, Elisa Budyn, Sang-Ho Lee, and Ted Belytschko. A method for growing multiple cracks without remeshing and its application to fatigue crack growth. *Modelling and Simulation in Materials Science and Engineering*, 12(5):901, 2004.

[70] Nicolas Moës, Eric Béchet, and Matthieu Tourbier. Imposing dirichlet boundary conditions in the extended finite element method. *International Journal for Numerical Methods in Engineering*, 67(12):1641–1669, 2006.

[71] Alireza Asadpoure, Soheil Mohammadi, and Abolhasan Vafai. Crack analysis in orthotropic media using the extended finite element method. *Thin-Walled Structures*, 44(9):1031–1038, 2006.

[72] A Asadpoure and S Mohammadi. Developing new enrichment functions for crack simulation in orthotropic media by the extended finite element method. *International Journal for Numerical Methods in Engineering*, 69(10):2150–2172, 2007.

[73] Stefan Loehnert and Ted Belytschko. A multiscale projection method for macro/microcrack simulations. *International Journal for Numerical Methods in Engineering*, 71(12):1466–1482, 2007.

[74] A Tabarraei and N23623821169 Sukumar. Extended finite element method on polygonal and quadtree meshes. *Computer Methods in Applied Mechanics and Engineering*, 197(5):425–438, 2008.

[75] Jack Chessa, Hongwu Wang, and Ted Belytschko. On the construction of blending elements for local partition of unity enriched finite elements. *International Journal for Numerical Methods in Engineering*, 57(7):1015–1038, 2003.

[76] Patrick Laborde, Julien Pommier, Yves Renard, and Michel Salaün. High-order extended finite element method for cracked domains. *International Journal for Numerical Methods in Engineering*, 64(3):354–381, 2005.

[77] Thomas-Peter Fries and Ted Belytschko. The intrinsic xfem: a method for arbitrary discontinuities without additional unknowns. *International journal for numerical methods in engineering*, 68(13):1358–1385, 2006.

[78] Thomas-Peter Fries. A corrected xfem approximation without problems in blending elements. *International Journal for Numerical Methods in Engineering*, 75(5):503–532, 2008.

[79] Robert Gracie, Hongwu Wang, and Ted Belytschko. Blending in the extended finite element method by discontinuous galerkin and assumed strain methods. *International Journal for Numerical Methods in Engineering*, 74(11):1645–1669, 2008.

[80] Kazuki Shibanuma and Tomoaki Utsunomiya. Reformulation of xfem based on pufem for solving problem caused by blending elements. *Finite Elements in Analysis and Design*, 45(11):806–816, 2009.

[81] S Loehnert, DS Mueller-Hoeppe, and P Wriggers. 3d corrected xfem approach and extension to finite deformation theory. *International Journal for Numerical Methods in Engineering*, 86(4-5):431–452, 2011.

[82] Julien Réthoré, Anthony Gravouil, and Alain Combescure. An energy-conserving scheme for dynamic crack growth using the extended finite element method. *International Journal for Numerical Methods in Engineering*, 63(5):631–659, 2005.

[83] Thomas Menouillard, Julien Rethore, Alain Combescure, and Harridh Bung. Efficient explicit time stepping for the extended finite element method (x-fem). *International Journal for Numerical Methods in Engineering*, 68(9):911–939, 2006.

[84] Thomas Menouillard, Julien Réthoré, Nicolas Moes, Alain Combescure, and Harridh Bung. Mass lumping strategies for x-fem explicit dynamics: application to crack propagation. *International Journal for Numerical Methods in Engineering*, 74(3):447–474, 2008.

[85] Thomas Elguedj, Anthony Gravouil, Hubert Maigre, and David Grégoire. An explicit dynamics extended finite element method with standard critical time step. In *2009 ASME International Mechanical Engineering Congress & Exposition*, page cdrom, 2009.

[86] Thomas-Peter Fries and Andreas Zilian. On time integration in the xfem. *International Journal for Numerical Methods in Engineering*, 79(1):69–93, 2009.

[87] Thomas Menouillard and Ted Belytschko. Dynamic fracture with meshfree enriched xfem. *Acta mechanica*, 213(1-2):53–69, 2010.

[88] Thomas Menouillard and Ted Belytschko. Smoothed nodal forces for improved dynamic crack propagation modeling in xfem. *International Journal for Numerical Methods in Engineering*, 84(1):47–72, 2010.

[89] Thomas Menouillard, Jeong-Hoon Song, Qinglin Duan, and Ted Belytschko. Time dependent crack tip enrichment for dynamic crack propagation. *International Journal of Fracture*, 162:33–49, 2010.

[90] D Motamedi and S Mohammadi. Dynamic crack propagation analysis of orthotropic media by the extended finite element method. *International Journal of Fracture*, 161:21–39, 2010.

[91] D Motamedi and S Mohammadi. Dynamic analysis of fixed cracks in composites by the extended finite element method. *Engineering Fracture Mechanics*, 77(17):3373–3393, 2010.

[92] Elie Chahine, Patrick Laborde, and Yves Renard. A quasi-optimal convergence result for fracture mechanics with xfem. *Comptes Rendus Mathematique*, 342(7):527–532, 2006.

[93] Juan Jose Ródenas, Octavio Andrés González-Estrada, José Enrique Tarancón, and Francisco Jose Fuenmayor. A recovery-type error estimator for the extended finite element method based on singular+ smooth stress field splitting. *International Journal for Numerical Methods in Engineering*, 76(4):545–571, 2008.

[94] Julien Panetier, Pierre Ladeveze, and Ludovic Chamoin. Strict and effective bounds in goal-oriented error estimation applied to fracture mechanics problems solved with xfem. *International Journal for Numerical Methods in Engineering*, 81(6):671–700, 2010.

[95] Juan José Ródenas, Octavio Andrés González-Estrada, Pedro Díez, and Francisco Javier Fuenmayor. Accurate recovery-based upper error bounds for the extended finite element framework. *Computer Methods in Applied Mechanics and Engineering*, 199(37-40):2607–2621, 2010.

[96] Yongxing Shen and Adrian Lew. An optimally convergent discontinuous galerkin-based extended finite element method for fracture mechanics. *International journal for numerical methods in engineering*, 82(6):716–755, 2010.

[97] Yongxing Shen and Adrian Lew. Stability and convergence proofs for a discontinuous-galerkin-based extended finite element method for fracture mechanics. *Computer Methods in Applied Mechanics and Engineering*, 199(37-40):2360–2382, 2010.

[98] Corinna Prange, Stefan Loehnert, and Peter Wriggers. Error estimation for crack simulations using the xfem. *International Journal for Numerical Methods in Engineering*, 91(13):1459–1474, 2012.

[99] Kyoungsoo Park, Jeronymo P Pereira, C Armando Duarte, and Glaucio H Paulino. Integration of singular enrichment functions in the generalized/extended finite element method for three-dimensional problems. *International Journal for Numerical Methods in Engineering*, 78(10):1220–1257, 2009.

[100] SE Mousavi and N Sukumar. Generalized gaussian quadrature rules for discontinuities and crack singularities in the extended finite element method. *Computer Methods in Applied Mechanics and Engineering*, 199(49-52):3237–3249, 2010.

[101] Stéphane PA Bordas, Timon Rabczuk, Nguyen-Xuan Hung, Vinh Phu Nguyen, Sundararajan Natarajan, Tino Bog, Nguyen Vinh Hiep, et al. Strain smoothing in fem and xfem. *Computers & structures*, 88(23-24):1419–1443, 2010.

[102] Casey L Richardson, Jan Hegemann, Eftychios Sifakis, Jeffrey Hellrung, and Joseph M Teran. An xfem method for modeling geometrically elaborate crack propagation in brittle materials. *International Journal for Numerical Methods in Engineering*, 88(10):1042–1065, 2011.

[103] Thomas-Peter Fries and Malak Baydoun. Crack propagation with the extended finite element method and a hybrid explicit–implicit crack description. *International Journal for numerical methods in engineering*, 89(12):1527–1558, 2012.

[104] M Baydoun and TP Fries. Crack propagation criteria in three dimensions using the xfem and an explicit–implicit crack description. *International journal of fracture*, 178:51–70, 2012.

[105] Hans Minnebo. Three-dimensional integration strategies of singular functions introduced by the xfem in the lefm. *International Journal for Numerical Methods in Engineering*, 92(13):1117–1138, 2012.

[106] Zdenek P Bazant and Jaime Planas. *Fracture and size effect in concrete and other quasibrittle materials*, volume 16. CRC press, 1997.

[107] Arne Hillerborg, Mats Modéer, and P-E Petersson. Analysis of crack formation and crack growth in concrete by means of fracture mechanics and finite elements. *Cement and concrete research*, 6(6):773–781, 1976.

[108] Donald S Dugdale. Yielding of steel sheets containing slits. *Journal of the Mechanics and Physics of Solids*, 8(2):100–104, 1960.

[109] Garth N Wells and LJ1013 Sluys. A new method for modelling cohesive cracks using finite elements. *International Journal for numerical methods in engineering*, 50(12):2667–2682, 2001.

[110] Nicolas Moës and Ted Belytschko. Extended finite element method for cohesive crack growth. *Engineering fracture mechanics*, 69(7):813–833, 2002.

[111] Goangseup Zi and Ted Belytschko. New crack-tip elements for xfem and applications to cohesive cracks. *International Journal for Numerical Methods in Engineering*, 57(15):2221–2240, 2003.

[112] Joris JC Remmers, R de Borst, and Alan Needleman. A cohesive segments method for the simulation of crack growth. *Computational mechanics*, 31:69–77, 2003.

[113] Stefano Mariani and Umberto Perego. Extended finite element method for quasi-brittle fracture. *International Journal for Numerical Methods in Engineering*, 58(1):103–126, 2003.

[114] Ted Belytschko, Hao Chen, Jingxiao Xu, and Goangseup Zi. Dynamic crack propagation based on loss of hyperbolicity and a new discontinuous enrichment. *International journal for numerical methods in engineering*, 58(12):1873–1905, 2003.

[115] Ragnar Larsson and Martin Fagerström. A framework for fracture modelling based on the material forces concept with xfem kinematics. *International Journal for Numerical Methods in Engineering*, 62(13):1763–1788, 2005.

[116] Pedro MA Areias and Ted Belytschko. Analysis of three-dimensional crack initiation and propagation using the extended finite element method. *International journal for numerical methods in engineering*, 63(5):760–788, 2005.

[117] QZ Xiao, Bhushan Lal Karihaloo, and XY Liu. Incremental-secant modulus iteration scheme and stress recovery for simulating cracking process in quasi-brittle materials using xfem. *International Journal for Numerical Methods in Engineering*, 69(12):2606–2635, 2007.

[118] Jesper L Asferg, Peter Noe Poulsen, and Leif Otto Nielsen. A consistent partly cracked xfem element for cohesive crack growth. *International Journal for Numerical Methods in Engineering*, 72(4):464–485, 2007.

[119] E Benvenuti. A regularized xfem framework for embedded cohesive interfaces. *Computer Methods in Applied Mechanics and Engineering*, 197(49-50):4367–4378, 2008.

[120] Arash Zamani, Robert Gracie, and M. Reza Eslami. Cohesive and non-cohesive fracture by higher-order enrichment ofxfem. *International Journal for Numerical Methods in Engineering*, 90(4):452–483, 2012.

[121] Jens Falkenskov Mougaard, Peter Noe Poulsen, and Leif Otto Nielsen. Complete tangent stiffness for extended finite element method by including crack growth parameters. *International journal for numerical methods in engineering*, 95(1):33–45, 2013.

[122] Jörg F Unger, Stefan Eckardt, and Carsten Könke. Modelling of cohesive crack growth in concrete structures with the extended finite element method. *Computer methods in applied mechanics and engineering*, 196(41-44):4087–4100, 2007.

[123] Debasis Deb and Kamal C Das. Extended finite element method for the analysis of discontinuities in rock masses. *Geotechnical and Geological Engineering*, 28:643–659, 2010.

[124] Yangjian Xu and Huang Yuan. Applications of normal stress dominated cohesive zone models for mixed-mode crack simulation based on extended finite element methods. *Engineering Fracture Mechanics*, 78(3):544–558, 2011.

[125] Elena Benvenuti and Antonio Tralli. Simulation of finite-width process zone in concrete-like materials by means of a regularized extended finite element model. *Computational Mechanics*, 50:479–497, 2012.

[126] Sherong Zhang, Gaohui Wang, and Xiangrong Yu. Seismic cracking analysis of concrete gravity dams with initial cracks using the extended finite element method. *Engineering Structures*, 56:528–543, 2013.

[127] Thomas-Peter Fries. Overview and comparison of different variants of the xfem. *Pamm*, 14(1):27–30, 2014.

[128] QZ Xiao and BL Karihaloo. Recent developments of the extended/generalized fem and a comparison with the fem. *Development and Applications of Solid Mechanics, University of Science and Technology of China Press, Hefei, China*, pages 303–324, 2005.

[129] C Armando Duarte and J Tinsley Oden. An hp adaptive method using clouds. *Computer methods in applied mechanics and engineering*, 139(1-4):237–262, 1996.

[130] James Albert Sethian. *Level set methods and fast marching methods: evolving interfaces in computational geometry, fluid mechanics, computer vision, and materials science*, volume 3. Cambridge university press, 1999.

[131] N Sukumar and EA Malsch. Recent advances in the construction of polygonal finite element interpolants. *Archives of Computational Methods in Engineering*, 13:129–163, 2006.

[132] A Tabarraei and N Sukumar. Extended finite element method on polygonal and quadtree meshes. *Computer Methods in Applied Mechanics and Engineering*, 197(5):425–438, 2008.

[133] F Mottaghian, A Darvizeh, and A Alijani. Extended finite element method for statics and vibration analyses on cracked bars and beams. *Journal of Solid Mechanics*, 10(4):902–928, 2018.

[134] Hamed Ghohani Arab and Mohammad Reza Ghasemi. Errors estimation of different numerical integration techniques on stiffness matrix and stress intensity factor in xfem. 2013.

[135] N Sukumar and J-H Prévost. Modeling quasi-static crack growth with the extended finite element method part i: Computer implementation. *International journal of solids and structures*, 40(26):7513–7537, 2003.

[136] James K Hahn. Realistic animation of rigid bodies. *ACM Siggraph computer graphics*, 22(4):299–308, 1988.

[137] Jan Bender, Kenny Erleben, and Jeff Trinkle. Interactive simulation of rigid body dynamics in computer graphics. In *Computer Graphics Forum*, volume 33, pages 246–270. Wiley Online Library, 2014.

[138] Bennert Machenhauer, Eigil Kaas, and Peter Hjort Lauritzen. Finite-volume methods in meteorology. In *Handbook of Numerical Analysis*, volume 14, pages 3–120. Elsevier, 2009.

[139] AH Stroud. Approximate calculation of multiple integrals. prentice-hall series in automatic computation. 1971.

[140] John C Amazigo and Lester A Rubenfeld. *Advanced calculus and its applications to the engineering and physical sciences*. Wiley, 1980.

[141] Philip J Davis and Philip Rabinowitz. *Methods of numerical integration*. Courier Corporation, 2007.

[142] J.-H. Lv, Y.-Y. Jiao, T. Rabczuk, X.-Y. Zhuang, X.-T. Feng, and F. Tan. A general algorithm for numerical integration of three-dimensional crack singularities in PU-based numerical methods. *Computer Methods in Applied Mechanics and Engineering*, 363, 2020.

[143] A. Düster and O. Allix. Selective enrichment of moment fitting and application to cut finite elements and cells. *Computational Mechanics*, 65(2):429–450, 2020.

[144] T. Ali, B. Mostefa, D. Abdelkader, A. Abdelkrim, and K. Habibe. Experimental and numerical fracture modeling using XFEM of aluminum plates. *International Journal of Engineering Research in Africa*, 46:45–52, 2020.

[145] M. Surendran, S. Natarajan, G.S. Palani, and S.P.A. Bordas. Linear smoothed extended finite element method for fatigue crack growth simulations. *Engineering Fracture Mechanics*, 206:551–564, 2019.

[146] T. Elguedj, Y. Jan, A. Combescure, B. Leblé, and G. Barras. X-fem analysis of dynamic crack growth under transient loading in thick shells. *International Journal of Impact Engineering*, 122:228–250, 2018.

[147] B. Müller, S. Krämer-Eis, F. Kummer, and M. Oberlack. A high-order discontinuous Galerkin method for compressible flows with immersed boundaries. *International Journal for Numerical Methods in Engineering*, 110(1):3–30, 2017.

[148] Y. Sudhakar, J.P. Moitinho de Almeida, and W.A. Wall. An accurate, robust, and easy-to-implement method for integration over arbitrary polyhedra: Application to embedded interface methods. *Journal of Computational Physics*, 273:393–415, 2014.

[149] P. Antonietti, M. Verani, C. Vergara, and S. Zonca. Numerical solution of fluid-structure interaction problems by means of a high order discontinuous Galerkin method on polygonal grids. *Finite Elements in Analysis and Design*, 159:1–14, 2019.

[150] S.E. Mousavi and N. Sukumar. Numerical integration of polynomials and discontinuous functions on irregular convex polygons and polyhedrons. *Computational Mechanics*, 47(5):535–554, 2011.

[151] J.-Y. Wu, J.-F. Qiu, V.P. Nguyen, T.K. Mandal, and L.-J. Zhuang. Computational modeling of localized failure in solids: XFEM vs PF-CZM. *Computer Methods in Applied Mechanics and Engineering*, 345:618–643, 2019.

[152] A. Martin, J.-B. Esnault, and P. Massin. About the use of standard integration schemes for X-FEM in solid mechanics plasticity. *Computer Methods in Applied Mechanics and Engineering*, 283:551–572, 2015.

[153] E. Benvenuti. XFEM with equivalent eigenstrain for matrix-inclusion interfaces. *Computational Mechanics*, 53(5):893–908, 2014.

[154] L. Formaggia, C. Vergara, and S. Zonca. Unfitted extended finite elements for composite grids. *Computers and Mathematics with Applications*, 76(4):893–904, 2018.

[155] L. Kudela, N. Zander, S. Kollmannsberger, and E. Rank. Smart octrees: Accurately integrating discontinuous functions in 3D. *Computer Methods in Applied Mechanics and Engineering*, 306:406–426, 2016.

[156] Konstantinos Agathos, Eleni Chatzi, and Stéphane PA Bordas. Multiple crack detection in 3d using a stable xfem and global optimization. *Computational mechanics*, 62:835–852, 2018.

[157] Ishai Oren. Admissible functions with multiple discontinuities. *Israel Journal of Mathematics*, 42:353–360, 1982.

[158] Sebastiano Fichera, Bruno Biondi, and Giulio Ventura. 2d finite elements for the computational analysis of crack propagation in brittle materials and the handling of double discontinuities. *Procedia Structural Integrity*, 42:1291–1298, 2022. 23 European Conference on Fracture.

[159] Gregorio Mariggiò, Giulio Ventura, and Mauro Corrado. A probabilistic fem approach for the structural design of glass components. *Engineering Fracture Mechanics*, 282:109157, 2023.

[160] Jan Bender, Kenny Erleben, and Jeff Trinkle. Interactive simulation of rigid body dynamics in computer graphics. *Comput Graph Forum*, 33:246–270, 2014.

[161] HG Timmer and JM Stern. Computation of global geometric properties of solid objects. *Computer-Aided Design*, 12(6):301–304, 1980.

[162] Adarsh Krishnamurthy and Sara McMains. Accurate gpu-accelerated surface integrals for moment computation. *Computer-Aided Design*, 43(10):1284–1295, 2011.

[163] TM Mamatha and B Venkatesh. Gauss quadrature rules for numerical integration over a standard tetrahedral element by decomposing into hexahedral elements. *Applied Mathematics and Computation*, 271:1062–1070, 2015.

[164] Eric B Chin and Natarajan Sukumar. An efficient method to integrate polynomials over polytopes and curved solids. *Computer Aided Geometric Design*, 82:101914, 2020.

[165] R.I. Saye. High-order quadrature methods for implicitly defined surfaces and volumes in hyperrectangles. *SIAM Journal on Scientific Computing*, 37(2):A993–A1019, 2015.

[166] Carl C Farrington. Numerical quadrature of discontinuous functions. In *Proceedings of the 1961 16th ACM national meeting*, pages 21–401, 1961.

[167] Simeon Hubrich, Paolo Di Stolfo, László Kudela, Stefan Kollmannsberger, Ernst Rank, Andreas Schröder, and Alexander Düster. Numerical integration of discontinuous functions: moment fitting and smart octree. *Computational Mechanics*, 60:863–881, 2017.

[168] Anna-Karin Tornberg. Multi-dimensional quadrature of singular and discontinuous functions. *BIT Numerical Mathematics*, 42:644–669, 2002.

[169] Ni Dai, Bin Zhang, Daogang Lu, and Yixue Chen. High-degree discontinuous finite element discrete quadrature sets for the boltzmann transport equation. *Progress in Nuclear Energy*, 153:104403, 2022.

[170] Sebastiano Fichera, Bruno Biondi, and Giulio Ventura. Implementation into opensees of xfem for analysis of crack propagation in brittle materials. In *Proceedings of the 2022 Eurasian OpenSees Days*, pages 157–165. Springer, 2023.

[171] E Pali, A Gravouil, A Tanguy, D Landru, and O Kononchuk. Three-dimensional x-fem modeling of crack coalescence phenomena in the smart cuttm technology. *Finite Elements in Analysis and Design*, 213:103839, 2023.

[172] Chao Song, Hongxin Zhang, Yuan Wu, and Hujun Bao. Cutting and Fracturing Models without Remeshing. In Falai Chen and Bert Jüttler, editors, *Advances in Geometric Modeling and Processing*, pages 107–118. Springer Berlin Heidelberg, 2008.

[173] Hayley N Iben and James F O'Brien. Generating surface crack patterns. *Graph Models*, 71(6):198–208, 2009.

[174] Erik da Rosa Rodriguez and Rodrigo Rossi. Assessment of eqp in xfem for weak discontinuities. *Journal of the Brazilian Society of Mechanical Sciences and Engineering*, 45(6):312, 2023.

[175] Peter J Davis and Philip Rabinowitz. *Methods of Numerical Integration (Second Edition)*. Academic Press, 2 edition, 1984.

[176] Zuorong Chen, AP Bunger, Xi Zhang, and Robert G Jeffrey. Cohesive zone finite element-based modeling of hydraulic fractures. *Acta Mechanica Solida Sinica*, 22(5):443–452, 2009.

[177] Renato Gutierrez Escobar, Eleazar Cristian Mejia Sanchez, Deane Roehl, and Celso Romanel. Xfem modeling of stress shadowing in multiple hydraulic fractures in multi-layered formations. *Journal of Natural Gas Science and Engineering*, 70:102950, 2019.

[178] Francisco Cruz, Deane Roehl, and Eurípedes do Amaral Vargas Jr. An xfem element to model intersections between hydraulic and natural fractures in porous rocks. *International Journal of Rock Mechanics and Mining Sciences*, 112:385–397, 2018.

[179] Tao Wang, ZhanLi Liu, QingLei Zeng, Yue Gao, and Zhuo Zhuang. Xfem modeling of hydraulic fracture in porous rocks with natural fractures. *Science China Physics, Mechanics & Astronomy*, 60:1–15, 2017.

[180] Yuxiao Wang, Akbar A Javadi, and Corrado Fidelibus. A hydro-mechanically-coupled xfem model for the injection-induced evolution of multiple fractures. *International Journal for Numerical and Analytical Methods in Geomechanics*, 2023.

[181] JAL Napier. Energy changes in a rockmass containing multiple discontinuities. *Journal of the Southern African Institute of Mining and Metallurgy*, 91(5):145–157, 1991.

[182] AS Sekhar. Multiple cracks effects and identification. *Mechanical Systems and Signal Processing*, 22(4):845–878, 2008.

[183] Masayuki Kamaya. A crack growth evaluation method for interacting multiple cracks. *JSME International Journal Series A Solid Mechanics and Material Engineering*, 46(1):15–23, 2003.

[184] Shuo Liu, Guodong Fang, Jun Liang, and Dongkai Lv. A coupling model of xfem/peridynamics for 2d dynamic crack propagation and branching problems. *Theoretical and Applied Fracture Mechanics*, 108:102573, 2020.

[185] Clemens Gebhardt and Michael Kaliske. An xfem-approach to model brittle failure of wood. *Engineering Structures*, 212:110236, 2020.

[186] Ashraf Idkaidek and Iwona Jasiuk. Cortical bone fracture analysis using xfem–case study. *International journal for numerical methods in biomedical engineering*, 33(4):e2809, 2017.

[187] Andre E Vellwock, Laura Vergani, and Flavia Libonati. A multiscale xfem approach to investigate the fracture behavior of bio-inspired composite materials. *Composites Part B: Engineering*, 141:258–264, 2018.

[188] Meysam Joulaian, Simeon Hubrich, and Alexander Düster. Numerical integration of discontinuities on arbitrary domains based on moment fitting. *Computational Mechanics*, 57:979–999, 2016.

[189] Alireza Abedian and Alexander Düster. Equivalent legendre polynomials: Numerical integration of discontinuous functions in the finite element methods. *Computer Methods in Applied Mechanics and Engineering*, 343:690–720, 2019.

[190] Jeen-Shang Lin. A mesh-based partition of unity method for discontinuity modeling. *Computer Methods in Applied Mechanics and Engineering*, 192(11-12):1515–1532, 2003.

[191] Alireza Abedian, Jamshid Parvizian, Alexander Düster, Hassan Khademyzadeh, and Ernst Rank. Performance of different integration schemes in facing discontinuities in the finite cell method. *International Journal of Computational Methods*, 10(03):1350002, 2013.

[192] Hojun You and Chongam Kim. Direct reconstruction method for discontinuous galerkin methods on higher-order mixed-curved meshes ii. surface integration. *Journal of Computational Physics*, 416:109514, 2020.

[193] Jeffrey Smith, Andrew Witkin, and David Baraff. Fast and controllable simulation of the shattering of brittle objects. In *Computer Graphics Forum*, volume 20, pages 81–91. Wiley Online Library, 2001.

[194] Alan Norton, Greg Turk, Bob Bacon, John Gerth, and Paula Sweeney. Animation of fracture by physical modeling. *The visual computer*, 7:210–219, 1991.

[195] James F O'brien and Jessica K Hodgins. Graphical modeling and animation of brittle fracture. In *Proceedings of the 26th annual conference on Computer graphics and interactive techniques*, pages 137–146, 1999.

[196] Ignacio Martin-Bragado, Antonio Rivera, Gonzalo Valles, Jose Luis Gomez-Selles, and María J Caturla. Mmonca: An object kinetic monte carlo simulator for damage irradiation evolution and defect diffusion. *Computer Physics Communications*, 184(12):2703–2710, 2013.

Appendix A

A.1 Equivalent polynomials computation in *Wolfram Mathematica*

Formal *Wolfram Mathematica* scripts to compute the equivalent polynomials for the domain shapes presented in chapter 5 crossed by two discontinuities is reported in the following.

In order to improve numerical efficiency and to obtain more compact results, the notation introduced in [27] is used in the computations, so that

$$\tilde{H}_\rho = \boldsymbol{C} \cdot \boldsymbol{m} \tag{A.1}$$

in which $\boldsymbol{m}$ is the vector collecting the monomials (see section 4.3.2) and $\boldsymbol{C}$ is the vector containing the equivalent polynomial coefficients. It is then possible to write eq. (4.16) as

$$\int_\Omega \boldsymbol{m}\,\boldsymbol{m}^T \,\mathrm{d}\Omega\,\boldsymbol{C} = \int_\Omega H_\rho \boldsymbol{m}\,\mathrm{d}\Omega \tag{A.2}$$

being

$$\begin{aligned} \boldsymbol{A} &= \int_\Omega \boldsymbol{m}\,\boldsymbol{m}^T \,\mathrm{d}\Omega \\ \boldsymbol{b} &= \int_\Omega H_\rho \boldsymbol{m}\,\mathrm{d}\Omega \end{aligned} \tag{A.3}$$

so that

$$C = A^{-1}b \tag{A.4}$$

and finally

$$\tilde{H}_\rho = m^T A^{-1} b \tag{A.5}$$

A.1.1 Equivalent polynomials computation for quadrilateral domains

(* Define discontinuity equation and the regularised Heaviside function *)

$d = a\xi + b\eta + c;$

$H = \dfrac{2}{1 + e^{-\rho d}} - 1;$

(* Monomial basis definition in the parent element domain and matrix A computation *)

$M = \{1, \xi, \eta, \xi\eta, \xi^2, \eta^2\};$

$A = [\text{Integrate} [\text{Outer} [\text{Times}, M\,M], \{\xi, -1, 1\}, \{\eta, -1, 1\}]];$

(* b vector analytic definition *)

$H_\xi = \text{Integrate} [H\,M, \xi];$

$T = \text{Simplify} [H_\xi [s] - H_\xi [-1]];$

$H_\eta = \text{Integrate} [T, \eta];$

$BV = \text{Simplify} [H_\eta [1] - H_\eta [-1]];$

(* b vector has to be computed for each discontinuity substituting the coefficients (a_1, b_1, c_1) and (a_2, b_2, c_2) *)

(* s is the abscissa of the discontinuities intersection point *)

(* Resultant b vector for the targeted portion is given by $b_1 - b_2$ and depends on the direction pointed by the discontinuities normals *)

(* Heqv: Equivalent Polynomial computation *)

$$BVres = BV1 - BV2;$$
$$CV = Inverse[A] \cdot BVres;$$
$$Heqv = CV \cdot M;$$

A.1.2 Equivalent polynomials computation for triangular domains

(* Define discontinuity equation and the regularised Heaviside function *)

$$d = a\xi + b\eta + c;$$
$$H = \frac{2}{1 + e^{-\rho d}} - 1;$$

(* Monomial basis definition in the parent element domain and matrix A computation *)

$$M = \{1\};$$
$$A = [Integrate[Outer[Times, M\,M], \{\xi, 0, 1\}, \{\eta, 0, 1 - \xi\}]];$$

(* b vector analytic definition *)

$$H_\eta = Integrate[H\,M, \eta];$$
$$T = Simplify[H_\eta[1 - \xi] - H_\eta[0]];$$
$$H_\xi = Integrate[T, \xi];$$
$$BV = Simplify[H_\xi[s] - H_\xi[0]];$$

(* b vector has to be computed for each discontinuity substituting the coefficients (a_1, b_1, c_1) and (a_2, b_2, c_2) *)

(* s is the abscissa of the discontinuities intersection point *)

(* Resultant b vector for the targeted portion is given by $b_1 - b_2$ and depends on the direction pointed by the discontinuities normals *)

(* Heqv: Equivalent Polynomial computation *)

$BVres = BV1 - BV2;$

$CV = Inverse[A] \, . \, BVres;$

$Heqv = CV \, . \, M;$

A.1.3 Equivalent polynomials computation for hexahedral domains

(* Define discontinuity equation and the regularised Heaviside function *)

$d = a\xi + b\eta + c\zeta + d;$

$H = \dfrac{2}{1 + e^{-\rho d}} - 1;$

(* Monomial basis definition in the parent element domain and matrix A computation *)

$M = \{1, \xi, \xi^2, \eta, \xi\eta, \xi^2\eta, \eta^2, \xi\eta^2, \xi^2\eta^2, \zeta, \xi\zeta, \xi^2\zeta, \eta\zeta,$
$\quad \xi\eta\zeta, \xi^2\eta\zeta, \eta^2\zeta, \xi\eta^2\zeta, \zeta^2, \xi\zeta^2, \xi^2\zeta^2, \eta\zeta^2, \xi\eta\zeta^2, \eta^2\zeta^2\};$

$A = [\text{Integrate}\,[\text{Outer}\,[\text{Times}, M\,M]\,, \{\xi, -1, 1\}, \{\eta, -1, 1\}, \{\zeta, -1, 1\}]];$

(* b vector analytic definition *)

$s = m\,\zeta + n;$

$H_\xi = \text{Integrate}\,[H\,M, \xi];$

$T = \text{Simplify}\,[H_\xi\,[s] - H_\xi\,[-1]];$

$H_\eta = \text{Integrate}\,[T, \eta];$

$T = \text{Simplify}\,[H_\eta\,[1] - H_\eta\,[-1]];$

$H_\zeta = \text{Integrate}\,[T, \zeta];$

$BV = \text{Simplify}\,[H_\zeta\,[\zeta_2] - H_\zeta\,[\zeta_1]];$

(* b vector has to be computed for each discontinuity substituting the coefficients (a_1, b_1, c_1, d_1) and (a_2, b_2, c_2, d_2) *)

(* s is the plane containing the discontinuities intersection line and with null normal wrt y-axis *)

(* ζ_1 and ζ_2 are the intersection between the discontinuities intersection line and $\xi = -1$ and $\xi = 1$ respectively *)

(* Resultant b vector for the targeted portion is given by $b_1 - b_2$ and depends on the direction pointed by the discontinuities normals *)

(* Heqv: Equivalent Polynomial computation *)

$BVres = BV1 - BV2;$

$\quad CV = Inverse[A] . BVres;$

$\ Heqv = CV . M;$

A.1.4 Equivalent polynomials computation for tetrahedral domains

(* Define discontinuity equation and the regularised Heaviside function *)

$d = a\xi + b\eta + c\zeta + d;$

$H = \dfrac{2}{1 + e^{-\rho d}} - 1;$

(* Monomial basis definition in the parent element domain and matrix A computation *)

$M = \{1\};$

$A = [\text{Integrate} [\text{Outer} [\text{Times}, M\,M], \{\xi, 0, 1 - \eta - \zeta\}, \{\eta, 0, 1 - \zeta\}, \{\zeta, 0, 1\}]];$

(* b vector analytic definition *)

$$s = m\,\zeta + n;$$
$$H_\xi = \text{Integrate}\left[H\,M \ast \text{Boole}[\xi \leq s], \xi\right];$$
$$T = \text{Simplify}\left[H_\xi\left[1 - \eta - \zeta\right] - H_\xi\left[0\right]\right];$$
$$H_\eta = \text{Integrate}\left[T, \eta\right];$$
$$T = \text{Simplify}\left[H_\eta\left[1 - \zeta\right] - H_\eta\left[0\right]\right];$$
$$H_\zeta = \text{Integrate}\left[T, \zeta\right];$$
$$BV = \text{Simplify}\left[H_\zeta\left[1\right] - H_\zeta\left[0\right]\right];$$

(* b vector has to be computed for each discontinuity substituting the coefficients (a_1, b_1, c_1, d_1) and (a_2, b_2, c_2, d_2) *)

(* s is the plane containing the discontinuities intersection line and with null normal wrt y-axis *)

(* Resultant b vector for the targeted portion is given by $b_1 - b_2$ and depends on the direction pointed by the discontinuities normals *)

(* Heqv: Equivalent Polynomial computation *)

$$BV\,res = BV1 - BV2;$$
$$CV = Inverse[A] \,.\, BV\,res;$$
$$Heqv = CV \,.\, M;$$

A.2   Fortran libraries source code

As discussed in chapters 4 and 5, a Fortran library for the integration of polynomials times step function over various domain shapes (*EQP*), and a Fortran library for the integration of polynomials times double step function over quadrilateral domains (*DD_EQP*) have been developed as a part of this PhD Thesis work.

The source code for both libraries, as well as some test files, are freely available at http://www.equivalent-polynomials.net/.

A.3   Section 5.8 numerical tests data

Detailed data used for the numerical tests reported in section 5.8 are reported in the following.

A.3.1   Data for test in section 5.8.1

Ω domain coordinates:

$$\mathbf{1} \equiv (-1,-1);$$
$$\mathbf{2} \equiv (1,-1);$$
$$\mathbf{3} \equiv (1,1);$$
$$\mathbf{4} \equiv (-1,1);$$

Intersection point coordinates:

$$\boldsymbol{P} \equiv (-0.40, 0.35);$$

Discontinuities equations:

$$d_1 : \ 1.87x + y + 0.40 = 0;$$
$$d_2 : \ 0.63x + y - 0.10 = 0;$$
$$d_3 : \ -0.07x + y - 0.38 = 0;$$
$$d_4 : \ -0.84x + y - 0.70 = 0;$$
$$d_5 : \ -2.68x + y - 1.44 = 0;$$

A.3.2   Data for test in section 5.8.2

Ω domain coordinates:

$$\mathbf{1} \equiv (-1, -1);$$
$$\mathbf{2} \equiv (1, -1);$$
$$\mathbf{3} \equiv (1, 1);$$
$$\mathbf{4} \equiv (-1, 1);$$

Intersection point coordinates:

$$\boldsymbol{P_1} \equiv (-0.74, -0.14);$$
$$\boldsymbol{P_2} \equiv (-0.18, 0.69);$$
$$\boldsymbol{P_3} \equiv (0.40, -0.29);$$

Discontinuities equations:

$$d_1 : \ 0.13x + y + 0.23 = 0;$$
$$d_2 : \ -1.46x + y - 0.94 = 0;$$
$$d_3 : \ 1.69x + y - 0.39 = 0;$$